

# Development of Electromagnetic Wave Absorption Properties of Graphene-Based Nanocomposites by Using Stochastic Optimization Methods

Submitted to the Graduate School of Natural and Applied Sciences  
in partial fulfillment of the requirements for the degree of

Master of Science

in Materials Science and Engineering

by

Kemal Bartu Aydın

ORCID 0000-0001-5980-9515

January, 2023

This is to certify that we have read the thesis **Development of Electromagnetic Wave Absorption Properties of Graphene-Based Nanocomposites by Using Stochastic Optimization Methods** submitted by **Kemal Bartu Aydın**, and it has been judged to be successful, in scope and in quality, at the defense exam and accepted by our jury as a MASTER'S THESIS.

**APPROVED BY:**

**Advisor:** **Assoc. Prof. Dr. Fethullah Güneş**  
İzmir Kâtip Çelebi University

**Co-advisor:** **Assoc. Prof. Dr. Levent Aydın**  
İzmir Kâtip Çelebi University

**Committee Members:**

**Assoc. Prof. Dr. Hüsnügül Yılmaz Atay**  
İzmir Kâtip Çelebi University

**Assoc. Prof. Dr. Mustafa Erol**  
Dokuz Eylül University

**Date of Defense: January 05, 2023**

# Declaration of Authorship

I, **Kemal Bartu Aydın**, declare that this thesis titled **Development of Electromagnetic Wave Absorption Properties of Graphene-Based Nanocomposites by Using Stochastic Optimization Methods** and the work presented in it are my own. I confirm that:

- This work was done wholly or mainly while in candidature for the Master's degree at this university.
- Where any part of this thesis has previously been submitted for a degree or any other qualification at this university or any other institution, this has been clearly stated.
- Where I have consulted the published work of others, this is always clearly attributed.
- Where I have quoted from the work of others, the source is always given. This thesis is entirely my own work, with the exception of such quotations.
- I have acknowledged all major sources of assistance.
- Where the thesis is based on work done by myself jointly with others, I have made clear exactly what was done by others and what I have contributed myself.

Date: 05.01.2023

---

# Development of Electromagnetic Wave Absorption Properties of Graphene-Based Nanocomposites by Using Stochastic Optimization Methods

## Abstract

Today, with the developing telecommunications and electronic technologies for civilian and military purposes, electromagnetic (EM) applications have a wide usage area, including different frequency ranges, such as radar, wireless information transfer, and medical technologies, as well as radio frequencies. However, the broad use of these technologies causes EM wave pollution, so they have a devastating effect not only on the working functionalities of electronic devices but also on human health. Therefore, the need to develop these technologies to prevent EM wave pollution is increasing daily. In line with this need, numerous studies have been recently conducted to develop EM interference (EMI) shielding composite materials. Generally, it is aimed to achieve maximum absorption performance with minimum reflection to develop EMI shielding composites. On the other hand, the increase in the number of parameters affecting the performance of these materials also increases the time and cost required for experimental studies. In this case, mathematical and statistical approaches play a crucial role in contributing to experimental studies to reduce time and cost.

In this thesis study, it is intended to develop a graphene foam/MnO<sub>2</sub> nanowire composite structure as an EMI shielding material in order to apply a comprehensive design-modeling-optimization study to the field of materials science. In line with this aim, hydrothermal process parameters (temperature, time, molar ratio) were determined as the design variables of the optimization problem, and the effects of these parameters on the EMI shielding effectiveness (SE) of the nanocomposite structure were investigated. Moreover, the objective of the problem was defined as maximizing the absorption effectiveness of nanocomposite while conserving minimum reflection effectiveness. Data modeling processes were performed via a nonlinear neuro-regression approach to achieve a robust objective function for the defined optimization problem. In the optimization stage of this study, four different stochastic optimization algorithms (Simulated Annealing, Differential Evolution, Nelder-Mead, Random Search) were utilized simultaneously to obtain global optima. It is envisaged that this thesis study would make big contributions to the design-based optimization studies in the materials science subject.

**Keywords:** graphene-based nanocomposite, electromagnetic interference shielding, materials design, neuro-regression approach, stochastic optimization

# Grafen Tabanlı Nanokompozitlerin Elektromanyetik Dalga Soğurma Özelliklerinin Stokastik Optimizasyon Yöntemleri Kullanılarak Geliştirilmesi

## ÖZ

Günümüzde, sivil ve askeri amaçlarla kullanılmak üzere geliştirilmekte olan haberleşme ve elektronik teknolojileri ile birlikte elektromanyetik (EM) uygulamalar, radyo frekanslarının yanı sıra mikrodalga, radar, kablosuz bilgi transferi ve tıbbi teknolojiler gibi farklı frekans aralıklarını içeren geniş bir kullanım alanına sahiptir. Söz konusu teknolojilerin yaygın kullanımı EM dalga kirliliğine yol açarak, elektronik cihazların kullanım fonksiyonlarının yanı sıra insan sağlığı üzerinde de olumsuz etkilere sahiptir. Bundan dolayı, EM dalga kirliliğinin engellenmesine yönelik teknolojilere duyulan ihtiyaç gün geçtikçe artmaktadır. Bu ihtiyaç doğrultusunda son yıllarda EM girişim koruyucu kompozit malzemelerin geliştirilmesine yönelik birçok çalışma yapılmaktadır. EM girişim koruyucu kompozit malzemelerin geliştirilmesi için genel olarak minimum yansıtma ile maksimum soğurma performansının elde edilmesi amaçlanmaktadır. Öte yandan, bu malzemelerin söz konusu performansını etkileyen parametre sayılarındaki artış, deneysel çalışmalar için gerekli olan zaman ve maliyeti de artırmaktadır. Bu durumda, matematiksel ve istatistiksel yaklaşımlar, zaman ve maliyeti azaltmak için deneysel çalışmalara katkıda bulunma konusunda büyük bir rol oynamaktadır.

Bu tez çalışmasında, kapsamlı bir tasarım-modelleme-optimizasyon çalışmasının malzeme bilimi alanına uygulanması adına EM girişim koruyucu malzeme olarak grafen köpük/MnO<sub>2</sub> nanotel kompozit yapısının geliştirilmesi amaçlanmıştır. Bu amaç doğrultusunda, hidrotermal üretim parametreleri (sıcaklık, zaman, molar oran), optimizasyon probleminin tasarım değişkenleri olarak belirlenmiş ve bu parametrelerin nanokompozit yapının EM girişim koruma özelliği üzerindeki etkileri incelenmiştir. Ek olarak, optimizasyon probleminin amacı, nanokompozit yapıdan minimum yansıtma etkinliğini korurken maksimum soğurma etkinliği elde etmek olarak belirlenmiştir. Tanımlanan optimizasyon problemi için yüksek tahmin kabiliyetine sahip bir amaç fonksiyonu elde etmek adına lineer olmayan nöro-regresyon yaklaşımı ile veri modelleme süreçleri gerçekleştirilmiştir. Çalışmanın optimizasyon aşamasında, global optimum değerlerini elde etmek için dört farklı stokastik optimizasyon algoritması (Simulated Annealing, Differential Evolution, Nelder-Mead, Random Search) eş zamanlı olarak kullanılmıştır. Bu tez çalışmasının, malzeme bilimi ve mühendisliği alanında gerçekleştirilecek tasarım tabanlı optimizasyon çalışmalarına büyük katkılar sağlayacağı öngörülmektedir.

**Anahtar Kelimeler:** grafen tabanlı nanokompozitler, elektromanyetik girişim koruma, malzeme tasarımı, nöro-regresyon yaklaşımı, stokastik optimizasyon

# Acknowledgment

First of all, I would like to express my gratitude for my advisors, Assoc. Prof. Dr. Fethullah Güneş and Assoc. Prof. Dr. Levent Aydın, for their guidance and supports during my graduate studies.

I would like to thank Prof. Dr. Merih Palandöken, Assoc. Prof. Dr. Mustafa Erol, and Assist. Prof. Dr. Ahmet Aykaç for their supports. I wish to express my gratitudes also for Evren Egesoy due to his support and friendship.

I'm also very thankful for The Scientific and Technological Research Council of Turkey (TÜBİTAK) – Science Fellowships and Grand Programmes Department (BİDEB) because I was funded within the scope of '2210/C National MSc/MA Scholarship Program in the Priority Fields in Science and Technology' during the term 2021/1. Moreover, I would like to thank İzmir Kâtip Çelebi University-Scientific Research Projects Unit for their financial support to this thesis study through projects with numbers 2021-GAP-MÜMF-0042 and 2022-TYL-FEBE-0018.

Besides, I would like to express my deepest appreciation to Melih Savran, Hande Parlak, Dr. Hazal Gergeroğlu, İpek Yoldaş, and Gülsüm Ersü for their invaluable support and friendships during my MSc studies.

I'm extremely grateful to my dear close friends, Arın Gürsel and İbrahim Gözütok, for their mental support and their solid friendship.

Apart from being my academic co-advisor, I also would like to specially thank Levent Aydın for his moral support and encouragement during my educational journey since my undergraduate education, as well as for his contributions to my view of life.

Of course, any acknowledgement section could not be thought without thanking Gülperi Feyza Yavuz. I could not have undertaken this journey without her. So, words cannot express my gratitude to Gülperi Feyza Yavuz.



Finally, the most special thanks go to my dear family members, Serpil Aydın, Gürbüz Aydın, and Oğuzhan Yılmaz Aydın, for their endless love and support throughout my life in every aspect.

*Kemal Bartu Aydın*

# Table of Contents

Declaration of Authorship.....	ii
Abstract .....	iii
Öz .....	v
Acknowledgment .....	vii
List of Figures .....	xii
List of Tables.....	xiii
List of Abbreviations.....	xv
<b>1 Introduction.....</b>	<b>1</b>
1.1 Literature Survey .....	1
1.2 Motivation .....	7
<b>2 Mathematical Background.....</b>	<b>9</b>
2.1 Design of Experiments (DoE) .....	9
2.1.1 Randomized Complete Block Design .....	10
2.1.2 Full Factorial Design.....	11
2.1.3 Fractional Factorial Design.....	11
2.1.4 Central Composite Design .....	12
2.1.5 Box-Behnken Design .....	12
2.1.6 Taguchi Design .....	12
2.1.7 Latin Hypercube Design .....	13
2.1.8 Optimal Design (D-Optimal) .....	13

2.2	Mathematical Modeling .....	14
2.2.1	Neuro-Regression Approach.....	15
2.2.2	Nonlinear Regression Analysis .....	15
2.3	Optimization.....	17
2.3.1	Simulated Annealing.....	19
2.3.2	Differential Evolution .....	20
2.3.3	Nelder-Mead .....	21
2.3.4	Random Search .....	23
2.4	Mathematica and Optimization .....	24
2.4.1	Random Search .....	25
2.4.2	Simulated Annealing.....	29
2.4.3	Differential Evolution .....	33
2.4.4	Nelder-Mead .....	34
2.4.5	NMaximize & NMinimize .....	36
<b>3</b>	<b>Preliminary Studies.....</b>	<b>38</b>
3.1	Stochastic Optimization of TiO <sub>2</sub> -Graphene Nanocomposite by Using Neuro-Regression Approach for Maximum Photocatalytic Degradation Rate .....	38
3.2	Modeling and Optimum Design of CNT/PVA Hybrid Nanofibers as EMI Shielding Material .....	43
3.2.1	Modeling Results .....	44
3.2.2	Optimization Results.....	48
<b>4</b>	<b>Results and Discussions .....</b>	<b>55</b>

4.1	Problem Definition .....	55
4.2	Modeling Results.....	57
4.3	Optimization Results .....	62
<b>5</b>	<b>Conclusion.....</b>	<b>68</b>
	<b>References .....</b>	<b>70</b>
	<b>Appendices .....</b>	<b>81</b>
	<b>Appendix A .....</b>	<b>82</b>
	<b>Appendix B .....</b>	<b>89</b>
	<b>Curriculum Vitae .....</b>	<b>90</b>

# List of Figures

Figure 1.1: Schematic representation of this thesis study.....	8
Figure 2.1: Flow diagram showing the steps of an optimal design process.....	9
Figure 2.2: SA Algorithm's Flowchart.....	20
Figure 2.3: DE Algorithm's Flowchart.....	21
Figure 2.4: NM Algorithm's Flowchart.....	22
Figure 2.5: RS Algorithm's Flowchart.....	23
Figure 2.6: Optimization procedure in Mathematica Software.....	25
Figure 2.7: The DE algorithm flowchart.....	33
Figure 3.1: 3D plots representations of the $SE_R$ (left) and $SE_A$ (right) functions depending on CNTs content (C) and frequency (F). Gray, yellow, blue, orange, and green surfaces indicate in which cases the thickness (T) values at 1, 1.5, 2, 2.5, and 3 mm, respectively.....	48
Figure 4.1: 3D plots representations of the $SE_R$ (left) and $SE_A$ (right) functions depending on temperature and time at certain concentration values. Green and orange surfaces indicate in which cases the concentration values at 0.07 and 0.2 M/M, respectively.....	62

# List of Tables

Table 2.1: Optimization types, algorithms, and relevant commands.....	24
Table 3.1: Dataset used through the study.....	40
Table 3.2: Accuracy check results of the attained model.....	41
Table 3.3: Optimization problem results (in continuous search space).....	42
Table 3.4: Optimization problem results (in integer search space).....	42
Table 3.5. Result comparison with the reference article.....	43
Table 3.6: All input and their corresponding output values classified as training and testing.....	44
Table 3.7: Types of multiple regression models used in the study.....	45
Table 3.8: Accuracy check results of obtained models for the $SE_R$ output in terms of $R^2$ values and boundedness check.....	46
Table 3.9: Accuracy check results of obtained models for the $SE_A$ output in terms of $R^2$ values and boundedness check.....	47
Table 3.10: Models determined as objective functions of defined optimization problems.....	47
Table 3.11: Optimization problem scenarios for $SE_R$ output and their results.....	49
Table 3.12: Optimization problem scenarios for $SE_A$ output and their results.....	52
Table 4.1: All inputs and their corresponding output values.....	56
Table 4.2: General representation of multiple logarithmic regression models.....	57

Table 4.3: Accuracy check results of obtained models for the $SE_R$ output in terms of $R^2$ values and boundedness check.....	58
Table 4.4: Accuracy check results of obtained models for the $SE_A$ output in terms of $R^2$ values and boundedness check.....	59
Table 4.5: Accuracy results of obtained hybrid models for each objective function.	61
Table 4.6: Optimization problem scenarios for $SE_R$ output and their results. ....	63
Table 4.7: Optimization problem scenarios for $SE_A$ output and their results. ....	65

# List of Abbreviations

GF	Graphene Foam
GF/MnO <sub>2</sub>	Graphene Foam/Manganese Dioxide
CNT	Carbon Nanotube
EM	Electromagnetic
EMI	Electromagnetic Interference
SE	Shielding Effectiveness
SE <sub>T</sub>	Total Shielding Effectiveness
SE <sub>A</sub>	Shielding Absorption Effectiveness
SE <sub>R</sub>	Shielding Reflection Effectiveness
RAM	Radar Absorbing Material
SA	Simulated Annealing
DE	Differential Evolution
NM	Nelder-Mead
RS	Random Search
DoE	Design of Experiment



# Chapter 1

## Introduction

### 1.1 Literature Survey

The electromagnetic (EM) wave absorption phenomenon recently had a great interest due to the need to decrease EM wave pollution from ever-growing electronic technologies used for several purposes. The detrimental effect of EM waves is known as EM interference (EMI) which is influential on human health in addition to the working of electronic devices. [1]. The EMI shielding term corresponds to a barrier for radio or microwave radiations to prevent their penetration [2]. Therefore, there is a high study interest in developing materials to enhance EMI shielding effectiveness (SE).

EM waves interact with materials mainly through reflection and absorption [3-5]. The EM wave reflection occurs on the material's surface because the charge carriers interact with the EM field. At the same time, absorption happens when electrical or magnetic dipoles interact with the EM field in the radiation. Additionally, absorbed EM waves by the medium are turned into thermal energy. Both of them are dependent on the electrical conductivity of the material. Another interaction of EM waves with the materials is multiple internal reflections that end up with the EM wave absorption by scattering at various interfaces within the material [5]. Moreover, the SE is attributed to the power loss realized by the EM radiation interaction with the material [2]. The total SE ( $SE_T$ ) involves mainly two interaction ways as absorption effectiveness ( $SE_A$ ) and reflection effectiveness ( $SE_R$ ). In addition, SE arising from the multiple internal reflections ( $SE_M$ ) is another mechanism, which is negligible when

$SE_T$  is greater than 15 dB. The  $SE_T$  interaction mechanism relationship can be represented by the following equations [2]:

$$SE_T = -10 \log_{10} |S_{21}|^2 \quad (1.1)$$

$$SE_R = -10 \log_{10}(1 - |S_{11}|^2) \quad (1.2)$$

$$SE_T = SE_A + SE_R + SE_M \quad (1.3)$$

$$SE_T = SE_A + SE_R \quad (\text{when } SE_T > 15 \text{ dB}) \quad (1.4)$$

In the related equations, the square of scattering parameters (S-parameters),  $|S_{11}|^2$  and  $|S_{21}|^2$ , denote the reflection and transmission coefficient, respectively, which should be considered as the fraction of the input powers during calculations instead of the dB unit [2]. The relevant S-parameters are obtained from the measurement via network analyzer instrument in a specific frequency bandwidth.

As seen from the abovementioned equations, both absorption and reflection of EM waves are directly proportional to the material's  $SE_T$ . Thus, improving both  $SE_R$  and  $SE_A$  mechanisms is a way to increase the  $SE_T$  of materials. However, the reflection is undesirable because it causes secondary EM pollution. Likewise, in the defense industry, the absorption capability is significant for stealth technology to prevent EM waves reflected from the target structure from reaching the receiving antenna by reducing the radar cross-section (RCS) [6, 7]. Therefore, absorption-dominant shielding materials must be developed, with the minimum  $SE_R$  as far as possible, for effective EMI SE characteristics.

In general, absorbing materials used to reduce unwanted EM waves should meet the properties such as lightness, low density, resistance to corrosion and high absorption in a wide frequency bandwidth [6, 8]. In addition, radar-absorbing materials (RAMs) with high thermal conductivity are desirable in stealth technology to prevent the target structure from being detected by thermal sensors due to the conversion of EM waves absorbed by the medium into thermal energy [6]. However, traditionally used materials

such as magnetic metal particles (e.g., iron, cobalt), ferrite and carbonyl iron powders are insufficient to provide high performance by meeting desirable features alone because of their disadvantages such as low stability, high density and low corrosion resistance [9-11]. Therefore, studies to develop absorber and shielding materials have recently focused on carbon-based nanomaterials such as carbon nanotubes (CNT) and graphene, which have properties such as low density, high corrosion resistance and high strength [6, 8, 10, 12]. Among these nanomaterials, graphene, presented to the literature for the first time in 2004, is a material consisting of one or more layers of graphite formed by  $sp^2$  hybridization of carbon atoms in a honeycomb-shaped hexagonal crystal lattice [13]. Graphene is preferred in many fields due to its high electron mobility, large surface area, and high electrical and thermal conductivity, and also frequently studied as an EM wave absorber material [8, 10, 14-17].

Furthermore, graphene is generally preferred in foam structures to meet the requirements of EMI shielding materials. Graphene foam (GF) provides a continuous network of flawless graphene sheets with high electrical conductivity without the formation of junction resistance [18]. In addition, GF has a high porosity of approximately 99.7%, making it an ideal material for use as a supporting surface compatible with other materials by creating synergistic effects [19]. There are sorts of production methods reported in the literature for graphene synthesis, which can be classified into two main approaches, bottom-up and top-down. Top-down methods such as chemical exfoliation, micromechanical separation and liquid phase exfoliation, in which graphite is used as a raw material, suffer from obtaining low-quality graphene, containing toxic chemical components, and therefore are unsuitable for commercial use [20]. On the contrary, the chemical vapor deposition (CVD) method is a bottom-up approach suitable for industrial applications due to its cost-effectiveness, high-quality, large surface area, and continuous graphene structure production. [17, 21-26]. However, graphene-derived structures are designed as EM wave absorber and EMI shielding materials mostly contain graphene oxide (GO) and reduced graphene oxide (rGO) foams [12, 27-29]. The fact that GO and rGO have low-quality limits their EM wave absorption property. On the contrary, CVD-based GF has significant potential as a shielding material with high electrical conductivity owing to its high quality. In addition to the advantages of graphene, its high electrical conductivity causes an impedance mismatch between the structure and free space.

Therefore, the desired performance cannot be achieved when graphene is used alone as shielding material [30]. To overcome the impedance mismatch, graphene can be combined with nanomaterials such as zinc oxide (ZnO), magnetite ( $\text{Fe}_3\text{O}_4$ ), and manganese dioxide ( $\text{MnO}_2$ ) by designing as hybrid structures to obtain the desired EM wave absorption characteristics [13, 30-33].

$\text{MnO}_2$  is one of the most common-used metal oxides in several applications, such as energy storage and photocatalytic applications, due to its high surface area, environment friendliness, natural abundance, and low cost [34-39]. The basic unit of  $\text{MnO}_2$  is formed by an octahedral close-packed structure ( $\text{MnO}_6$ ). Accordingly, several crystallographic derivatives (e.g.,  $\delta$ ,  $\beta$ , and  $\alpha$ ) of  $\text{MnO}_2$  can be achieved by linking octahedral units differently [40-42]. In general, there are some methods to synthesize  $\text{MnO}_2$  nanostructures, such as electrochemical synthesis, hydrothermal, and sol-gel methods [43-45]. Among these techniques, hydrothermal is a cost-effective method that allows simple nanostructure synthesis in low temperatures. Moreover, the most effective crystal and morphologic structure for the relevant applications can be achieved by controlling hydrothermal process parameters (e.g., temperature, time, and solution concentration).  $\text{MnO}_2$  is also an ideal candidate to be used as an EM wave absorber owing to its functionality offers a choice to optimize the absorption characteristic through materials design since its features differ depending on both its morphological and crystallographic forms. For example, in the study by Song et al., the EM wave absorption performance of different morphological and crystalline phases of  $\text{MnO}_2$  nanomaterials ( $\alpha$ - $\text{MnO}_2$  nanowire,  $\alpha$ - $\text{MnO}_2$  microsphere,  $\delta$ - $\text{MnO}_2$  nanowires,  $\delta$ - $\text{MnO}_2$  microspheres) were compared [45]. It is found that the  $\alpha$ - $\text{MnO}_2$  has a higher dipolar moment than other phases, and the best EM wave absorption was achieved from the  $\alpha$ - $\text{MnO}_2$  nanowire. The high performance of the nanowire form was attributed to its high surface area and having more trapping sites for the EM wave. However, because  $\text{MnO}_2$  nanostructures are insufficient to meet the requirement of absorbers alone, they are combined widely with suitable materials, such as graphene, to obtain an effective EM wave absorption performance [46-49]. By keeping the abovementioned considerations of the relevant materials in mind, this thesis study is focused on developing the CVD-based graphene foam/ $\text{MnO}_2$  nanowire (GF/ $\text{MnO}_2$  NW) composite structure as an effective EMI shielding materials.

Furthermore, materials' EMI SE capability depends on several variables, such as the incident wave frequency, thickness of the structure, and the amount and size of the material included in the structure [50-52]. The increase in the number of variables in such engineering problems leads to a rise in the raw material consumption, time, and cost required for the experimental process. Hence, obtaining the interactions between the variables required to achieve the desired performance by experimental methods becomes challenging. A systematic mathematical optimization approach considering the applications' requirements can help to overcome this problem. Therefore, obtaining a robust objective function for the specified problem is crucial in accurately defining the physical phenomenon. At this point, data science plays a big role in materials science. Therefore, data-driven modeling approaches have been frequently utilized by researchers recently to design, develop, and discover new materials [53-55]. In the literature, there are great efforts to develop a method to achieve a robust model to estimate the phenomenon realistically and reliably. Therefore, statistical and mathematical-based approaches such as artificial neural networks (ANN), response surface methodology (RSM), and regression analysis (RA) have been used for the design of EM wave absorbers [56-63]. These methods are utilized to attain a function that includes the correlation between parameters and probable outcomes of experiments. For example, in the study by Nasouri et al., a carbon nanotube/polyvinyl alcohol (CNT/PVA) hybrid nanofiber structure is used as EMI shield material [64]. The effects of CNT concentration ( $x_1$ ), structure thickness ( $x_2$ ), and EM wave frequency ( $x_3$ ) on the EMI properties of the structure were examined. It is stated that the RSM is used to model and optimize the EM wave absorption and reflection properties of the hybrid nanofiber structure. Thus, they obtained two objective functions by expressing the absorption and reflection properties of the structure with quadratic polynomial functions depending on  $x_1$ ,  $x_2$ , and  $x_3$ . It is reported that the structure will show maximum EM wave absorption performance with minimum EM wave reflection when the design variables  $x_1$ ,  $x_2$ , and  $x_3$  have 7.7 wt.%, 3 mm and 12 GHz values, respectively.

Salah et al. used the ANN to predict the EM wave absorption property of the polycarbonate/CNT (PC/CNT) composite structure depending on different weight percentages of carbon nanotube [65]. According to the outputs of the method used in the study, it has been estimated that the PC/CNT composite structure containing 5

wt.% CNT concentration will reach the best EM wave absorption index. In another study by Green et al., a data-driven approach was used to build a predictive model to achieve an optimum microwave absorption performance of polypyrrole/paraffin composite [66]. The objective of the problem is designated to minimize reflection loss (RL) (or to maximize the absolute value of RL) with maximum bandwidth corresponding to the band where RL is smaller than -10 dB. Moreover, the effects of parameters such as polypyrrole content, structure thickness, complex features of the material, and frequency were investigated. As a result, it is reported that -62.6 dB of RL and 7.7 GHz of bandwidth are achieved for the relevant structure.

In the study by Toktas et al., a multi-objective problem, including surrogate modeling, was defined to design a multi-layer radar absorber by considering each layer's material type and thickness [67]. The outputs were determined to minimize the total reflection and all structure thickness. Furthermore, the absorber was designed through multiple radar bandwidths (0.2-2, 2-8, 8-12, 12-18, and 2-18 GHz). The obtained optimum design was reported for each bandwidth in order as the total reflection and thickness values of -27.83 dB and 3.38 mm, -22.31 dB and 2.13 mm, -25.24 dB and 1.11 mm, -25.47 dB and 1.0426 mm, and -18.88 dB and 2.69 mm.

On the other hand, inadequate approaches are encountered when the relevant methods preferred in literature studies are examined. Firstly, current data modeling approaches are based on considering one or two different regression model types with the accuracy step by checking  $R^2$  values only. Nevertheless, achieving a high  $R^2$  value is unsuitable for complex engineering problems. Therefore, different regression model forms must be considered to define the relevant phenomenon realistically. Another shortcoming is that the current methods cannot provide a boundedness check for the candidate models. However, whether the candidate models are limited to the parameter intervals of the considered phenomenon should be checked. To overcome these problems, in previous studies, a comprehensive mathematical approach has been reported to enable reliable predictions by using the neuro-regression analysis, a systematic combination of RA and ANN methods [68-72].

## 1.2 Motivation

CVD-based GF has a high potential to be used as EMI shielding material since it provides a large surfaced 3D network of high-quality graphene. Moreover, it is an ideal candidate to be used as a template in the hydrothermal method to synthesize  $\text{MnO}_2$  nanostructures for various applications. However, there is a very limited study concerning the hydrothermal process parameters' effect on the EMI shielding effectiveness through the characteristics of the  $\text{MnO}_2$  nanostructure on the CVD-based GF. Therefore, it would be very insightful to understand the interaction of the structural forms of  $\text{MnO}_2$  nanomaterials growth on the GF with hydrothermal process parameters in order to achieve the most effective properties for the EMI shielding.

For the above-stated reasons, this thesis study intends to conduct a design-based optimization procedure considering the nanocomposite structure of GF/ $\text{MnO}_2$  NW as EMI shielding material. In line with this purpose, hydrothermal process parameters' effects on the nanocomposite material's EM wave absorption and reflection effectiveness characteristics are examined. First, the mathematical optimization problem is defined considering design variables (time, temperature,  $\text{KMnO}_4/\text{HCl}$  molar ratio) and objective functions ( $\text{SE}_R$  and  $\text{SE}_A$  of material). Then, the obtained data is modeled by a multiple nonlinear neuro-regression approach to achieve robust objective functions for the optimization problem. In this step, several regression model types (linear, trigonometric, polynomial, logarithmic, exponential, and their rational and hybrid forms) are considered to attain an objective function that defines the phenomenon accurately and realistically. Accordingly, four-distinct direct search optimization algorithms (Simulated Annealing, Nelder-Mead, Differential Evolution, Random Search), which have a different fundamental basis from each other, were performed simultaneously to offer an optimum design. Figure 1.1 represents the general procedure steps of this thesis study schematically.

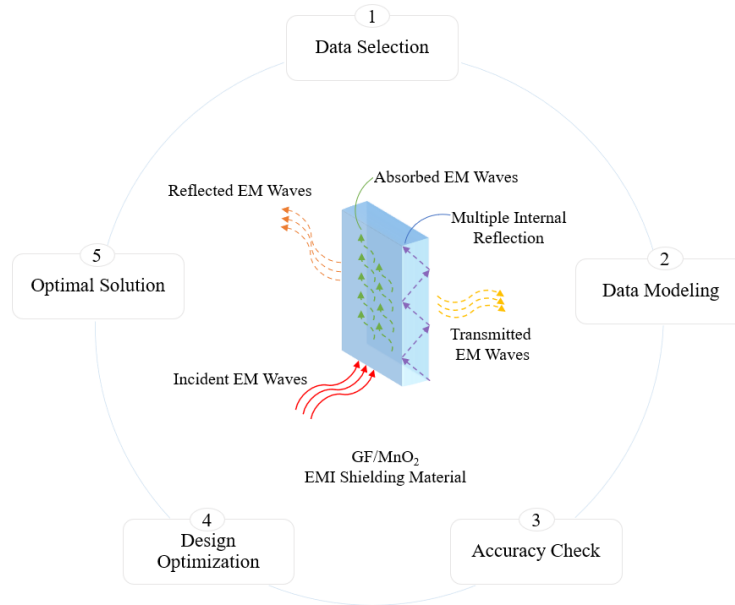


Figure 1.1: Schematic representation of this thesis study.

Furthermore, in the literature, there have been numerous recent studies on the materials informatics field implementing data-driven approaches to design and develop materials with minimum time and costs. However, as mentioned before, the current methods have some deficiencies, and more effort is needed to develop a systematic perspective to predict the relevant properties of materials during the design process. Therefore, the motivation of this thesis is based on presenting a systematic approach for materials modeling and optimization through statistical and mathematical basis by considering graphene-based nanocomposite as a case study. This method would allow the materials used in the relevant fields to be designed and optimized to have desired performance. Furthermore, the proposed method has a high potential to meet the fundamentals of materials science within the scope of processing-structure-properties-performance relationships. In this respect, it is practicable for not only the EMI shielding materials but also the modeling-design-optimization processes of any materials science-concerned subject.



# Chapter 2

## Mathematical Background

In this chapter, it is introduced the background of mathematical instruments used throughout the thesis. The main goal of this chapter is to briefly explain the processes for design-based optimization in engineering through the methods used in this study. In this regard, the design of experiments, mathematical modeling, and optimization processes are presented. Figure 2.1 displays all these steps for an optimal design process. Furthermore, optimization processes in Mathematica software, which is the tool utilized to perform mathematical procedures in this study, are mentioned.

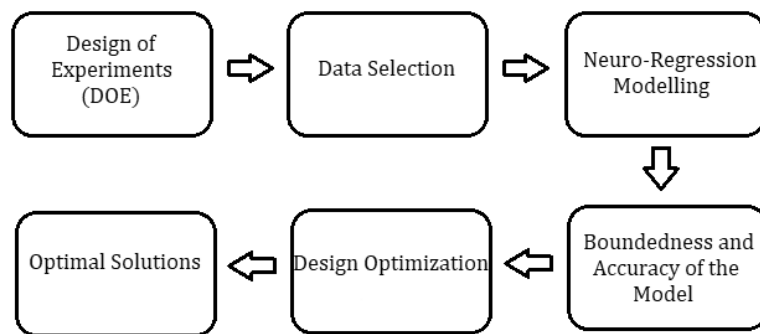


Figure 2.1: Flow diagram showing the steps of an optimal design process.

### 2.1 Design of Experiments (DoE)

In manufacturing processes, experiments are conducted to increase our knowledge and understanding of them. Hence, the correlations between the main factors of the inputs and the output behaviors can be observed [73, 74]. One of the most popular strategies in engineering is One-Variable-At-a-Time (OVAT). In this method, one parameter is

changed at a time, with all others kept constant in all experiments. However, this method may give a misleading conclusion to processes, making the results unreliable and wasteful. Furthermore, it is known that not all parameters have an equal effect on the outcomes. Hence, an elaborate design aims to identify the effect level of process parameters on the output [73, 75, 76]. If multiple factors influence a given characteristic of a component, then the best option is design of experiments (DoE) [73, 74, 77]. DoE is a useful technique for discovering new processes, gaining a deep insight into existing processes, and optimizing their performance. This method ensures high efficiency and more consistent process results by saving time and cost.

It is vital to decide on the most appropriate statistical tools to analyze data since the results can be affected by noise to a considerable extent. Replication, randomization, and blocking are the core principles of statistical approaches in DoE. Replication is based on repeating experimental runs to attain more precise results and decrease experimental error. Randomization process designates a random order for the experiments to be performed. The purpose of blocking is to isolate a known systematic bias impact and to prevent the major effects from vagueness [73, 75]. The determination of the proper DoE method depends on the objectives of experiments and the number of factors to be addressed. The remaining part of this section presents a list and brief explanation of some DoE methods, which are Randomized Complete Block Design, Full Factorial, Fractional Factorial, Central Composite, Box-Behnken, Taguchi, Latin Hypercube, and D-Optimal Design [75]. It should be noted that the techniques presented here do not comprise a complete list since it is aimed to acquaint the readers with the topic by presenting the approaches widely used in practice.

### 2.1.1 Randomized Complete Block Design

There is no strict limitation on the distribution of treatment for experimental constituents. However, there are practical situations in which the data obtained from experiments varies considerably. In such cases, the design made in relation is referred to as a Randomized Complete Block Design (RCBD). The chief purpose of blocking is the minimization of variability between experimental units within a block and the maximization of variation between blocks.

### *Advantages*

- Removing the treatments or replicates from the analysis is possible.
- Some multiple treatments can be more often replicated than others.
- The number of treatments or replicates is not strictly restricted.
- There can be valid comparisons, although the experimental error is not homogeneous [73, 78].

### *Disadvantages*

- A smaller error on  $df$  exists for a small number of treatments.
- It is possible to acquire a substantial error term if there are too many treatments and considerable variations between experimental units.

RCBD is not good at experimental efficiency when data deficiency exists.

## 2.1.2 Full Factorial Design

Factorial designs at two or three levels are generally recognized as the most often employed DoE method in manufacturing industries and can enable obtaining consistent results on the effect of the variables. Factorial designs can be divided into as full and fractional factorials. Full factorial design is an approach that identifies the experimental runs by combining each factor setting with every other one. If the concerned response is affected by five or more factors, full factorial design needs a substantial number of runs and is not very useful. In such circumstances, the fractional factorial design can be preferable [73, 74].

## 2.1.3 Fractional Factorial Design

In practice, time and funding are mostly insufficient to carry out experiments via full factorial design. However, in case of some higher-order correlations are not indispensable, the main influences and two-order interactions can be obtained by utilizing a fraction of the full factorial experiment to decrease the time and cost of the experiments. Fractional factorial design is a type of orthogonal array layout that allows

researchers to investigate the most important and necessary impacts of relationships with a minimum number of workouts or experimental runs [73, 74, 78, 79].

#### 2.1.4 Central Composite Design

Central composite design (CCD), which generates a factorial design, is one of the most common response surface designs and is conducted with five factorial levels. Checking the corner points is one of the most important advantages of CCD. Accordingly, if the curvature is inconsiderable, then it is accomplished. On the other hand, the main task is to create the star runs if the curvature is significant [77].

#### 2.1.5 Box-Behnken Design

Box-Behnken design is a popular DoE technique compatible with using three factorial levels. This approach is based on the midpoints instead of the cube edge corner points, resulting in fewer runs. However, apart from CCD, all runs must also be done in Box-Behnken. Furthermore, it is superior in which cases the curvature specified in the screening experiment is likely necessary [73].

#### 2.1.6 Taguchi Design

Taguchi design is a statistical method which helps to enhance engineering efficiency significantly. The main goal of the Taguchi method is to maintain the output fluctuation at the minimum even in the noise existence. Therefore, this approach helps to ensure product quality by considering the noise factors and the error amount. Furthermore, Taguchi design focuses on improving the primary function of the design process, and thereby flexible designs can be presented [73, 78].

##### *Advantages*

- It is easily adaptable to various engineering problems, which enables it to be a robust tool.
- It improves the product quality, within some qualification constraints, by considering a mean production feature value comparable to the final one rather than just a value.

- It enables to examine the several variables without an impractically large number of runs.

#### *Disadvantages*

- Obtained results are comparative and do not determine which parameter has the most significant effect on the desired feature accurately.
- It cannot be used to figure out interactions of all variables because orthogonal arrays only analyze some parameter combinations.
- Parameter interactions are hard to be considered.

It is offline, so that inconvenient for procedures having dynamic changes as in computer simulations.

### 2.1.7 Latin Hypercube Design

This approach is a method which creates a near-random sample of parameter values from Multidimensional Distribution. Furthermore, Latin Hypercube design is a generalization of the Latin Square concept to an arbitrary number of dimensions. In this method, the first step is to determine how many sample points are to be addressed and along which row and column the sample point was utilized for each. Besides, this approach ensures a set of random numbers representing the actual fluctuation, while standard random sampling is only a set of random numbers without assurance [73-75].

### 2.1.8 Optimal Design (D-Optimal)

D-Optimal is a computer-aided design containing the best part of entire possible experiments. The final design may differ depending on the tool employed so software tools may possess different processes to create D-Optimal designs [73, 79]. Selection method generates the best design based on a predetermined factor and the number of runs. D-Optimal design approach is very useful in which cases that traditional design methods are not used. These cases are:

- When supplies of factor configurations are restrained.
- If the number of experimental runs must be reduced.

- When using the operation and mixing variables in the same design.
- When previously performed experiments must be comprised.
- If the experimental region is unstable [73, 76, 77].

## 2.2 Mathematical Modeling

Mathematical modeling plays a key role in design-based engineering optimization studies to obtain a robust objective function for the problem. Therefore, selecting an appropriate data modeling methodology is important to define the considered phenomenon accurately. In this manner, researchers employ various modeling methodologies such as Regression Analysis, Response Surface Methodology (RSM), Finite Difference Technique (FDT), and Artificial Neural Networks (ANN). Nevertheless, studies preferred popular methods regarding engineering optimization have some inadequate approaches, as follows:

- (i) It is not a satisfying description of updating one input while maintaining the others constant because this approach causes to neglect the nonlinear impact of input variables. So, it is necessary to consider the interactions between all experimental and constructional parameters in terms of optimization perspective.
- (ii) Most data modeling methods include utilizing one or two traditional regression models as an objective function for the problem. Accordingly, the model's reliability is checked by calculating  $R^2$  values, which indicate the proximity of the fitted model results to the experimental data. However, achieving a high  $R^2$  value does not always mean a good fit for the engineering systems. Furthermore, since the model describes only the experimental data rather than the fundamental behavior of the phenomenon, different regression model types and approaches should be considered.
- (iii) Another critical point is to consider the boundedness of the model function. All the engineering parameters are known as finite, so the function should be bounded to model the engineering systems realistically. Hence, the proposed model should be checked to determine whether it is limited to the parameter intervals of the respective phenomenon.

(iv) Although it is vital to unveil the inherent behaviors of the stochastic search processes, some studies on engineering systems optimization do not consider the reliability, sensitivity, and robustness of the algorithms.

In order to overcome the abovementioned deficiencies of the most widely used modeling and optimization approaches, it has been stated in the literature that it is possible to perform realistic engineering design optimization studies [68, 70]. Therefore, with the optimization process including the simultaneous use of four distinct direct search algorithms, a multiple nonlinear neuro-regression analysis is introduced to present a comprehensive aspect of the modeling-design-optimization processes.

### 2.2.1 Neuro-Regression Approach

Neuro-regression approach is a hybrid data modeling technique that draws on the advantages of regression analysis and Artificial Neural Network (ANN) to enhance prediction accuracy. At the beginning of this approach, all data is split randomly into two sets of 80% and 20% to be used as training and testing, respectively. The goal of the training step is to minimize the error between the experimental and predicted values by specifying the regression models and their coefficients. Accordingly, testing data are used to obtain the estimated results by minimizing the effects of regression model inconsistencies, and this step gives an understanding of the candidate models' prediction capability.  $R^2$  values of the models are achieved in the training and testing steps. As a final phase of the approach, appropriate models in terms of  $R^2$  values are subjected to a boundedness check. In this regard, the boundary of the candidate models is determined as the minimum and maximum values in the given interval for each design variable. This step is crucial to confirm whether the models are meaningful regarding the considered problem. As a result, chosen models are expected to meet each criterion required for robustness.

### 2.2.2 Nonlinear Regression Analysis

Models which are not linear in their parameter are known as nonlinear regression models. They can be utilized for three distinct purposes [80]:

- To test the validity of the model (or compare the hypothesis),
- To characterize the model (i.e., prediction of parameters),
- To estimate the behavior of the system (interpolation and calibration).

The nonlinear regression model can be written in general form as follows:

$$y = f(x, \beta) + \varepsilon \quad (2.1)$$

where  $x$ ,  $\beta$ , and  $\varepsilon$  are vector of  $p$  predictors, a vector of  $k$  parameters, and an error term, respectively.  $f(-)$  represents a known regression function.

For nonlinear regression, mathematical modeling processes can be conducted systematically considering the main properties as follows:

- Since the function does not need to be linear or linearizable, nonlinear regression offers more flexibility than linear regression. Hence, the nonlinear regression ensures a variety of choices to match the data.
- In cases where the  $f$  function can be linearized, nonlinear regression may be more applicable than transformations and linear regression.
- Nonlinear regression necessitates a knowledge of the  $f$  function (e.g., polynomial, trigonometric, exponential), which requires a comprehensive insight into the studied process. However, linear regression models are appropriate for process forecasts in which the relationship between input and output parameters is roughly certain, but precise clarity is not required.

Functionally generalized states cannot be written because nonlinear regression models involve the most general mathematical terms. However, some fundamental model types utilized in engineering fields are given as examples of nonlinear equations as follows:

$$y = a_0 + a_1x + a_2x^2 + \dots + a_nx^n \quad (2.2)$$

$$y = a_0 + a_1e^x + a_2e^{x^2} + \dots + a_n e^{x^n} \quad (2.3)$$



$$y = a_0 + a_1 \sin x + a_2 \sin x^2 + \dots + a_n \sin x^n \quad (2.4)$$

$$y = \frac{a_0 + a_1 x + a_2 x^2 + \dots + a_n x^n}{b_0 + b_1 x + b_2 x^2 + \dots + b_n x^n} \quad (2.5)$$

Furthermore, multivariable states having multiple inputs of the abovementioned model types can be constructed with a similar approach. Another pertinent point is that special functions (e.g., Bessel, Laguerre, Lambert, Gamma), as well as different combinations of traditional functions, can be chosen with a deeper understanding of mathematical functions.

## 2.3 Optimization

In engineering, optimization can be defined as obtaining an optimum design by maximizing or minimizing predetermined objective(s) to meet the considered problem requirements. The objective of an engineering problem can be expressed as a function dependent on design variables. Furthermore, optimization problems are defined as single- or multi-objective approaches. Single-objective optimization problems, including an objective function, design variables, and constraints, can be mathematically expressed as follows:

$$\text{minimize/maximize} \quad f(\theta_1, \theta_2, \dots, \theta_n)$$

$$\text{constraints} \quad g_i(\theta_1, \theta_2, \dots, \theta_n) \leq 0 \quad i = 1, 2, \dots, m$$

$$h_j(\theta_1, \theta_2, \dots, \theta_n) = 0 \quad j = 1, 2, \dots, p$$

$$\theta^L \leq \theta_1, \theta_2, \dots, \theta_n \leq \theta^U$$

where  $f$  is an objective function dependent on the design variables which are  $\theta_1, \theta_2, \dots, \theta_n$ , and both  $g$  and  $h$  represent the constraints of the problem.  $\theta^L$  and  $\theta^U$  indicates the lower and upper bounds of design variables.

On the other hand, modern engineering design and optimization problems often need to deal with conflicting multiple objectives to be minimized and/or maximized [81]. Therefore, multi-objective optimization approaches are used in these cases, and Pareto

optimal solution sets are obtained. However, in a multi-objective optimization approach, it is not possible to find an optimum solution for all objectives; hence, only one solution from the solution set is chosen for engineering applications in practice [82, 83]. A multi-objective optimization problem can be mathematically expressed as follows:

$$\begin{aligned}
 \text{minimize/maximize} \quad & f_1(\theta_1, \theta_2, \dots, \theta_n), f_2(\theta_1, \theta_2, \dots, \theta_n), \dots, f_t(\theta_1, \theta_2, \dots, \theta_n) \\
 \text{constraints} \quad & g_i(\theta_1, \theta_2, \dots, \theta_n) \leq 0 \quad i = 1, 2, \dots, m \\
 & h_j(\theta_1, \theta_2, \dots, \theta_n) = 0 \quad j = 1, 2, \dots, p \\
 & \theta^L \leq \theta_1, \theta_2, \dots, \theta_n \leq \theta^U
 \end{aligned}$$

where  $f_1, f_2, \dots, f_t$  indicate objective functions of the relevant optimization problem [84]. In addition, penalty function formulation rather than the classical multi-objective optimization approach may be more suitable in some cases to benefit from its advantage of converting constrained problems into unconstrained ones [82].

Furthermore, optimization algorithms are mainly divided into traditional (deterministic) and non-traditional (stochastic) methods. Traditional optimization approaches, such as Lagrange multipliers, are analytical methods [70, 81]. Therefore, they give optimum solutions based on exact input values for only continuous and differentiable functions. However, one of the most prevalent issues in applied mathematics is finding an optimal solution approximately for a function defined on a subset of finite-dimensional space. Combinatorial optimization problems, essential for most machine learning approaches, have objective functions to be optimized to attain an optimal solution approximation. With the advance of computer technology, stochastic optimization approaches have come to the forefront in several areas, such as engineering, science, and statistics, as solid tools to meet the requirements of modern optimization problems. Stochastic optimization is a process grounded on minimizing or maximizing a statistical or mathematical function when multiple input parameters depend on random variables. The randomness can be either Monte Carlo randomness or noise in measurements in the search procedure or both [84-86]. Unlike traditional methods, stochastic optimization algorithms ensure approximate rather than exact solutions. Additionally, because stochastic optimization techniques include

probability, their simultaneous utilization in a problem increases the reliability of results.

The following subsections include a brief overview of Simulated Annealing (SA), Differential Evolution (DE), Nelder-Mead (NM), and Random Search (RS), which are optimization algorithms used in this study.

### 2.3.1 Simulated Annealing

Simulated Annealing (SA) algorithm is one of the most effective stochastic optimization methods and is based on an analogy of the annealing process. An annealing process can be defined as increasing a solid's temperature to a certain level and then decreasing it to obtain a low-energy state of a solid. At the maximum temperature, all crystal molecules are shifted randomly into a liquid phase. Then, the melted crystal is cooled to a certain level (e.g., room temperature). A crystal structure with optimum stability is achieved when the cooling process is appropriately conducted. Otherwise, defects and instabilities in the structure occur if the cooling process is carried out rapidly. In the optimization perspective, the solid's states correspond to probable solutions of optimization problems, while the energy states of the solid represent objective function values of solutions [87].

SA algorithm is inspired by achieving a low-energy state of a solid in the analogy and is quite useful to obtain the global optimum of a function. This method can ensure the global optimum with a substantial number of independent variables. Furthermore, this algorithm is utilized to find the minimum value of a function in mixed-integer, discrete, or continuous optimization problems. SA method is based on using a random search regarding Markov Chain, which keeps some non-ideal changes in addition to accepting changes that develop the objective function. Figure 2.2 shows a flowchart representing the steps of the SA algorithm. In this process, a new point is created randomly, and the algorithm ends when any stopping criteria are met. The distance between the new and current point is based on Boltzmann Probability Distribution with a scale proportionally to the temperature. Boltzmann Probability Distribution can be defined as follows [85, 88-90]:

$$P(E) = e^{-E/kT} \quad (2.6)$$

where  $k$ ,  $T$ , and  $P(E)$  denote Boltzmann constant, temperature, and the probability of achieving the energy level ( $E$ ), respectively.

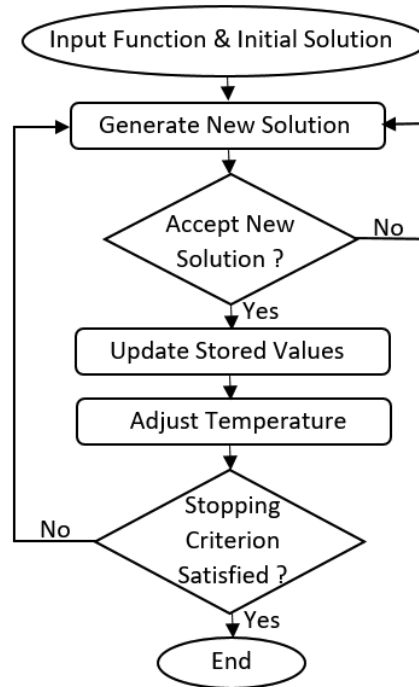


Figure 2.2: SA Algorithm's Flowchart [88].

### 2.3.2 Differential Evolution

Differential Evolution (DE) is one of the most efficient real-parameter optimization algorithms for problems in continuous domains [91]. The DE algorithm consists of four main steps: selection, crossover, mutation, and initialization. Furthermore, this algorithm has three real control parameters: differentiation/mutation constant, crossover constant, and population size. The DE technique's performance depends on the target and difference vector manipulation to attain a trial vector. Other control parameters of this algorithm are: i) problem dimension that scales the case difficulty, ii) boundary constraints, and iii) the maximum number of generations known as a

stopping condition [85, 90]. Figure 2.3 shows a flowchart of the process of this algorithm.

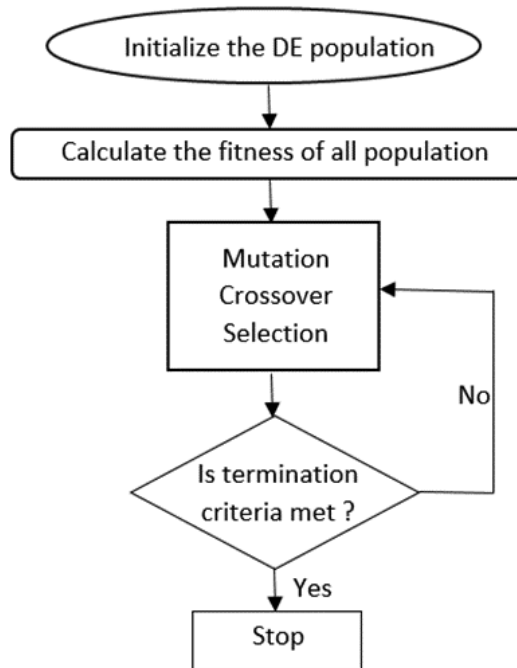


Figure 2.3: DE Algorithm's Flowchart

Besides, the DE method is a population-based algorithm based on the mutation operation as a primary search mechanism. This operation relies on the differences between randomly sampled pairs of solutions. Although the DE algorithm is numerically uneconomical, it is powerful enough to achieve a global optimum and to maintain the local minimum regardless of initial points [92-94].

### 2.3.3 Nelder-Mead

Nelder-Mead (NM) is a simplex search algorithm designed for unconstrained optimization problems by Nelder and Mead at first [95]. NM is a traditional local search rather than a global optimization algorithm; however, it works quite well for optimization problems with few local minima in practical applications. The NM algorithm possesses four main control option procedures: reflection, expansion,

contraction, and shrinkage. Furthermore, the NM algorithm often gives significant enhancements in the first few iterations characteristically and creates good results quickly. Additionally, this algorithm typically requires only one or two function evaluations per iteration, except for shrink transformations, which are highly unusual in practice. Therefore, this feature makes the NM algorithm significant in such cases that each function evaluation is expensive or time-wasting. The NM algorithm has high flexibility to discover difficult domains since the simplex can alter its shape, orientation, and size to adjust to the objective function's local contour [96]. Figure 2.4 displays a flowchart showing the steps of the NM algorithm process.

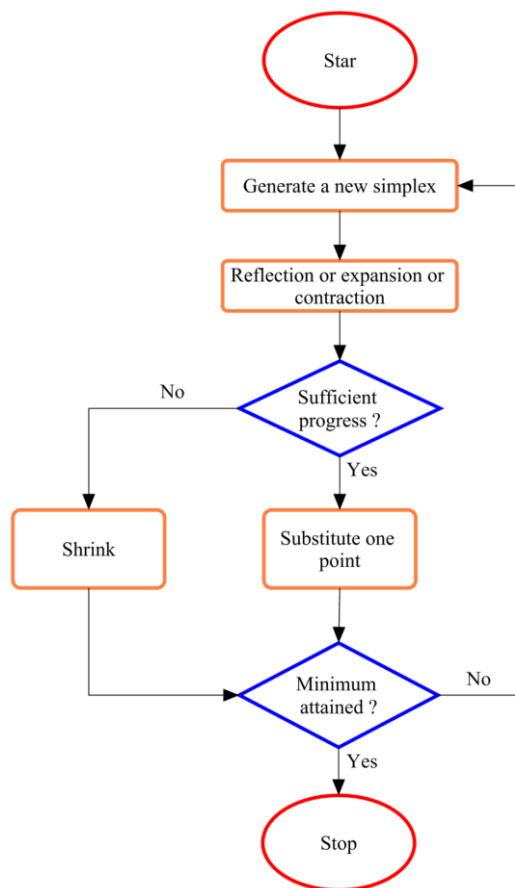


Figure 2.4: NM Algorithm's Flowchart

### 2.3.4 Random Search

Random Search (RS) is a stochastic algorithm which may also be known as the Monte Carlo method. Since the RS algorithm is based on randomness or probability to provide asymptotic convergence, it completely differs from deterministic optimization techniques such as interval analysis, tunnelling methods, and branch and bound [97-99]. Within the stochastic process, a set of methods and programs based on a pseudo-number creator are available. Obtained values should be scaled and converted to approach any desired distribution. Moreover, the RS technique is frequently preferred because it ensures the solution quickly and easily, which is an important feature of computational effort. One of the most prominent advantages of the RS algorithm is that it is useful for complex optimization problems in cases being nonconvex, nondifferentiable, and discontinuous over a continuous, discrete, or continuous-discrete domain. Therefore, the RS algorithm is known as robust in terms of achieving beneficial information quickly for complex problems [82, 100]. Figure 2.5 represents the flowchart of the RS algorithm followed through the thesis.

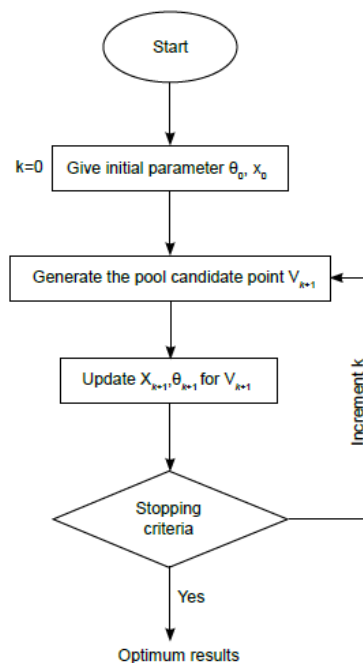


Figure 2.5: RS Algorithm's Flowchart

## 2.4 Mathematica and Optimization

Wolfram Mathematica is a solid technical computing software allowing to study of various fields, such as data science, machine learning, symbolic computation, and optimization. It has commands group work for exact-numeric optimization to solve linear-nonlinear and constrained-unconstrained problems [101]. In this regard, commands, *Minimize* and *Maximize* are used only in exact global optimization, while *NMinimize* and *NMaximize* commands are proper for numeric global optimization. Additionally, the *FindMinimum* command is utilized to conduct numeric local optimization. Table 2.1 and Figure 2.6 present in detail which commands and algorithms are used for what kind of problem.

Table 2.1: Optimization types, algorithms, and relevant commands [102].

Types	Algorithms	Mathematica Commands
Numerical Local Optimization	- Linear Programming Methods (LPM) - Nonlinear Interior Point Algorithms	<i>FindMinimum</i> <i>FindMaximum</i>
Numerical Global Optimization	- LPM - SA - DE - NM - RS	<i>NMinimize</i> <i>NMaximize</i>
Exact Global Optimization	- LPM - Cylindrical Algebraic Decomposition - Lagrange Multipliers - Integer Linear Programming	<i>Minimize</i> <i>Maximize</i>
Linear Optimization	- Linear Programming Methods (simplex, revised simplex, interior point)	<i>Linear Programming</i>



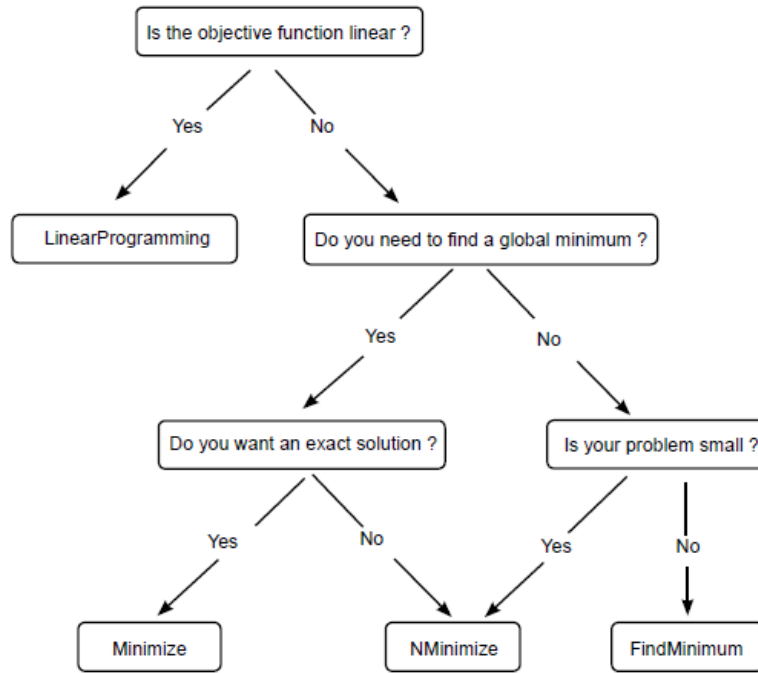


Figure 2.6: Optimization procedure in Mathematica Software [101].

### 2.4.1 Random Search

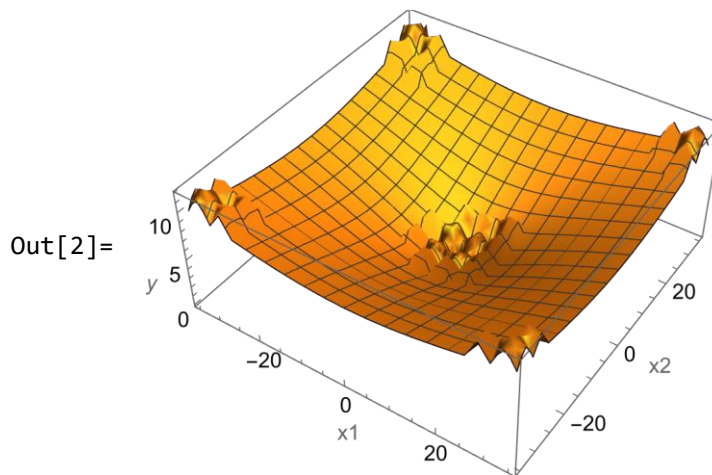
The RS algorithm embedded in Mathematica consists of population involving random starting points. Accordingly, the starting points' convergence behavior to the local minimum is evaluated using the *FindMinimum* local search method. The following options occur during the process:

- (i) The starting points number as per the “min(10 f,100)” expression is determined by *SearchPoints* (where f denotes the variable number),
- (ii) The starting value for the random number generator is arranged by *RandomSeed*,
- (iii) Method is used to identify by which method to be employed for minimizing the objective function by *FindMinimum*. The *FindMinimum* command employs the Quasi-Newton as a search approach for unconstrained problems, which does not need the computation of the second derivatives (Hessian matrix); rather, the Hessian is updated by examining successive gradient vectors. In the constrained problem case, the *FindMinimum* command uses the non-linear interior point as the search method,
- (iv) *PostProcess* option can be chosen as Karush-Kuhn-Tucker (KKT) conditions or *FindMinimum*. Finally, the best local minimum is determined as the solution.

In the RS algorithm, the options *InitialPoints*, *Method*, *PenaltyFunction*, *PostProcess*, and *SearchPoints* are controlled automatically by Mathematica, and proper values are chosen according to the optimization problems [101].

Separable and non-separable multimodal test functions having multiple local minima are used to evaluate the performance capacity of the RS algorithm in achieving the global optimum. In case of an algorithm is not designed properly, this kind of global optimization problem becomes quite hard. So, it can be inserted into local minima without finding the global minima, or not all global minima can be found. In this regard, the first chosen test function is Ackley which has global minima at  $f(0,0) = 0$  [102]. The Mathematica syntax for the definition of Ackley function with its 3D plot in an interval is given as follows:

```
In[1]:= f[x1_,x2_] := -20Exp[(-0.02Sqrt[0.5(x1^2+x2^2)])]
-Exp[(0.5(Cos[2Pix1]+Cos[2Pix2]))]+20+Exp[1];
In[2]= Plot3D[f[x1,x2],{x1,-35,35},{x2,-35,35},
AxesLabel->{x1,x2,y}]
```



It should be noted that the *RandomSearch* command may fail to identify a global minimum if its options are not changed.

```
In[3]:= NMinimize[{f[x1,x2],-35<=x1<=35,-35<=x2<=35},
{x1,x2},Method->"RandomSearch"]
Out[3]= {2.83635, {x1->-5.99749,x2->8.99623}}
```

Sometimes altering the search point option, which defines the point number to start searches, can be an effective move in achieving a global minimum.

```
In[4]:= Do[Print[NMinimize[{f[x1,x2],-35≤x1≤35,-35≤x2≤35},
{x1,x2},Method->{"RandomSearch","SearchPoints"->i}],
{i,500,3000,500}]
{0.39531,{x1->0.996345,x2->0.996345}}
{0.280127,{x1->-5.04225*10^-24,x2->-0.9948}}
{0.280127,{x1->-5.04225*10^-24,x2->-0.9948}}
{0.280127,{x1->-5.04225*10^-24,x2->-0.9948}}
{0.280127,{x1->-5.04225*10^-24,x2->-0.9948}}
{1.2012*10^-9,{x1->-8.42728*10^-10,x2->-4.16243*10^-9}}
```

The *RandomSeed* option effect is examined below. In the previous example, the “*SearchPoints*→500” is insufficient to reach the global optimum. Therefore, in the following case, a global minimum can be attained by adjusting the values of the *RandomSeed* and *SearchPoints* to 5 and 500, respectively.

```
In[5]:= Do[Print[NMinimize[{f[x1,x2],-35≤x1≤35,-35≤x2≤35},
{x1,x2},Method->{"RandomSearch","SearchPoints"->500,
"RandomSeed"->i}],{i,5}]
{0.280127,{x1->-7.38323*10^-25,x2->0.9948}}
{7.40815*10^-10,{x1->6.89861*10^-10,
x2->-2.52669*10^-9}}
{0.280127,{x1->5.59478*10^-24,x2->0.9948}}
{0.39531,{x1->0.996345,x2->0.996345}}
{1.37499*10^-9,{x1->-3.64123*10^-9,
x2->-3.22083*10^-9}}
```

Herein, points are generated on a grid to use as initial points. If the problem’s approximate solution range can be predicted, the solution is achieved more easily when designating a starting point.

```
In[6]:= Print[NMinimize[{f[x1,x2],-35≤x1≤35,-35≤x2≤35},
{x1,x2},Method->{"RandomSearch","InitialPoints"-
>Flatten[Table[{i,j},{i,-35,35,5},{j,-35,35,5}],1}]]]
Out[6]= {-4.44089*10^-16,{x1->-1.52703*10^-15,
x2->-1.52703*10^-15}}
```

Since the *PostProcess* methods (KKT option) and *FindMinimum* give the same results, the *PostProcess* option does not have primary importance for this problem.

```

In[7]:= Print[NMinimize[{f[x1,x2], -35≤x1≤35, -35≤x2≤35},
{x1,x2},Method->{"RandomSearch", "SearchPoints"->3000,
"PostProcess"->KKT}]]
Out[7]= {1.2012*10^-9, {x1->-8.42726*10^-10,
x2->-4.16243*10^-9}}
In[8]:= Print[NMinimize[{f[x1,x2], -35≤x1≤35, -35≤x2≤35},
{x1,x2},Method->{"RandomSearch", "SearchPoints"->3000,
"PostProcess"->FindMinimum}]]
Out[8]= {1.2012*10^-9, {x1->-8.42728*10^-10,
x2->-4.16243*10^-9}}

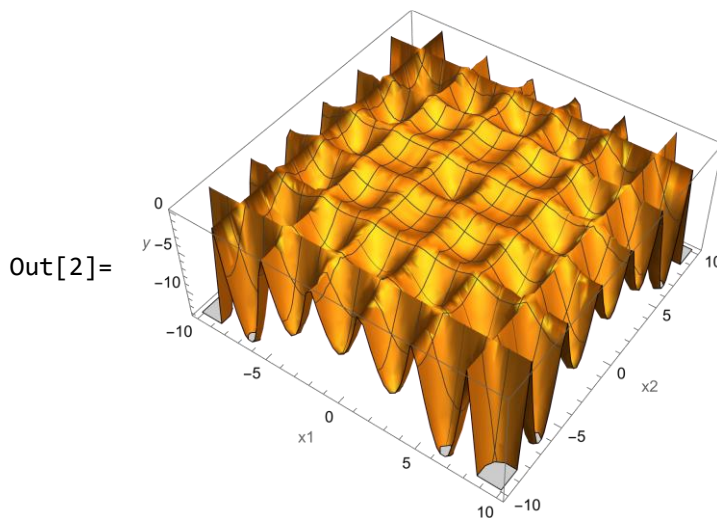
```

Another test function, “Holder Table 1”, which is separable and multimodal, is used to assess the *RandomSearch* command’s capability in obtaining the global minimum [102]. The test function has global optima at  $f(\pm 9.646168, \pm 9.646168) = -26.920336$ . The definition of “Holder Table 1” function and its 3D plot is performed in Mathematica syntax as follows:

```

Clear[f];
In[9]:= f[x1_,x2_] := -Abs[Cos[x1]Cos[x2]Exp
[Abs[1 - ((x1^2+x2^2)^0.5)/Pi]]];
In[10]:= Plot3D[f[x1,x2], {x1, -10, 10}, {x2, -10, 10}]

```



The RS algorithm attains one of the global minimum points without changing its options for this problem.

```

In[11]:= NMinimize[{f[x1,x2],-10<=x1<=10,-10<=x2<=10},
{x1,x2},Method->"RandomSearch"]
Out[11]= {-26.9203, {x1 -> -9.64617, x2 -> -9.64617}}
In[12]:= Do[Print[NMinimize[{f[x1,x2],-10<=x1<=10,-10<=x2<=10},
{x1,x2},Method->{"RandomSearch", "RandomSeed"->i}],
{i,{1,6,7}}]
{-26.9203, {x1->-9.64617, x2->9.64617}}
{-26.9203, {x1->-9.64617, x2->-9.64617}}
{-26.9203, {x1->9.64617, x2->9.64617}}

```

## 2.4.2 Simulated Annealing

In the Simulated Annealing algorithm embedded in Mathematica software, the working process involves that the startup solution, “Z”, which is generated first. Then, “Z<sub>new</sub>” is produced in the neighborhood of the “Z” point, and then “Z<sub>best</sub>” is identified. If  $f(Z_{new}) \leq f(Z_{best})$ , Z<sub>new</sub> substitutes Z<sub>best</sub> and Z. Otherwise, it replaces with Z. *InitialPoints*, *SearchPoints*, and *RandomSeed* options in this loop can determine the initial guess, its number, and starting value, respectively.

In the SA algorithm, random movements in the search space based on the Boltzmann probability distribution,  $e^{D(k,\Delta f,f_0)}$ , where D, k, and  $\Delta f$  denotes the function defined by *BoltzmannExponent*, current iteration, and change in the objective function, respectively. Mathematica software defines D automatically as  $\frac{\Delta f \log(k+1)}{10}$  by *BoltzmannExponent*.

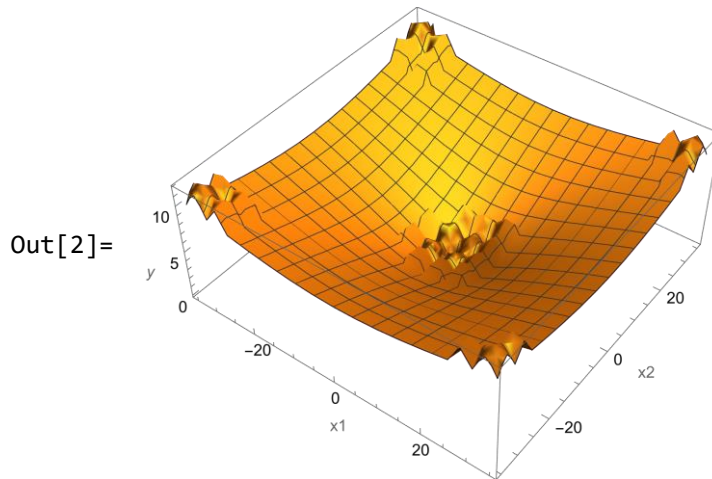
For all starting points, the SA algorithm process is returned by the time either the algorithm converges to a point or remains at the same point due to the iteration number appointed by the *LevelIterations* [103].

“Ackley” and “Holder Table 1” functions are utilized to assess the SimulatedAnnealing command’s performance in achieving the global minimum.

```

In[1]:= f[x1_,x2_]:= -20 Exp[(-0.02 Sqrt[0.5 (x1^2+x2^2)])]-
Exp[(0.5 (Cos[2 Pi x1]+Cos[2 Pi x2]))]+20+Exp[1];
In[2]= Plot3D[f[x1,x2],{x1,-35,35},{x2,-35,35},
AxesLabel->{x1,x2,y}]

```



The SA algorithm may not obtain a global minimum by using the default options.

```
In[3]:= NMinimize[{f[x1,x2], -35<=x1<=35, -35<=x2<=35},
  {x1,x2},Method->{"SimulatedAnnealing"}]
Out[3]= {2.37578, {x1 -> 7.99584, x2 -> 3.99792}}
```

The *BoltzmannExponent* is a substantial command that presents the way to attain a global minimum since it involves a function that determines a new point at iteration. The found result can be altered if this function is used without a default value. In the following case, however, altering this option alone has not been sufficient to obtain the global minimum.

```
In[4]:= NMinimize[{f[x1,x2], -35<=x1<=35, -35<=x2<=35}, {x1,x2},
  Method->{"SimulatedAnnealing", "BoltzmannExponent"
  ->Function[{i,df,f0},-df/(Exp[i/10])]}]
Out[4]= {0.830095, {x1 -> -2.99495, x2 -> 6.41153*10^-9}}
```

Furthermore, even though the *PerturbationScale* changes the result, altering this option alone has still not been enough to attain the global minimum.

```
In[5]:= Do[Print[NMinimize[{f[x1, x2], -35 ≤ x1 ≤ 35, -35 ≤ x2
≤ 35}, {x1, x2}, Method -> {"SimulatedAnnealing",
"PerturbationScale" -> i}]], {i, 15}]
{2.37578, {x1->7.99584, x2->3.99792}}
{2.40345, {x1->0.999488, x2->8.99539}}
{1.0993, {x1->-1.04986*10^-9, x2->3.99502}}
{3.8527, {x1->-1.99944, x2->14.9958}}
{6.15308, {x1->-23.9966, x2->-9.9986}}
{4.50046, {x1->14.9966, x2->-9.99773}}
{4.26698, {x1->11.9971, x2->-11.9971}}
{4.27353, {x1->7.99805, x2->-14.9963}}
{2.63697, {x1->5.99725, x2->-7.99634}}
{6.15308, {x1->-23.9966, x2->-9.9986}}
{6.15308, {x1->-23.9966, x2->-9.9986}}
{6.15308, {x1->-23.9966, x2->-9.9986}}
{6.15308, {x1->-23.9966, x2->-9.9986}}
{6.15308, {x1->-23.9966, x2->-9.9986}}
{6.15308, {x1->-23.9966, x2->-9.9986}}
{6.15308, {x1->-23.9966, x2->-9.9986}}
```

A global minimum can be obtained by using much more *SearchPoints*.

```
In[6]:= Do[Print[NMinimize[{f[x1, x2], -35 ≤ x1 ≤ 35, -35 ≤ x2 ≤ 35},
{x1, x2}, Method -> {"SimulatedAnnealing",
"SearchPoints" -> i}]], {i, 100, 500, 100}]
{0.830095, {x1->-2.99495, x2->7.32049*10^-10}}
{0.62186, {x1->1.99543, x2->-0.997715}}
{0.280127, {x1->-1.64485*10^-9, x2->-0.9948}}
{0.280127, {x1->0.9948, x2->5.25186*10^-12}}
{1.937*10^-9, {x1->-2.31279*10^-9, x2->-6.44598*10^-9}}
```

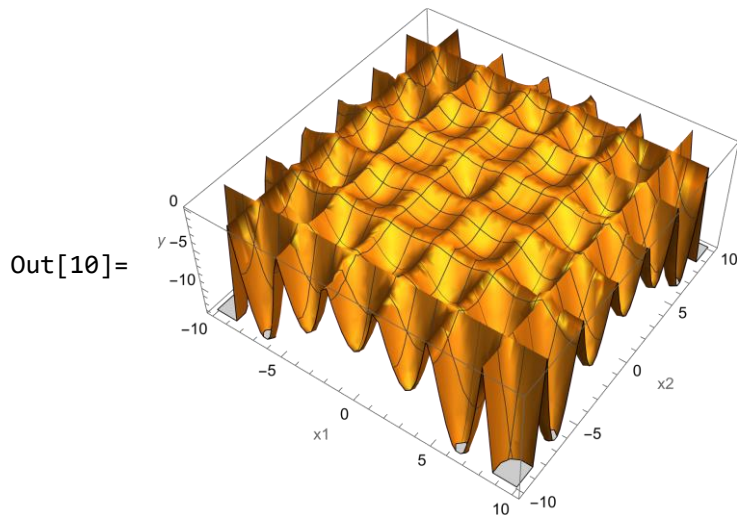
As seen before, although altering the search points alone is adequate to achieve the global optimum, the algorithm obtains the local minima in the case of performing a search utilizing the *PerturbationScale*, *RandomSeed*, and *BoltzmannExponent*.

```
In[7]:= Do[Print[NMinimize[{f[x1, x2], -35 ≤ x1 ≤ 35,
-35 ≤ x2 ≤ 35}, {x1, x2}, Method ->
{"SimulatedAnnealing", "RandomSeed" -> i}]], {i, 0, 10}]
{2.37578, {x1->7.99584, x2->3.99792}}
{0.557056, {x1->-4.99634*10^-9, x2->1.99487}}
{2.15456, {x1->7.99533, x2->-0.999416}}
{0.39531, {x1->0.996345, x2->0.996345}}
{3.46466, {x1->-8.99708, x2->9.99676}}
{0.993567, {x1->2.99583, x2->1.99722}}
{1.58244, {x1->-2.9975, x2->-4.99584}}
{1.22508, {x1->-3.99557, x2->1.99779}}
{1.46596, {x1->1.99819, x2->-4.99546}}
{0.39531, {x1->-0.996345, x2->0.996345}}
{2.29034, {x1->4.99729, x2->6.9962}}
```

```

Clear[f]
In[9]:= f[x1_,x2_] := -Abs[Cos[x1]Cos[x2]
Exp[Abs[1 - ((x1^2+x2^2)^0.5)/Pi]]];
In[10]:= Plot3D[f[x1,x2],{x1,-10,10},{x2,-10,10}]

```



For this problem, the SA algorithm attains one of the global minimum points without changing of its options.

```

In[11]:= NMinimize[{f[x1,x2],-10<=x1<=10,-10<=x2<=10},{x1,x2},
Method->"SimulatedAnnealing"]
Out[11]= {-26.9203, {x1 -> 9.64617, x2 -> 9.64617}}

```

Unlike the RS, four different global minimum points can be achieved by utilizing the SA algorithm.

```

In[12]:= Do[Print[NMinimize[{f[x1,x2],-10<=x1<=10,
-10<=x2<=10},{x1,x2},Method->
{"SimulatedAnnealing","RandomSeed"->i}],
{i,{1,2,3,11}}]
{-26.9203, {x1->9.64617,x2->9.64617}}
{-26.9203, {x1->-9.64617,x2->-9.64617}}
{-26.9203, {x1->-9.64617,x2->9.64617}}
{-26.9203, {x1->9.64617,x2->-9.64617}}

```



### 2.4.3 Differential Evolution

The Differential Evolution algorithm embedded in Mathematica software generates a new population of  $k$  points in iterations. Then, the  $j^{\text{th}}$  new point is generated considering three random points (e.g.,  $z_1$ ,  $z_2$ , and  $z_3$ ) from the population created before. After that, a new formation by  $z_s = z_3 + s(z_1 - z_2)$  is built where  $s$  denotes the real scaling factor. A new point,  $z_{\text{new}}$ , is created from  $z_j$  and  $z_s$  by selecting the  $i^{\text{th}}$  coordinate or another coordinate of  $j^{\text{th}}$  from  $z_s$  with the probability of  $p$ . Then,  $z_{\text{new}}$  substitutes by  $z_j$  if  $h(z_{\text{new}}) < h(z_j)$  [101].

The *DifferentialEvolution* command involves specific arrangement options, *CrossProbability* ( $P$ ), *InitialPoints*, *PenaltyFunction*, *PostProcess*, *RandomSeed*, *ScalingFactor*, *SearchPoints*, and *Tolerance*, even if none of them guarantees to achieve global optima. The DE algorithm process in Mathematica software is illustrated in Figure 2.7 [104].

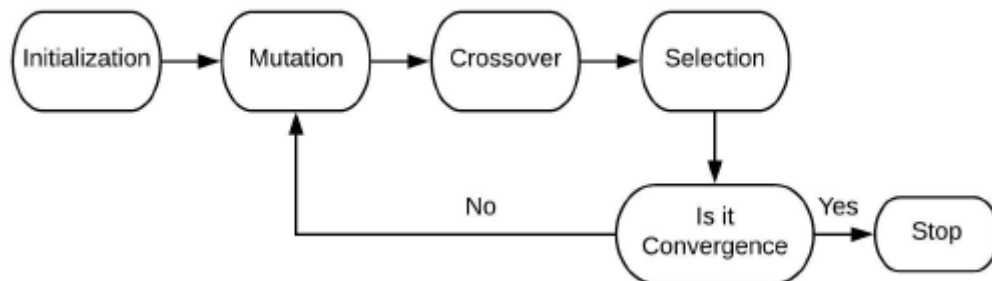


Figure 2.7: The DE algorithm flowchart [104].

To examine the DE algorithm performance, the same test functions are utilized as they were in previous algorithms.

```
In[3]:= NMinimize[{f[x1,x2], -35<=x1<=35, -35<=x2<=35}, {x1,x2},  
Method->"DifferentialEvolution"]  
Out[3]= {2.2587*10^-9, {x1 -> -1.63413*10^-9,  
x2 -> -7.81672*10^-9}}
```

Better results are obtained considering the global optima when the default value of *ScalingFactor* is set from 0.6 to 0.7.

```
In[5]:= NMinimize[{f[x1,x2],-35≤x1≤35,-35≤x2≤35},{x1,x2},  
Method->{"DifferentialEvolution",  
"ScalingFactor"->0.7}]  
Out[5]= {3.74914*10^-10, {x1 -> 8.68579*10^-10,  
x2 -> -1.00129*10^-9}}
```

However, better global optima were not produced by changing *ScalingFactor*, *RandomSeed*, *CrossProbability*, or *SearchPoints*. So, the relevant solvers were kept as default.

Moreover, the global minima of Holder Table 1 were tried to attain by the SA algorithm. The initial steps are same with algorithms used before.

```
In[10]:= NMinimize[{f[x1,x2],-10≤x1≤10,-10≤x2≤10},{x1,x2},-  
Method->"DifferentialEvolution"]  
Out[10]= {-26.9203, {[x1 -> 9.64617, x2 -> -9.64617]}}
```

In this case, any parameters different from their default values attain neither different results nor better global minima.

#### 2.4.4 Nelder-Mead

As other algorithms, the NM algorithm embedded in the Mathematica has certain options allowing flexibility: *ContractRatio*, *ExpandRatio*, *InitialPoints*, *PenaltyFunction*, *PostProcess*, *RandomSeed*, *ReflectRatio*, *ShrinkRatio*, and *Tolerance*. The NM algorithm is capable of working well for the problem with less local minima, although it does not ensure the full specifications that a precise global optimization approach should have. As done for other algorithms, the NM algorithm is utilized to achieve the global optimum for Ackley and Holder Table 1 [101].

```
In[5]:= NMinimize[{f[x1,x2],-35≤x1≤35,-35≤x2≤35},{x1,x2},  
Method->"NelderMead"]  
Out[5]= {0.87404, {x1 -> -0.998405, x2 -> -2.99522}}
```

As can be seen, the first trial outcomes by DE are outperformed, while NM obtains better global optima than RS and SA for Ackley test functions in default mode.

A critical adjustment parameter of the NM algorithm, *RandomSeed*, may influence the performance directly to obtain global minima.

```
In[6]:= Do[Print[NMinimize[{f[x1,x2], -35<=x1<=35, -35<=x2<=35},
{x1,x2},Method->{"NelderMead",
"RandomSeed"->i}],{i,5}]
Out[6]= {0.557056, {x1->8.15872*10^-25, x2->-1.99487}}
{0.280127, {x1->0.9948, x2->-6.32493*10^-9}}
{7.12481, {x1->-20.9977, x2->-22.9975}}
{2.32486*10^-10, {x1->4.63269*10^-10,
x2->-6.78982*10^-10}}
{1.3908, {x1->-4.99519, x2->-0.999038}}
```

Compared with the trial carried out in the default setting, the *RandomSeed* arrangement ensured a better value.

Other helpful options in the NM for adjusting to obtain better results are *ShrinkRatio*, *ContractRatio*, and *ReflectRatio*. Nevertheless, global minima could not be achieved in the following case for the Ackley test function.

```
In[7]:= Do[Print[NMinimize[{f[x1,x2], -35<=x1<=35, -35<=x2<=35},
{x1,x2},Method->{"NelderMead", "ShrinkRatio"->0.95,
"ContractRatio"->0.95, "ReflectRatio"->2,
"RandomSeed"->i}],{i,5}]
Out[7]= {0.39531, {x1->-0.996345, x2->-0.996345}}
{0.783523, {x1->-1.99642, x2->1.99642}}
{7.37952, {x1->-5.99939, x2->-31.9967}}
{0.39531, {x1->-0.996345, x2->0.996345}}
{2.40704*10^-9, {x1->-2.92841*10^-9,
x2->-7.99045*10^-9}}
```

Holder Table 1 function was minimized via command *NMinimize* in default mode as follows:

```
In[12]:= NMinimize[{f[x1,x2], -10<=x1<=10, -10<=x2<=10}, {x1,x2}, -
Method->"NelderMead"]
Out[12]= {-26.9203, {x1 -> 9.64617, x2 -> 9.64617}}
```

As used previously, the first adjustment has been made by the *RandomSeed* to obtain global value.

```
In[13]:= Do[Print[NMinimize[{f[x1,x2],-10<=x1<=10,-10<=x2<=10},
{x1,x2},Method->{"NelderMead",
"RandomSeed"->i}]],{i,5}]
Out[13]= {-26.9203,{x1->-9.64617,x2->-9.64617}}
{-9.13635,{x1->3.24199,x2->-9.71802}}
{-26.9203,{x1->9.64617,x2->-9.64617}}
{-7.76664,{x1->2.08542*10^-8,x2->9.73295}}
{-7.76664,{x1->-7.64705*10^-9,x2->-9.73295}}
```

The results show that the *RandomSeed* was not sufficient to reach minimum value. Therefore, other possible parameters useful to attain global value for the *NelderMead* were utilized.

```
In[14]:= Do[Print[NMinimize[{f[x1,x2],-10<=x1<=10,-10<=x2<=10},
{x1,x2},Method->{"NelderMead", "ShrinkRatio"->0.95,
"ContractRatio"->0.95,"ReflectRatio"->2,
"RandomSeed"->i}]],{i,5}]
Out[14]= {-26.9203,{x1->-9.64617,x2->-9.64617}}
{-26.9203,{x1->-9.64617,x2->-9.64617}}
{-26.9203,{x1->-9.64617,x2->-9.64617}}
{-26.9203,{x1->-9.64617,x2->-9.64617}}
{-26.9203,{x1->-9.64617,x2->-9.64617}}
```

In the relevant case, the adjustment parameters could not ensure a global minimum differing from the obtained values by the default mode.

## 2.4.5 NMaximize & NMinimize

In Mathematica, *NMaximize* and *NMinimize* commands provide users to optimize complex engineering and science problems with their specific characteristics utilizing search algorithms. However, even without constraints and boundary conditions, finding optimum results might be difficult even though *NMaximize* and *NMinimize* methods are solid to find the global optimum. This kind of case can be overcome by optimizing the given functions with distinct initial conditions. The commands are

evaluated using the test functions, Ackley and Holder Table 1, as functions of  $f(x_1, x_2)$  and  $g(x_3, x_4)$ , respectively.

```
In[15]:= NMinimize[{f[x1,x2], -35<=x1<=35, -35<=x2<=35}, {x1,x2}]
Out[15]= {0.8740, {x1->-0.9984, x2->-2.9952}}
In[4]:= NMaximize[{f[x1,x2], -35<=x1<=35, -35<=x2<=35}, {x1,x2}]
Out[4]= {12.3202, {x1->34.5137, x2->34.51377}}
In[7]:= NMinimize[{g[x3,x4], -10<=x3<=10, -10<=x4<=10}, {x3,x4}]
Out[7]= {-26.9203, {x3->9.6461, x4->9.6461}}
In[8]:= NMaximize[{g[x3,x4], -10<=x3<=10, -10<=x4<=10}, {x3,x4}]
Out[8]= {-2.5326x[10]^(-13), {x3->-4.7498, x4->-4.7123}}
```

It can be seen that the global minima and maxima of the Ackley function could be achieved, while they could not be for Holder Table 1 function. Therefore, parameter adjustment or altering the restriction region may be effective in finding global values.

Furthermore, constraints can be defined either in the list form or rational combination of domain options, inequalities, and equalities. For instance, if results require to be obtained in the integer domain, the unknown parameter  $z$  should be indicated as  $z \in \text{Integers}$  in line to restrict the solutions as only integers. Moreover, to begin the optimization process, the *NMinimize* command entails a rectangular starting region which means that all variables of a given function should have a finite upper and lower boundary. Additionally, the *Method* option allows the user to perform other search algorithms types, ensuring a non-automatic solution set as used before in the SA and RS algorithms. Herein, if an objective function and constraints are linear, the default setting is *LinearProgramming* in the solving process. If the objective function's central part is not numerical, and the variables are integer, the DE is the default algorithm. Otherwise, the NM is the search algorithm. However, it can be altered with DE to attain optimum values when the NM provides undesirable solutions [101].

# Chapter 3

## Preliminary Studies

This section aims to demonstrate the applicability of the methodology utilized throughout this thesis in different materials science subjects. Therefore, prestudies worked and published within the scope of this thesis are presented briefly [72, 105].

### 3.1 Stochastic Optimization of TiO<sub>2</sub>-Graphene Nanocomposite by Using Neuro-Regression Approach for Maximum Photocatalytic Degradation Rate

Improvement in photocatalytic activity to design photocatalysts is crucial for applications such as water treatment and air purification. TiO<sub>2</sub> nanomaterials and its hybrid form with graphene have come to the fore recently to achieve the desired performance of photocatalysts.

This study intends to offer an optimum design to synthesize graphene oxide/TiO<sub>2</sub> (GO/TiO<sub>2</sub>) nanocomposite. Parameters of defined optimization problems include process parameters (EtOH/water ratio, hydrothermal reaction time, and GO content) as design variables (input) and the 2-hydroxyterephthalic acid (HTPA) formation rate as an objective function (output). Dataset was obtained from a literature study [106] and data modeling process were modeled by multiple nonlinear neuro-regression approach. In addition, four different optimization algorithms (DE, RS, SA, NM) were utilized in the optimization stage. Problem definition of this study is as follows [105]:

***Find***

$$v, v \in [4.55, 105.00]$$

$$g, g \in [0.06, 1.24]$$

$$t, t \in [0.23, 24.00]$$

***Maximizing***

$$K(v, g, t)$$

***Constraints***

$$\text{Scenario 1} \quad 4.55 \leq v \leq 105.00, 0.06 \leq g \leq 1.24, 0.23 \leq t \leq 24.00$$

$$\text{Scenario 2} \quad 4.55 \leq v \leq 105.00, 0.06 \leq g \leq 1.24, 0.23 \leq t \leq 24.00 \quad \{v, g, t\} \in \text{Integers}$$

***Design variables***

$$v, g, t$$

where  $v$ ,  $g$ , and  $t$  denote EtOH/water ratio, GO content, and reaction time, respectively.  $K$  represents the objective function, HTPA formation rate.

Data modeling process were performed by starting to separate dataset into 75% and 25% for training and testing, respectively. Training data were used to build a model via the multiple nonlinear neuro-regression approach. Accordingly, all testing data were used to test the obtained data. Table 3.1 shows dataset used in this study [106].

Table 3.1: Dataset used through the study [106].

	Run	EtOH/Water (v/v%) v	GO Content (wt.%) g	Reaction Time (h) t	Rate (min <sup>-1</sup> ) K
Training	1	55.00	0.06	12.00	0.27
	2	55.00	0.65	24.00	0.40
	3	105.00	0.65	12.00	0.20
	4	4.55	0.65	12.00	0.22
	5	55.00	1.24	12.00	0.25
	6	55.00	0.65	0.23	0.21
	7	85.00	0.30	5.00	0.27
	8	25.00	0.30	5.00	0.23
	9	55.00	0.65	12.00	0.32
	10	55.00	0.65	12.00	0.29
	11	55.00	0.65	12.00	0.31
	12	55.00	0.65	12.00	0.30
	13	85.00	1.00	19.00	0.28
	14	55.00	0.65	12.00	0.32
	15	25.00	1.00	19.00	0.32
Testing	16	25.00	1.00	5.00	0.23
	17	85.00	0.30	19.00	0.33
	18	55.00	0.65	12.00	0.29
	19	85.00	1.00	5.00	0.18
	20	25.00	0.30	19.00	0.35

The obtained model by the proposed approach to define a function of HTPA formation rate (K) depending on the design variables is given as follows:



$$\begin{aligned}
K = & 0.123727 - 0.00245074v - 0.161525g + 0.00735434t \\
& + 0.0873669 \ln v + 0.0537129 \ln g \\
& + 0.00158895 \ln t
\end{aligned} \tag{3.1}$$

The accuracy of the objective function is represented in Table 3.2.  $R^2$  values for training and testing are 0.99 and 0.96, respectively. Additionally, boundedness check step gives the interval in between 0.1 to 0.42  $\text{min}^{-1}$ . The boundedness check stage was performed in the search space of input values. Therefore, the proposed model gives realistic and meaningful results in accordance with the specified engineering phenomenon.

Table 3.2: Accuracy check results of the attained model

Data	$R^2$	$R^2_{\text{adjusted}}$	Minimum K ( $\text{min}^{-1}$ )	Maximum K ( $\text{min}^{-1}$ )
Training	0.99	0.9293	0.11155	0.417288
Testing	0.96	-		

Tables 3.3 and 3.4 give the suggested optimum design for the maximum HTPA formation rate according to four optimization methods. In the optimization process, the integer and continuous search spaces are considered. Table 3.3 represents the first scenario considering continuous search space so that all input values as real numbers. As the table shows, all algorithms working independently from each other obtain the same K value, 0.42  $\text{min}^{-1}$ . Furthermore, inputs are obtained almost the same from the algorithms.

Table 3.3: Optimization problem results (in continuous search space).

Optimization Algorithms	Design Variables			Formation Rate (K) (min <sup>-1</sup> )
	EtOH/Water Ratio (v/v%)	GO Content (wt.%)	HT Reaction Time (h)	
RS	35.6492	0.332535	24	0.417288
SA	35.6493	0.332537	24	0.417288
DE	35.6493	0.332535	24	0.417288
NM	35.6492	0.332535	24	0.417288

Table 3.4 gives the suggested optimal design considering the integer search space. Unlike the first scenario, the same K values were not obtained. However, very close values, 0.37 min<sup>-1</sup>, were achieved.

Table 3.4: Optimization problem results (in integer search space).

Optimization Algorithms	Design Variables			Formation Rate (K) (min <sup>-1</sup> )
	EtOH/Water Ratio (v/v%)	GO Content (wt.%)	HT Reaction Time (h)	
NM	36	1	24	0.36861
SA	37	1	24	0.368553
DE	36	1	24	0.36861
RS	53	1	24	0.360739

The results of this study with the referenced article are given in Table 3.5 for comparison. The comparison shows that higher values than the results in reference study was achieved.

Table 3.5. Result comparison with the reference article

Study	Design Variables			Formation Rate (K) (min <sup>-1</sup> )
	EtOH/Water Ratio (v/v%)	GO Content (wt.%)	HT Reaction Time (h)	
Reference Study [106]	51.49	0.48	19	0.36
Our study (continuous)	35.65	0.33	24	~ 0.42
Our study (integer)	36	1	24	~ 0.37

### 3.2 Modeling and Optimum Design of CNT/PVA Hybrid Nanofibers as EMI Shielding Material

As mentioned in the introduction section, recent studies have focused on developing absorption-dominant EMI shielding material to eliminate secondary EM wave pollution. Therefore, in this published work, a design-based optimization study on CNT/PVA nanofiber composite structure was performed for high EMI SE with maximum absorption and minimum reflection [72]. Dataset was obtained from a literature study that uses an RSM-based design for the same aim [64]. Data modeling process was performed via multiple nonlinear neuro-regression approach, while the optimization process includes DE, RS, SA, and NM algorithms.

The optimization problem of this study was defined considering multi-walled CNT (MWCNT) content, thickness, and frequency parameters as design variables with the objective functions,  $SE_R$  and  $SE_A$ . Accordingly, the problem is defined as the equivalent single objective approach considering the objective functions. In the modeling, 12 different regression types (linear, quadratic, trigonometric, exponential, and rational forms) were achieved for each objective function to attain the most accurate one for the phenomenon. Besides, six-distinct scenarios were specified for the optimization to evaluate the problem widely. The purpose here is to achieve maximum absorption with minimum  $SE_R$  of the structure. All data is represented as training and testing in Table 3.6.

Table 3.6: All input and their corresponding output values classified as training and testing [64].

	Run	CNTs content, C (wt%)	Thickness, T (mm)	Frequency, F (GHz)	SE <sub>R</sub> (dB)	SE <sub>A</sub> (dB)
Training	1	0	1	12	1.5	2.4
	2	5	2	10	7.0	13.7
	3	2.5	2	10	4.3	7.1
	4	0	1	8	2.1	2.2
	5	10	1	12	10.5	31.4
	6	5	2	10	7.2	14.5
	7	7.5	2	10	10.6	24.1
	8	10	3	8	12.4	35.2
	9	5	2	11	6.6	15.9
	10	5	2	10	7.4	13.7
	11	5	2	10	7.1	14.1
	12	0	3	12	1.1	3.1
	13	10	3	12	10.8	44.7
Testing	14	0	3	8	1.9	2.9
	15	5	1.5	10	7.2	12.1
	16	5	2.5	10	7.3	16.7
	17	5	2	9	7.7	12.2
	18	10	1	8	13.0	26.3

### 3.2.1 Modeling Results

In this section, results of mathematical modeling stage are presented. Table 3.7 show the general representation of multiple regression model types considered through

modeling stage. Different kinds of model types were considered to find the most accurate models.

Table 3.7: Types of multiple regression models used in the study.

Model Name	Nomenclature	Formula
Multiple linear	L	$Y = \sum_{i=1}^3 (a_i x_i) + c$
Multiple linear rational	LR	$Y = \frac{\sum_{i=1}^3 (a_i x_i) + c_1}{\sum_{i=1}^3 (\beta_i x_i) + c_2}$
2 <sup>nd</sup> order multiple nonlinear	SON	$Y = \sum_{j=1}^3 \sum_{i=1}^3 (b_i x_i x_j) + \sum_{i=1}^3 (a_i x_i) + c$
2 <sup>nd</sup> order multiple nonlinear rational	SONR	$Y = \frac{\sum_{j=1}^3 \sum_{i=1}^3 (b_i x_i x_j) + \sum_{i=1}^3 (a_i x_i) + c_1}{\sum_{j=1}^3 \sum_{i=1}^3 (\gamma_i x_i x_j) + \sum_{i=1}^3 (\beta_i x_i)} + c_2$
1 <sup>st</sup> order exponential multiple nonlinear	FOEN	$Y = \sum_{i=1}^3 (a_i e^{x_i}) + c$
1 <sup>st</sup> order exponential multiple nonlinear rational	FOENR	$Y = \frac{\sum_{i=1}^3 (a_i e^{x_i}) + c_1}{\sum_{i=1}^3 (\beta_i e^{x_i})} + c_2$
2 <sup>nd</sup> order exponential multiple nonlinear	SOEN	$Y = \sum_{i=1}^3 (a_i e^{x_i^2}) + c$
2 <sup>nd</sup> order exponential multiple nonlinear rational	SOENR	$Y = \frac{\sum_{i=1}^3 (a_i e^{x_i^2}) + c_1}{\sum_{i=1}^3 (\beta_i e^{x_i^2})} + c_2$
1 <sup>st</sup> order trigonometric multiple nonlinear	FOTN	$Y = \sum_{i=1}^3 (a_i \sin x_i + \mu_i \cos x_i) + c$
1 <sup>st</sup> order trigonometric multiple nonlinear rational	FOTNR	$Y = \frac{\sum_{i=1}^3 (a_i \sin x_i + b_i \cos x_i) + c_1}{\sum_{i=1}^3 (\beta_i \sin x_i + \gamma_i \cos x_i)} + c_2$
2 <sup>nd</sup> order trigonometric multiple nonlinear	SOTN	$Y = \sum_{i=1}^3 (a_i \sin x_i + b_i \cos x_i) + \sum_{i=1}^3 (\beta_i \sin^2 x_i + \gamma_i \cos^2 x_i) + \sum_{i=1}^3 (\mu_i \sin x_i \cos x_i) + \sum_{j=1}^3 \sum_{i=1}^3 (\rho_i \sin x_i \sin x_j) + \sum_{j=1}^3 \sum_{i=1}^3 (\delta_i \cos x_i \cos x_j) + c$
2 <sup>nd</sup> order trigonometric multiple nonlinear rational	SOTNR	$Y = \frac{\sum_{i=1}^3 (a_i \sin x_i + b_i \cos x_i) + \sum_{i=1}^3 (\beta_i \sin^2 x_i + \gamma_i \cos^2 x_i) + \sum_{i=1}^3 (\mu_i \sin x_i \cos x_i) + \sum_{j=1}^3 \sum_{i=1}^3 (\rho_i \sin x_i \sin x_j) + \sum_{j=1}^3 \sum_{i=1}^3 (\delta_i \cos x_i \cos x_j) + c_1}{\sum_{i=1}^3 (h_i \sin x_i + k_i \cos x_i) + \sum_{i=1}^3 (l_i \sin^2 x_i + m_i \cos^2 x_i) + \sum_{i=1}^3 (n_i \sin x_i \cos x_i) + \sum_{j=1}^3 \sum_{i=1}^3 (\theta_i \sin x_i \sin x_j) + c_2}$

Tables 3.8 and 3.9 give the accuracy results of the obtained candidate models regarding  $R^2$  values and boundedness control for outputs  $SE_R$  and  $SE_A$ . Both tables are prepared to compare all models following the accuracy steps. Herein, models are expected to pass each of the steps.

Table 3.8: Accuracy check results of obtained models for the  $SE_R$  output in terms of  $R^2$  values and boundedness check.

Nomenclature*	$R^2_{\text{training}}$	$R^2_{\text{training-adjusted}}$	$AIC_{\text{training}}$	$BIC_{\text{training}}$	$R^2_{\text{testing}}$	Minimum Value (dB)	Maximum Value (dB)
L1	0.99	0.99	39.3453	44.4299	0.98	1.22	12.70
LR1	0.99	0.99	31.0368	36.1213	0.99	1.03	12.64
SON1	0.99	1.00	-	-	0.11	-3.8	17.6
SONR1	0.99	1.00	-	-	-0.71	0.90	25.06
FOEN1	0.91	0.75	81.6794	86.764	0.53	3.83	13.46
FOENR1	0.99	0.99	29.9443	35.0289	-1.92	$-8.62 \times 10^{14}$	$1.41 \times 10^{16}$
SOEN1	0.91	0.77	80.5601	85.6446	0.71	2.17	14.54
SOENR1	0.99	0.99	37.7508	42.8354	-0.0009	$-4.71 \times 10^{11}$	11.08
FOTN1	0.91	2.12	-	-	0.79	2.76	11.88
FOTNR1	0.97	1.36	-	-	0.93	$-6.21 \times 10^8$	46.30
SOTN1	0.99	1.00	-	-	0.04	0.66	12.19
SOTNR1	0.99	1.00	-	-	-4.36	$-1.43 \times 10^{11}$	$9.81 \times 10^{16}$

\* Corresponding functions are available in the appendices of the cited article [72].

Table 3.9: Accuracy check results of obtained models for the  $SE_A$  output in terms of  $R^2$  values and boundedness check.

Nomenclature	$R^2_{\text{training}}$	$R^2_{\text{training-adjusted}}$	$AIC_{\text{training}}$	$BIC_{\text{training}}$	$R^2_{\text{testing}}$	Minimum Value (dB)	Maximum Value (dB)
L2	0.98	0.94	90.1634	95.248	0.86	-3.72	37.26
LR2	0.99	0.99	45.0651	50.1496	0.97	1.69	44.74
SON2	0.99	1.00	-	-	0.79	-4.18	45.36
SONR2	0.99	1.00	-	-	0.65	2.41	50.16
FOEN2	0.92	0.79	106.234	111.318	0.16	9.13	39.42
FOENR2	0.99	0.98	75.6496	80.7342	-1.37	$-8.46 \times 10^{15}$	$9.74 \times 10^{16}$
SOEN2	0.91	0.76	107.778	112.862	0.04	8.73	39.60
SOENR2	0.96	0.90	96.1488	101.233	-0.39	3.1	33.85
FOTN2	0.89	2.49	-	-	0.82	-0.66	37.49
FOTNR2	0.95	1.67	-	-	0.96	2.24	46.48
SOTN2	0.99	1.000	-	-	0.19	-2.28	28.42
SOTNR2	0.99	1.000	-	-	-2.99	$-1.19 \times 10^{17}$	$4.48 \times 10^{16}$

\* Corresponding functions are available in the appendices of the cited article [72].

It is obvious from both Tables 3.8 and 3.9 that it will be made wrong assessment by considering the validity of the models according to  $R^2$  values only because all models have  $R^2$  values very close to 1. However, the point is that the models possessing high  $R^2$  values are incapable of meeting the remainder accuracy stages. Furthermore, Table 3.10 represents the models determined as problems' objective functions as a consequence of evaluating the accuracy steps.

Table 3.10: Models determined as objective functions of defined optimization problems.

Output	Type	Model	$R^2_{\text{training}}$	$R^2_{\text{training-adjusted}}$	$R^2_{\text{testing}}$	Min. (dB)	Max. (dB)
$SE_R$	LR1	$\frac{8733.82 + 4216.07 C - 747.909 T - 255.528 F}{1838.33 + 91.8026 C - 60.0513 T + 138.879 F}$	0.99	0.99	0.99	1.03	12.64
$SE_A$	LR2	$\frac{931.323 + 2468.74 C - 146.956 T + 214.237 F}{1891.11 - 44.8854 C - 133.037 T - 35.2433 F}$	0.99	0.99	0.97	1.69	44.74

In Figure 3.1, 3D plots are given to show the change behavior of reflection and absorption effectiveness by CNT content (wt%) and frequency (GHz). These plots include the relationships in which thickness parameters are kept at 1, 1.5, 2, 2.5, and 3 mm values. It can be seen from the left plot that the reflection effectiveness value increases as the CNT content increases, and the change rate decreases. Additionally, frequency effect is almost negligible on output 1. Besides, the right-hand plot demonstrates that different thickness values cause distinct absorption effectiveness values, although these differences are insufficient to alter the main behavior. In addition, absorption effectiveness also increases as CNT content increases, and the change rate increases, unlike the  $SE_R$ . Moreover, the absorption effectiveness increases as frequency increases.

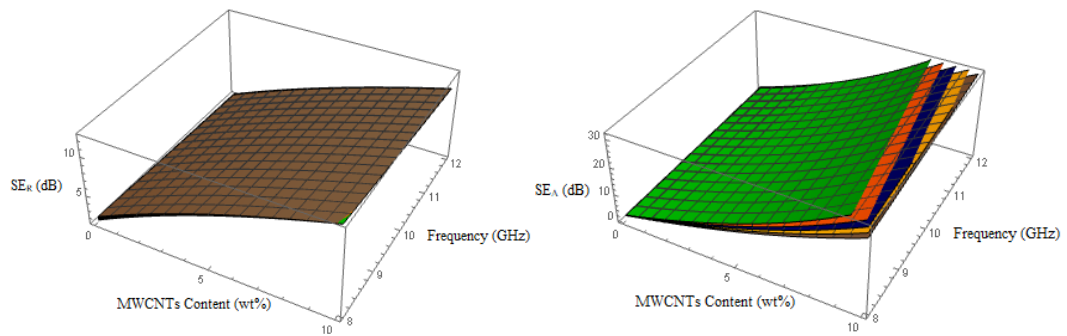


Figure 3.1: 3D plots representations of the  $SE_R$  (left) and  $SE_A$  (right) functions depending on CNTs content (C) and frequency (F). Gray, yellow, blue, orange, and green surfaces indicate in which cases the thickness (T) values at 1, 1.5, 2, 2.5, and 3 mm, respectively.

### 3.2.2 Optimization Results

Six-distinct scenarios were analyzed for each output in the optimization step where DE, NM, RS, and SA algorithms were used. Table 3.11 presents the results of all scenarios for minimizing the  $SE_R$  as the objective function of the problem.



Table 3.11: Optimization problem scenarios for  $SE_R$  output and their results.

Scenario No	Optimization Problem	Optimization Algorithm	$SE_R$ (dB)*	$SE_A$ (dB)	Suggested Design
1		NM	1.03	2.86	C = 0, T = 3, F = 12
	Min. $SE_R$ $0 \leq C \leq 10$ $1 \leq T \leq 3$ $8 \leq F \leq 12$	DE	1.03	2.86	C = 0, T = 3, F = 12
		SA	1.03	2.86	C = 0, T = 3, F = 12
		RS	1.03	2.86	C = 0, T = 3, F = 12
2		NM	1.03	2.86	C = 0, T = 3, F = 12
	Min. $SE_R$ $0 \leq C \leq 10$ $1 \leq T \leq 3$ $8 \leq F \leq 12$ {C, T, F} $\in$ Integers	DE	1.03	2.86	C = 0, T = 3, F = 12
		SA	1.16	2.58	C = 0, T = 3, F = 11
		RS	1.36	2.42	C = 0, T = 2, F = 11
3		NM	1.03	2.86	C = 0, T = 3, F = 12
	Min. $SE_R$ {C=0    C=2.5    C=5    C=7.5    C=10 & T=1    T=1.5    T=2    T=2.5    T=3 & F=8    F=9    F=10    F=11    F=12}	DE	1.03	2.86	C = 0, T = 3, F = 12
		SA	1.03	2.86	C = 0, T = 3, F = 12
		RS	1.03	2.86	C = 0, T = 3, F = 12
4		NM	5.96	16.24	C = 4.47185, T = 3, F = 12
	Min. $SE_R$ $SE_A > 16.2389$ $0 \leq C \leq 10$ $1 \leq T \leq 3$ $8 \leq F \leq 12$	DE	5.96	16.24	C = 4.47185, T = 3, F = 12
		SA	5.96	16.24	C = 4.47185, T = 3, F = 12
		RS	5.96	16.24	C = 4.47185, T = 3, F = 12
5		NM	6.48	18.24	C = 5, T = 3, F = 12
	Min. $SE_R$ $SE_A > 16.2389$ $0 \leq C \leq 10$ $1 \leq T \leq 3$ $8 \leq F \leq 12$ {C, T, F} $\in$ Integers	DE	6.48	18.24	C = 5, T = 3, F = 12
		SA	6.48	18.24	C = 5, T = 3, F = 12
		RS	6.79	17.26	C = 5, T = 3, F = 11
6		NM	6.48	18.24	C = 5, T = 3, F = 12
	Min. $SE_R$ $SE_A > 16.2389$ {C=0    C=2.5    C=5    C=7.5    C=10 & T=1    T=1.5    T=2    T=2.5    T=3 & F=8    F=9    F=10    F=11    F=12}	DE	6.48	18.24	C = 5, T = 3, F = 12
		SA	6.48	18.24	C = 5, T = 3, F = 12
		RS	6.48	18.24	C = 5, T = 3, F = 12

\* Gray-filled boxes indicate the objective function of the problem.

In the first scenario, all inputs are taken into consideration as real numbers in the continuous search space. The input intervals are  $0 \leq C \leq 10$ ,  $1 \leq T \leq 3$ , and  $8 \leq F \leq 12$ . It is apparent from Table 3.1 that all algorithms gave the same value as 1.03 dB for  $SE_R$  and 2.9 dB for  $SE_A$  with the suggested (optimum) design,  $C=0$  wt%,  $T=3$  mm, and  $F=12$  GHz. However, the corresponding values of  $SE_A$  are not good results for the EM wave absorption, which is valid for the entire scenarios when the objective function is taken as minimizing the  $SE_R$  in Table 3.1.

In the second scenario, the same intervals were used as a constraint for the input variables within the integer search space. Herein, the same values as in the first one were obtained from both DE and NM, while different values were obtained from SA and RS algorithms. However, the values are still very near to each other, 1.16 and 1.36 dB for  $SE_R$  and 2.58 and 2.42 dB for  $SE_A$  by SA and RS, respectively. The suggested design obtained from SA is  $T=3$  mm,  $C=0$  wt%, and  $F=11$  GHz, while from RS is  $T=2$  mm,  $C=0$  wt%, and  $F=11$  GHz.

The third scenario includes the optimum case when the design variables have to be certain values as 0, 2.5, 5, 7.5, or 10 wt% for CNTs content, 1, 1.5, 2, 2.5, or 3 mm for thickness, and 8, 9, 10, 11, or 12 GHz for frequency. In the third scenario, the same values were obtained from each optimization algorithm as 1.03 dB for reflection and 2.86 dB for absorption effectiveness. The suggested design is obtained when content is 0 wt%, thickness is 3 mm, and frequency is 12 GHz.

Besides, because the satisfying values for absorption effectiveness could not be achieved in the first three scenarios, the fourth, fifth, and sixth scenarios were defined. In the last three scenarios, a constraint was defined as the  $SE_A$  values must be higher than their mean value, 16.24 dB, in the dataset. Other constraints were considered the same as the first three scenarios corresponding to the last three scenarios orderly. In the fourth scenario, the same values as 5.96 dB for reflection and 16.24 dB for absorption are obtained from all algorithms with optimum design as 3 mm for  $T$ , 4.47 wt% for  $C$ , and 12 GHz for  $F$ .

In the last two scenarios, 6.48 dB for reflection and 18.24 dB for absorption effectiveness are attained from all algorithms except the RS algorithm in the fifth one. The optimum design is suggested as  $T=3$  mm,  $C=5$  wt%, and  $F=12$  GHz. In the fifth

one, the RS algorithm gave the  $SE_R$  values, 6.79 dB and  $SE_A$  values, 17.26 dB with suggested design values,  $T=3$  mm,  $C= 5$  wt%, and  $F=11$  GHz. However, in the fifth scenario, the RS algorithm's results are still very close to the values achieved from the others in the fifth and sixth scenarios. When the results obtained from the scenarios are considered, it can be seen that the reflection effectiveness tends to increase with the increase in absorption effectiveness of the structure.

Furthermore, Table 3.12 includes the six-distinct scenarios for the optimization problems with the objective function of absorption effectiveness for maximizing. All constraints were considered the same as the scenarios in Table 3.11 orderly. Additionally, the last three scenarios consist of the constraint specified with a lower reflection value than the mean of all reflection effectiveness values, 6.98 dB, in the dataset.

Table 3.12: Optimization problem scenarios for  $SE_A$  output and their results.

Scenario No	Optimization Problem	Optimization Algorithm	$SE_R$ (dB)	$SE_A$ (dB)*	Suggested Design
1	Max. $SE_A$ $0 \leq C \leq 10$ $1 \leq T \leq 3$ $8 \leq F \leq 12$	NM	10.74	44.74	C = 10, T = 3, F = 12
		DE	10.74	44.74	C = 10, T = 3, F = 12
		SA	10.74	44.74	C = 10, T = 3, F = 12
		RS	10.74	44.74	C = 10, T = 3, F = 12
2	Max. $SE_A$ $0 \leq C \leq 10$ $1 \leq T \leq 3$ $8 \leq F \leq 12$ {C, T, F} $\in$ Integers	NM	11.17	42.01	C = 10, T = 3, F = 11
		DE	10.74	44.74	C = 10, T = 3, F = 12
		SA	10.74	44.74	C = 10, T = 3, F = 12
		RS	9.54	30.32	C = 8, T = 3, F = 11
3	Max. $SE_A$ {C=0    C=2.5    C=5    C=7.5    C=10 & T=1    T=1.5    T=2    T=2.5    T=3 & F=8    F=9    F=10    F=11    F=12}	NM	10.74	44.74	C = 10, T = 3, F = 12
		DE	10.74	44.74	C = 10, T = 3, F = 12
		SA	10.74	44.74	C = 10, T = 3, F = 12
		RS	10.74	44.74	C = 10, T = 3, F = 12
4	Max. $SE_A$ $SE_R < 6.98333$ $0 \leq C \leq 10$ $1 \leq T \leq 3$ $8 \leq F \leq 12$	NM	6.98	20.39	C = 5.53677, T = 3, F = 12
		DE	6.98	20.39	C = 5.53677, T = 3, F = 12
		SA	6.98	20.39	C = 5.53677, T = 3, F = 12
		RS	6.98	20.39	C = 5.53677, T = 3, F = 12
5	Max. $SE_A$ $SE_R < 6.98333$ $0 \leq C \leq 10$ $1 \leq T \leq 3$ $8 \leq F \leq 12$ {C, T, F} $\in$ Integers	NM	6.57	15.91	C = 5, T = 2, F = 12
		DE	6.48	18.24	C = 5, T = 3, F = 12
		SA	6.48	18.24	C = 5, T = 3, F = 12
		RS	6.79	17.26	C = 5, T = 3, F = 11
6	Max. $SE_A$ $SE_R < 6.98333$ {C=0    C=2.5    C=5    C=7.5    C=10 & T=1    T=1.5    T=2    T=2.5    T=3 & F=8    F=9    F=10    F=11    F=12}	NM	6.48	18.24	C = 5, T = 3, F = 12
		DE	6.48	18.24	C = 5, T = 3, F = 12
		SA	6.48	18.24	C = 5, T = 3, F = 12
		RS	6.48	18.24	C = 5, T = 3, F = 12

\* Gray-filled boxes indicate the objective function of the problem.

In scenarios one and three, the values for absorption and reflection effectiveness were achieved from the algorithms as 44.74 and 10.74 dB, respectively, with the design variable values,  $T=3$  mm,  $C=10$  wt%, and  $F=12$  GHz.

Algorithms DE and SA in the second scenario gave the same values as obtained from the first and third ones. However, 42.01 dB for absorption and 11.17 dB for reflection values were obtained from the NM algorithm. The values from the NM algorithm are very close to the achieved values from the other algorithms except for RS. The values obtained from the RS algorithm are 30.32 dB and 9.54 dB for absorption and reflection, respectively. Accordingly, the suggested design is  $T=3$  mm,  $C=8$  wt%, and  $F=11$  GHz. These results from the RS method in the second scenario can be interpreted as follows: the inconsistency occurred for the relevant conditions because the RS method is not robust for the problem, which has an integer programming solution.

In the fourth one, the same values for absorption and reflection effectiveness of the nanocomposite were achieved as 20.39 and 6.98 dB, respectively, with the design variable values,  $F=12$  GHz,  $T=3$  mm,  $C=5.54$  wt%.

In scenarios five and six, all approaches gave the identical values as 6.48 dB for reflection and 18.24 dB for absorption excepting NM and RS methods in the fifth one. Accordingly, the input parameters are found as 3 mm of  $T$ , 5 wt% of  $C$ , and 12 GHz of  $F$ . However, NM and RS approaches gave different values in the conditions of scenario five, but the results are still close to the values from the other methods in the scenarios five and six. In the fifth scenario conditions, NM method gave the values 6.57 dB and 15.91 dB for reflection and absorption, respectively, with the optimum design is achieved as  $T=2$  mm,  $C=5$  wt%, and  $F=12$  GHz. Furthermore, in the fifth scenario, RS approach gives the values of 6.79 dB for reflection and of 17.26 dB for absorption while the suggested design parameters are  $F=11$  GHz,  $C=5$  wt%, and  $T=3$  mm.

Consequently, both optimization problems, including the constraints presented in Tables 3.11 and 3.12, demonstrate design variables' influences on the outputs. Accordingly, materials content is the most effective parameter for both cases of objective functions of the problem. Both reflection and absorption features of respective nanocomposite material increase with the increase in the content of the

material. Furthermore, the EM wave frequency is another effective parameter on the outputs. The results show that the frequency parameters are either 11 or 12 GHz varying with the defined constraints. However, the thickness parameter has the least effect on the absorption and reflection properties of the structure because they have the same values (3 mm) in all scenarios, except the NM algorithm in the fifth scenario condition having the objective function as the maximization of absorption. The attained results related to the effects of the input parameters on the outputs are fully coherent with the referenced article [64]. Additionally, in the first and third scenarios shown in Table 3.12, the maximum absorption with the minimum reflection effectiveness was obtained as 44.74 and 10.74 dB, respectively [72].

# Chapter 4

## Results and Discussions

### 4.1 Data Acquisition

The data modeled in this thesis was obtained from the experimental studies conducted by the collaborative research group within the scope of the project (2021-GAP-MÜMF-0042) funded by İzmir Kâtip Çelebi University, Scientific Research Projects Unit. This project involves graphene synthesis on a nickel foam substrate via the CVD method. After etching the nickel away from the structure, the obtained pristine GF was used as a template to synthesize MnO<sub>2</sub> nanowires by hydrothermal method considering the different combinations of process parameters to obtain the most effective structural form for the EMI SE. Because the nanowire structure of MnO<sub>2</sub> was intended to be synthesized, the hydrothermal process parameters' (temperature (°C), time (h), and molar concentration ratio (M/M)) intervals were specified experimentally. This process was performed with multiple repetitions of experimental processes. Although several morphologic and crystallographic forms of MnO<sub>2</sub> nanostructures were possible to synthesize, the relevant intervals of parameters were determined considering the domination of the nanowire structure of MnO<sub>2</sub> on the GF. During the experimental studies performed to identify the parameters' interval, Scanning Electron Microscopy (SEM, Carl Zeiss, İKÇÜ), X-Ray Diffractometer (XRD, Bruker D2 Phaser, İKÇÜ), and Raman Spectroscopy (Raman Spectrometer, Renishaw/In Via, İKÇÜ) analysis were conducted to identify the morphological, crystallographic, and quality characteristics (e.g., layer numbers and crystallinity of GF) of obtained structures. After determining the parameters' interval, a 2-level full factorial design was carried out to obtain a combination of these parameters using Design-Expert software. The research group performed the experimental procedures according to the obtained

experimental runs from the Design of Experiment (DoE) method with the relevant characterization of the samples. The EMI SE of the samples were measured in 8-12 GHz bandwidth (X-band) via a two-port vector network analyzer (VNA, Agilent Technologies N5230C, DEU/EMUM) by converting the S-parameters to SE characteristics considering the equations (1.1), (1.2), (1.3), and (1.4). The respective dataset is presented in Table 4.1.

Table 4.1: All inputs and their corresponding output values

	Run	Temperature (°C)	Time (h)	Concentration (M/M)	SE <sub>R</sub> (dB)	SE <sub>A</sub> (dB)
Training	1	140	6	0.07	10.351	21.8931
	2	140	12	0.07	9.4474	19.1939
	3	180	12	0.07	8.9753	16.2173
	4	140	6	0.2	9.01002	25.0281
	5	180	6	0.2	9.75106	17.7674
	6	140	12	0.2	8.87389	40.2124
Testing	7	180	6	0.07	9.95189	23.2322
	8	180	12	0.2	8.7958	17.4203

## 4.2 Problem Definition

This thesis intends to perform a systematic design-based optimization study on GF/MnO<sub>2</sub> NW nanocomposite as an EMI shielding material. In line with this purpose, mathematical optimization problems were defined considering the hydrothermal process parameters (temperature (T), time (t), concentration (C)) as design variables with objective functions SE<sub>R</sub> and SE<sub>A</sub> of the nanocomposite structure. Herein, the problem is defined as the equivalent single objective approach considering both objective functions. Since this thesis study's objective includes developing absorption-dominant shielding material, the objective function is to maximize SE<sub>A</sub> with minimum SE<sub>R</sub> instead of maximizing the SE<sub>T</sub>. The data modeling step was conducted via multiple nonlinear neuro-regression approach, and 16 different regression types (linear, logarithmic, trigonometric, exponential, quadratic, and their rational forms) were compared for each objective function to achieve the most accurate one. The optimization procedure was carried out via four direct search algorithms (SA, NM, RS,



and DE). Besides, three-distinct scenarios were identified for each optimization problem to evaluate the phenomenon widely.

### 4.3 Modeling Results

The mathematical modeling stage results are presented in this section. In this step, different regression model types were considered to find the most accurate models. Table 4.2 shows the general representation of multiple logarithmic regression forms used in the modeling stage, together with the model types given in Table 3.7.

Table 4.2: General representation of multiple logarithmic regression models.

Model Name	Nomenclature	Formula
1 <sup>st</sup> order logarithmic multiple nonlinear	FOLN	$Y = \sum_{i=1}^3 (a_i \text{Log}[x_i]) + c$
1 <sup>st</sup> order logarithmic multiple nonlinear rational	FOLNR	$Y = \frac{\sum_{i=1}^3 (a_i \text{Log}[x_i]) + c_1}{\sum_{j=1}^3 (\beta_j \text{Log}[x_j])} + c_2$
2 <sup>nd</sup> order logarithmic multiple nonlinear	SOLN	$Y = \sum_{k=1}^3 \sum_{j=1}^3 (a_j \text{Log}[x_j x_k]) + \sum_{i=1}^3 (a_i \text{Log}[x_i]) + c$
2 <sup>nd</sup> order logarithmic multiple nonlinear rational	SOLNR	$Y = \frac{\sum_{k=1}^3 \sum_{j=1}^3 (a_j \text{Log}[x_j x_k]) + \sum_{i=1}^3 (a_i \text{Log}[x_i]) + c_1}{\sum_{m=1}^3 \sum_{l=1}^3 (a_l \text{Log}[x_l x_m]) + \sum_{n=1}^3 (a_n \text{Log}[x_n])} + c_2$

Tables 4.3 and 4.4 give the obtained models' accuracy results regarding  $R^2$  values and boundedness control for both outputs,  $SE_R$  and  $SE_A$ , respectively. Both tables are prepared to compare all models in accordance with accuracy steps. The eligibility criteria as follows:

- (i) It can be determined the prediction ability of the candidate models' absorption and reflection effectiveness of the nanocomposite by considering  $R^2$  values.
- (ii) It can be specified whether the obtained models have functional limitation by considering their intervals.

Table 4.3: Accuracy check results of obtained models for the  $SE_R$  output in terms of  $R^2$  values and boundedness check.

Nomenclature*	$R^2_{\text{training}}$	$R^2_{\text{training-adjusted}}$	$AIC_{\text{training}}$	$BIC_{\text{training}}$	$R^2_{\text{testing}}$	Minimum Value (dB)	Maximum Value (dB)
L1	0.99	1	-	-	0.92	8.62	10.16
LR1	1	1	-	-	-2997.64	$-\infty$	$\infty$
SON1	1	1	-	-	0.40	8.87	10.74
SONR1	0.99	1	-	-	-0.92	8.40	11.01
FOEN1	0.99	1	-	-	0.92	8.62	10.16
FOENR1	0.99	1	-	-	0.73	9.1	9.8
SOEN1	1	1	-	-	-1.09	8.42	11.17
SOENR1	0.99	1	-	-	0.09	8.36	9.56
FOLN1	0.99	1	-	-	0.92	8.62	10.16
FOLNR1	0.99	1	-	-	0.73	$-3.56 \times 10^{14}$	$4.72 \times 10^8$
SOLN1	1	1	-	-	0.55	8.06	10.35
SOLNR1	0.99	1	-	-	0.32	8.49	10.55
FOTN1	0.99	1	-	-	0.92	-5.45	14.46
FOTNR1	0.73	1	-	-	-200.15	$-1.05 \times 10^{14}$	$7.3 \times 10^{13}$
SOTN1	1	1	-	-	-0.92	-7.55	14.11
SOTNR1	0.75	1	-	-	-194.58	$-4.86 \times 10^7$	$9.76 \times 10^{12}$

\* Corresponding functions are available in the appendices.

Table 4.4: Accuracy check results of obtained models for the  $SE_A$  output in terms of  $R^2$  values and boundedness check.

Nomenclature*	$R^2_{\text{training}}$	$R^2_{\text{training-adjusted}}$	$AIC_{\text{training}}$	$BIC_{\text{training}}$	$R^2_{\text{testing}}$	Minimum Value (dB)	Maximum Value (dB)
L2	0.98	1.1	-	-	-17.6	7.83	35.74
LR2	0.92	1.2	-	-	-2.69	13.6	28.9
SON2	1	1	-	-	-14.5	16.2	40.2
SONR2	0.93	1	-	-	-2.95	17.1	30.3
FOEN2	0.98	1.1	-	-	-17.6	7.83	35.74
FOENR2	0.93	1	-	-	-0.03	20.19	29.67
SOEN2	1	1	-	-	-25.5	14.97	49.9
SOENR2	0.93	1	-	-	0.03	19.32	20.14
FOLN2	0.98	1.1	-	-	-17.6	7.83	35.74
FOLNR2	0.99	1	-	-	-5.76	14.3	39.5
SOLN2	1	1	-	-	-17.5	16.2	40.2
SOLNR2	1	1	-	-	-5.3	16.2	40.2
FOTN2	0.98	1	-	-	-17.6	-26.1	50
FOTNR2	0.98	1	-	-	-8.7	$-6.6 \times 10^{12}$	$4.07 \times 10^{11}$
SOTN2	1	1	-	-	-25.7	-122.7	76.97
SOTNR2	0.87	1	-	-	-41.15	$-2.02 \times 10^8$	$1.3 \times 10^{12}$

\* Corresponding functions are available in the appendices.

As seen from Table 4.3, the  $R^2_{\text{training}}$  values of all models are almost 1 except for FOTNR1 and SOTNR1, which have values of almost 0.75. However, only four models, L1, FOEN1, FOLN1, and FOTN1, have valid  $R^2$  testing value, 0.92. Among them, when considering the phenomenon, the FOTN1 model form was defined in the unrealistic interval because the minimum reflection effectiveness value is -5.45 dB. On the contrary, the boundedness check is also successful for L1, FOEN1, and FOLN1 models because of having intervals from 8.62 to 10.16 dB. Furthermore, all models have training  $R^2$  values between almost 0.90-1 for the  $SE_A$  output, as shown in Table 4.4. However, none of them has valid testing  $R^2$  values.

It is obvious from both Tables 4.3 and 4.4 that if the model validity is carried out according to  $R^2$  values only, it will be made wrong assessment because almost entire models have  $R^2$  values very close to 1. Nevertheless, the point is that the models possessing high  $R^2$  values are incapable of meeting the remainder accuracy stages. Therefore, mathematical optimization studies to design engineering phenomena must be performed systematically. Additionally, if any traditional regression model types would not meet the criteria, their hybrid forms should be considered to achieve a solid objective function. In the case of this thesis study, it can be seen from Table 4.4 that all models failed to pass the accuracy steps. Therefore, a hybrid model was achieved to identify the  $SE_A$  of nanocomposite structure. Furthermore, although some valid models were obtained for the objective function  $SE_R$ , a hybrid model was also attained to find a more accurate model. The obtained models determined as objective functions are shown in Mathematica language form as follows:

$$SE_R = 8 - \text{Abs}[-0.215556 - 0.301347 \text{Cos}[x_1] + 0.194855 \text{Cos}[x_1]^2 + 0.188714 \text{Cos}[x_1]^3 + 0.142409 \text{Cos}[x_2] - 1.2434 \text{Cos}[x_1] \text{Cos}[x_2] - 0.516784 \text{Cos}[x_1]^2 \text{Cos}[x_2] + 0.0342264 \text{Cos}[x_2]^2 - 0.961969 \text{Cos}[x_1] \text{Cos}[x_2]^2 - 0.261268 \text{Cos}[x_2]^3 + 0.380922 \text{Cos}[x_3] - 1.0033 \text{Cos}[x_1] \text{Cos}[x_3] + 0.507617 \text{Cos}[x_1]^2 \text{Cos}[x_3] + 1.43094 \text{Cos}[x_2] \text{Cos}[x_3] - 0.771072 \text{Cos}[x_1] \text{Cos}[x_2] \text{Cos}[x_3] - 0.394824 \text{Cos}[x_2]^2 \text{Cos}[x_3] - 0.101567 \text{Cos}[x_3]^2 + 0.155897 \text{Cos}[x_1] \text{Cos}[x_3]^2 + 0.583046 \text{Cos}[x_2] \text{Cos}[x_3]^2 - 0.0372116 \text{Cos}[x_3]^3 - 0.182722 \text{Sin}[x_1] + 0.0785989 \text{Cos}[x_1] \text{Sin}[x_1] + 0.231365 \text{Cos}[x_1]^2 \text{Sin}[x_1] + 0.291949 \text{Cos}[x_2] \text{Sin}[x_1] + 0.0134971 \text{Cos}[x_1] \text{Cos}[x_2] \text{Sin}[x_1] + 0.341456 \text{Cos}[x_2]^2 \text{Sin}[x_1] + 0.546507 \text{Cos}[x_3] \text{Sin}[x_1] - 0.923421 \text{Cos}[x_1] \text{Cos}[x_3] \text{Sin}[x_1] + 0.430724 \text{Cos}[x_2] \text{Cos}[x_3] \text{Sin}[x_1] - 0.271307 \text{Cos}[x_3]^2 \text{Sin}[x_1] + 0.163751 \text{Sin}[x_1]^2 - 0.347657 \text{Cos}[x_1] \text{Sin}[x_1]^2 - 0.165957 \text{Cos}[x_2] \text{Sin}[x_1]^2 + 0.14073 \text{Cos}[x_3] \text{Sin}[x_1]^2 + 0.183718 \text{Sin}[x_1]^3 + 0.0851726 \text{Sin}[x_2] - 1.00378 \text{Cos}[x_1] \text{Sin}[x_2] - 0.232983 \text{Cos}[x_1]^2 \text{Sin}[x_2] - 0.302517 \text{Cos}[x_2] \text{Sin}[x_2] - 1.0819 \text{Cos}[x_1] \text{Cos}[x_2] \text{Sin}[x_2] + 0.569202 \text{Cos}[x_2]^2 \text{Sin}[x_2] + 1.40112 \text{Cos}[x_3] \text{Sin}[x_2] - 1.36763 \text{Cos}[x_1] \text{Cos}[x_3] \text{Sin}[x_2] - 1.177 \text{Cos}[x_2] \text{Cos}[x_3] \text{Sin}[x_2] + 0.529925 \text{Cos}[x_3]^2 \text{Sin}[x_2] - 0.459805 \text{Sin}[x_1] \text{Sin}[x_2] - 0.277556 \text{Cos}[x_1] \text{Sin}[x_1] \text{Sin}[x_2] + 0.378513 \text{Cos}[x_2] \text{Sin}[x_1] \text{Sin}[x_2] + 1.09321 \text{Cos}[x_3] \text{Sin}[x_1] \text{Sin}[x_2] - 0.145587 \text{Sin}[x_1]^2 \text{Sin}[x_2] - 0.631895 \text{Sin}[x_2]^2 - 0.474564 \text{Cos}[x_1] \text{Sin}[x_2]^2 - 0.340187 \text{Cos}[x_2] \text{Sin}[x_2]^2 - 0.339871 \text{Cos}[x_3] \text{Sin}[x_2]^2 - 0.292429 \text{Sin}[x_1] \text{Sin}[x_2]^2 - 0.212368 \text{Sin}[x_2]^3 - 0.780192 \text{Sin}[x_3] - 1.1163 \text{Cos}[x_1] \text{Sin}[x_3] + 0.371579 \text{Cos}[x_1]^2 \text{Sin}[x_3] - 3.31548 \text{Cos}[x_2] \text{Sin}[x_3] - 1.85931 \text{Cos}[x_1] \text{Cos}[x_2] \text{Sin}[x_3] - 0.607195 \text{Cos}[x_2]^2 \text{Sin}[x_3] - 2.2713 \text{Cos}[x_3] \text{Sin}[x_3] + 0.0411471 \text{Cos}[x_1] \text{Cos}[x_3] \text{Sin}[x_3] - 2.1418 \text{Cos}[x_2] \text{Cos}[x_3] \text{Sin}[x_3] - 0.127016 \text{Cos}[x_3]^2 \text{Sin}[x_3] - 1.14506 \text{Sin}[x_1] \text{Sin}[x_3] + 0.0755503 \text{Cos}[x_1] \text{Sin}[x_1] \text{Sin}[x_3] - 5.52406 \text{Cos}[x_2] \text{Sin}[x_1] \text{Sin}[x_3] - 0.587712 \text{Cos}[x_3] \text{Sin}[x_1] \text{Sin}[x_3] - 0.0143231 \text{Sin}[x_1]^2 \text{Sin}[x_3] - 3.73874 \text{Sin}[x_2] \text{Sin}[x_3] - 0.817386 \text{Cos}[x_1] \text{Sin}[x_2] \text{Sin}[x_3] - 1.83274 \text{Cos}[x_2] \text{Sin}[x_2] \text{Sin}[x_3] - 2.08975 \text{Cos}[x_3] \text{Sin}[x_2] \text{Sin}[x_3] - 9.65885 \text{Sin}[x_1] \text{Sin}[x_2] \text{Sin}[x_3] + 0.067117 \text{Sin}[x_2]^2 \text{Sin}[x_3] + 0.114418 \text{Sin}[x_3]^2 - 0.0348673 \text{Cos}[x_1] \text{Sin}[x_3]^2 - 0.167593 \text{Cos}[x_2] \text{Sin}[x_3]^2 + 0.217548 \text{Cos}[x_3] \text{Sin}[x_3]^2 + 0.301428 \text{Sin}[x_1] \text{Sin}[x_3]^2 - 0.802783 \text{Sin}[x_2] \text{Sin}[x_3]^2 - 0.311073 \text{Sin}[x_3]^3]$$

$$SE_A = 15 - \text{Abs}[-0.277656 + 1.90073 \text{Cos}[x_1] - 1.41002 \text{Cos}[x_1]^2 + 0.352302 \text{Cos}[x_1]^3 + 0.192292 \text{Cos}[x_2] - 0.885104 \text{Cos}[x_1] \text{Cos}[x_2] - 0.815926 \text{Cos}[x_1]^2 \text{Cos}[x_2] - 0.285923 \text{Cos}[x_2]^2 - 1.41538 \text{Cos}[x_1] \text{Cos}[x_2]^2 + 0.580158 \text{Cos}[x_2]^3 + 0.625201 \text{Cos}[x_3] - 0.219247 \text{Cos}[x_1] \text{Cos}[x_3] + 1.15688 \text{Cos}[x_1]^2 \text{Cos}[x_3] - 0.27043 \text{Cos}[x_2] \text{Cos}[x_3] + 4.86946 \text{Cos}[x_1] \text{Cos}[x_2] \text{Cos}[x_3] - 0.341995 \text{Cos}[x_2]^2 \text{Cos}[x_3] - 0.856523 \text{Cos}[x_3]^2 + 0.752303 \text{Cos}[x_1] \text{Cos}[x_3]^2 + 0.704503 \text{Cos}[x_2] \text{Cos}[x_3]^2 - 0.197564 \text{Cos}[x_3]^3 - 1.34174 \text{Sin}[x_1] - 3.43043 \text{Cos}[x_1] \text{Sin}[x_1] + 1.11257 \text{Cos}[x_1]^2 \text{Sin}[x_1] - 2.24298 \text{Cos}[x_2] \text{Sin}[x_1] + 1.94825 \text{Cos}[x_1] \text{Cos}[x_2] \text{Sin}[x_1] + 0.963312 \text{Cos}[x_2]^2 \text{Sin}[x_1] + 3.39432 \text{Cos}[x_3] \text{Sin}[x_1] + 1.8599 \text{Cos}[x_1] \text{Cos}[x_3] \text{Sin}[x_1] + 21.1618 \text{Cos}[x_2] \text{Cos}[x_3] \text{Sin}[x_1] - 1.57153 \text{Cos}[x_3]^2 \text{Sin}[x_1] + 0.445736 \text{Sin}[x_1]^2 - 0.910283 \text{Cos}[x_1] \text{Sin}[x_1]^2 - 1.31401 \text{Cos}[x_2] \text{Sin}[x_1]^2 - 2.5867 \text{Cos}[x_3] \text{Sin}[x_1]^2 - 0.111804 \text{Sin}[x_1]^3 - 2.9033 \text{Sin}[x_2] - 0.821197 \text{Cos}[x_1] \text{Sin}[x_2] - 1.58375 \text{Cos}[x_1]^2 \text{Sin}[x_2] - 3.64402 \text{Cos}[x_2] \text{Sin}[x_2] - 0.91265 \text{Cos}[x_1] \text{Cos}[x_2] \text{Sin}[x_2] - 0.717054 \text{Cos}[x_2]^2 \text{Sin}[x_2] + 1.82845 \text{Cos}[x_3] \text{Sin}[x_2] + 9.77616 \text{Cos}[x_1] \text{Cos}[x_3] \text{Sin}[x_2] + 1.11167 \text{Cos}[x_2] \text{Cos}[x_3] \text{Sin}[x_2] + 2.4794 \text{Cos}[x_3]^2 \text{Sin}[x_2] - 3.31401 \text{Sin}[x_1] \text{Sin}[x_2] + 0.440401 \text{Cos}[x_1] \text{Sin}[x_1] \text{Sin}[x_2] - 0.870828 \text{Cos}[x_2] \text{Sin}[x_1] \text{Sin}[x_2] + 41.4474 \text{Cos}[x_3] \text{Sin}[x_1] \text{Sin}[x_2] - 0.857045 \text{Sin}[x_1]^2 \text{Sin}[x_2] - 2.08265 \text{Sin}[x_2]^2 - 0.863726 \text{Cos}[x_1] \text{Sin}[x_2]^2 - 0.326158 \text{Cos}[x_2] \text{Sin}[x_2]^2 - 2.87838 \text{Cos}[x_3] \text{Sin}[x_2]^2 - 1.63424 \text{Sin}[x_1] \text{Sin}[x_2]^2 + 0.865007 \text{Sin}[x_2]^3 + 5.38396 \text{Sin}[x_3] + 1.79234 \text{Cos}[x_1] \text{Sin}[x_3] + 0.80522 \text{Cos}[x_1]^2 \text{Sin}[x_3] - 10.393 \text{Cos}[x_2] \text{Sin}[x_3] - 26.3819 \text{Cos}[x_1] \text{Cos}[x_2] \text{Sin}[x_3] - 0.57547 \text{Cos}[x_2]^2 \text{Sin}[x_3] + 12.0351 \text{Cos}[x_3] \text{Sin}[x_3] - 5.6129 \text{Cos}[x_1] \text{Cos}[x_3] \text{Sin}[x_3] - 15.5835 \text{Cos}[x_2] \text{Cos}[x_3] \text{Sin}[x_3] + 0.437466 \text{Cos}[x_3]^2 \text{Sin}[x_3] + 14.6156 \text{Sin}[x_1] \text{Sin}[x_3] - 7.86441 \text{Cos}[x_1] \text{Sin}[x_1] \text{Sin}[x_3] - 134.153 \text{Cos}[x_2] \text{Sin}[x_1] \text{Sin}[x_3] + 12.4834 \text{Cos}[x_3] \text{Sin}[x_1] \text{Sin}[x_3] + 2.88235 \text{Sin}[x_1]^2 \text{Sin}[x_3] - 53.1822 \text{Sin}[x_2] \text{Sin}[x_3] - 55.7568 \text{Cos}[x_1] \text{Sin}[x_2] \text{Sin}[x_3] - 39.3815 \text{Cos}[x_2] \text{Sin}[x_2] \text{Sin}[x_3] - 52.9824 \text{Cos}[x_3] \text{Sin}[x_2] \text{Sin}[x_3] - 333.141 \text{Sin}[x_1] \text{Sin}[x_2] \text{Sin}[x_3] + 9.49698 \text{Sin}[x_2]^2 \text{Sin}[x_3] + 1.60241 \text{Sin}[x_3]^2 - 1.98064 \text{Cos}[x_1] \text{Sin}[x_3]^2 + 0.37143 \text{Cos}[x_2] \text{Sin}[x_3]^2 + 1.16013 \text{Cos}[x_3] \text{Sin}[x_3]^2 - 0.890825 \text{Sin}[x_1] \text{Sin}[x_3]^2 - 2.39199 \text{Sin}[x_2] \text{Sin}[x_3]^2 - 0.113068 \text{Sin}[x_3]^3]$$

where  $x_1$ ,  $x_2$ , and  $x_3$  indicate the hydrothermal process parameters, temperature, time, solution concentration, respectively.

Furthermore, Table 4.5 shows the accuracy results of each objective functions. As can be seen, all accuracy step was met via both obtained hybrid models.

Table 4.5: Accuracy results of obtained hybrid models for each objective function.

Output	$R^2_{\text{training}}$	$R^2_{\text{training-adjusted}}$	$R^2_{\text{testing}}$	Min. (dB)	Max. (dB)
SE <sub>R</sub>	1	1	1	8	12.63
SE <sub>A</sub>	1	1	1	15	66.17

Additionally, Figure 4.1 shows the 3D plots to evaluate the relationships between the hydrothermal process parameters, temperature and time with SE<sub>A</sub> and SE<sub>R</sub>. The plots were prepared considering the concentration value taken as constant at 0.07 and 0.2 M/M representing the minimum and maximum values of its interval. It is apparent from Figure 4.1 that both graphs have almost the same nonlinear behavior that is valid for the relevant constant values of concentration. When the left-hand figure is observed, the SE<sub>R</sub> function has multiple maximum and minimum points depending on the time and temperature. Moreover, the repetitive behavior of the 3D plots belonging to the SE<sub>R</sub> function is changed more frequently with altering in the temperature than the time variable. In addition, even if the two-distinct constant concentration values do not change the fundamental behavior of the curves, they shift the peak locations in line with the temperature axis with almost the same results. Besides, the same interpretations can be made for the relationships between the SE<sub>A</sub> with temperature and time parameters when the figure on the right is considered. However, the two-distinct concentration values significantly affect obtaining the maximum absorption effectiveness of nanocomposite. Accordingly, when the concentration value is kept at 0.2 M/M, the SE<sub>A</sub> function can increase over 60 dB at specific time and temperature values.

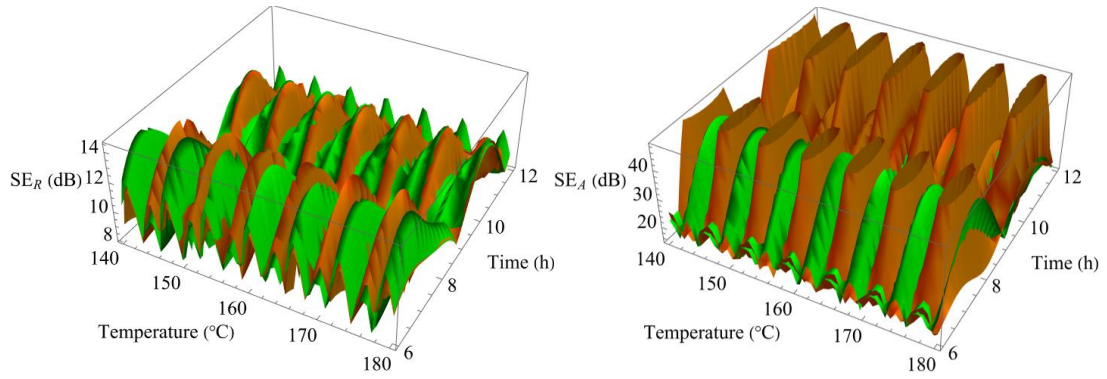


Figure 4.1: 3D plots representations of the  $SE_R$  (left) and  $SE_A$  (right) functions depending on temperature and time at certain concentration values. Green and orange surfaces indicate in which cases the concentration values at 0.07 and 0.2 M/M, respectively.

### 4.3 Optimization Results

In the optimization step, three distinct scenarios were analyzed for each output. The defined optimization problems were solved via NM, SA, DE, and RS algorithms. Table 4.6 show the results of all scenarios for minimizing reflection effectiveness as objective function of the problem.

Table 4.6: Optimization problem scenarios for  $SE_R$  output and their results.

Scenario No	Optimization Problem	Optimization Algorithm	$SE_R$ (dB)*	$SE_A$ (dB)	Suggested Design
1	Min. $SE_R$ $140 \leq T \leq 180$ $6 \leq t \leq 12$ $0.07 \leq C \leq 0.2$	NM	8	16.07	$T = 160.66, t = 9.07, C = 0.13$
		SA	8	16.57	$T = 140.23, t = 9.2, C = 0.10$
		DE	8	15.86	$T = 150.16, t = 9.11, C = 0.15$
		RS	8	56.25	$T = 159.33, t = 11.41, C = 0.2$
2	Min. $SE_R$ $140 \leq T \leq 180$ $6 \leq t \leq 12$ $0.07 \leq C \leq 0.2$ {T, t} $\in$ Integers	NM	8	15.43	$T = 176, t = 9, C = 0.11$
		SA	8	15.57	$T = 176, t = 9, C = 0.14$
		DE	8	15.71	$T = 176, t = 9, C = 0.17$
		RS	8	40.42	$T = 159, t = 8, C = 0.16$
3	Min. $SE_R$ {T=150    T=160    T=170    & t=8    t=10 & C=0.08    C=0.09    C=0.1}	NM	8.66	29.3505	$T = 150, t = 8, C = 0.08$
		SA	8.66	29.3505	$T = 150, t = 8, C = 0.08$
		DE	8.66	29.3505	$T = 150, t = 8, C = 0.08$
		RS	8.66	29.3505	$T = 150, t = 8, C = 0.08$

\* Gray-filled boxes indicate the objective function of the problem.

The first case scenario includes all inputs considered as real numbers in the continuous search space. In other words, these constraints were determined to examine whether nanocomposite structures can achieve the optimum SE in any value of hydrothermal process parameters' interval,  $140 \leq T \leq 180$ ,  $6 \leq t \leq 12$ , and  $0.07 \leq C \leq 0.2$ . As seen from Table 4.6, all algorithms gave the same value, 8 dB, for the objective function  $SE_R$ . However, different  $SE_A$  values were obtained by four algorithms because the same value of  $SE_R$  was achieved from each at different independent variable values of the objective function. Accordingly, except for the RS method, close results were obtained for the  $SE_A$  value as 16.07, 16.57, and 15.86 dB by NM, SA, and DE, respectively, with different suggested design values. The NM algorithm gave the suggested design as  $T=160.66$  °C,  $t=9.07$  h, and  $C=0.13$  M/M, while  $T=140.23$  °C,  $t=9.2$  h, and  $C=0.1$  M/M values were obtained from the SA algorithm. Furthermore, the suggested design values by the DE algorithm are  $T=150.16$  °C,  $t=9.11$  h, and  $C=0.15$  M/M. Unlike the three algorithms, a higher  $SE_A$  value, 56.25 dB, was obtained

from the RS approach when design variables are 159.33 °C, 11.41 h, and 0.2 M/M for T, t, and C, respectively.

In the second case scenario, the constraints were identified as integer search space for T and t variables with the same intervals as scenario one. In other words, since any random values might not be adjusted depending on the sensibility of experimental conditions, this scenario was identified to investigate whether the nanocomposite structure can possess any optimum SE value when the process parameters (T and t) are controllable integer values experimentally. Herein, the same value (8 dB) with distinct suggested design parameters was also acquired from the entire algorithms for the objective function  $SE_R$ . However, the obtained  $SE_A$  values from each method differ from the first scenario. Thus, close values of each other were achieved from NM, SA, and DE approaches as 15.43, 15.57, and 15.71 dB, respectively. Additionally, these three algorithms gave the same values, 176 °C for T and 9 h for t, but obtained C values from NM, SA, and DE are different as 0.11, 0.14, and 0.17 M/M, respectively. On the other hand, a higher value, 40.42 dB, for  $SE_A$  was achieved from the RS algorithm with the suggested design, T=159 °C, t=8 h, and C=0.16 M/M. The results from both scenarios demonstrate that the same values for objective function can be achieved from all. For the relevant case, obtaining different optimum designs and, therefore, different  $SE_A$  values reveals that there are distinct combinations to reach the same output values. Furthermore, the RS results obtained in the first two scenarios demonstrate that there are some points for input variables achieving a high  $SE_A$  value with minimum  $SE_R$  when the problem is defined as minimizing  $SE_R$ .

In the third case scenario, optimum cases were examined when the design variables are specific values as 150, 160, or 170 °C for T, 8 or 9 h for t, and 0.08, 0.09, or 0.1 M/M for C. Since the obtained data have been subjected to the full factorial design with 2-level before experimental processes, these values were determined considering intermediate values of inputs. Herein, it was aimed to predict whether any desirable optimal SE value of nanocomposites is possible when hydrothermal process parameters are any of the relevant values. Accordingly, the same results for all parameters were attained from the four algorithms as  $SE_R=8.66$  dB and  $SE_A=29.35$  dB when T=150 °C, t=8 h, and C=0.08 M/M. From the optimization perspective, the third



scenario results show that all algorithms give consistent results in the relevant conditions, even if the value, 29.35 dB, is not satisfying for the  $SE_A$  phenomenon.

Moreover, Table 4.7 represents the optimization problem results in which the objective function is considered as maximizing the absorption effectiveness of the nanocomposite structure. It should be noted that all scenarios are the same, as considered in Table 4.6. In the first scenario, SA, DE, and RS algorithms gave the same results for  $SE_A$  and  $SE_R$ , as 67.03 and 11.7 dB, respectively. Among them, SA and DE methods ensure the result with the same input values as  $T=152.2$  °C,  $t=7.45$  h, and  $C=0.2$  M/M, while the RS ensures the same values with different T, 158.48 °C. However, the NM algorithm obtained different values, 66.17 dB for  $SE_A$  and 8.74 dB for  $SE_R$ , by ensuring close values to other methods for the respective condition. Accordingly, the suggested optimum design by the NM algorithm is  $T=152.43$  °C,  $t=10.91$  h, and  $C=0.2$  M/M.

Table 4.7: Optimization problem scenarios for  $SE_A$  output and their results.

Scenario No	Optimization Problem	Optimization Algorithm	$SE_R$ (dB)	$SE_A$ (dB)*	Suggested Design
1	Max. $SE_A$ $140 \leq T \leq 180$ $6 \leq t \leq 12$ $0.07 \leq C \leq 0.2$	NM	8.74	66.17	$T = 152.43, t = 10.91, C = 0.2$
		SA	11.7	67.03	$T = 152.2, t = 7.45, C = 0.2$
		DE	11.7	67.03	$T = 152.2, t = 7.45, C = 0.2$
		RS	11.7	67.03	$T = 158.48, t = 7.45, C = 0.2$
2	Max. $SE_A$ $140 \leq T \leq 180$ $6 \leq t \leq 12$ $0.07 \leq C \leq 0.2$ {T, t} $\in$ Integers	NM	8.25	63.83	$T = 152, t = 11, C = 0.2$
		SA	8.50	65.77	$T = 146, t = 11, C = 0.2$
		DE	8.61	66.03	$T = 165, t = 11, C = 0.2$
		RS	8.39	65.08	$T = 171, t = 11, C = 0.2$
3	Max. $SE_A$ {T=150    T=160    T=170    & t=8    t=10 & C=0.08    C=0.09    C=0.1}	NM	8.66	29.35	$T = 150, t = 8, C = 0.08$
		SA	8.66	29.35	$T = 150, t = 8, C = 0.08$
		DE	8.66	29.35	$T = 150, t = 8, C = 0.08$
		RS	8.66	29.35	$T = 150, t = 8, C = 0.08$

\* Gray-filled boxes indicate the objective function of the problem.

For the second case scenario, NM, SA, DE, and RS approaches gave very close results to each other as 63.83, 65.77, 66.03, and 65.08 dB for  $SE_A$ , and 8.25, 8.50, 8.61, and 8.39 dB for  $SE_R$ , respectively. In addition, all algorithms attained the relevant results suggesting the same  $t$  and  $C$  values, 11 h and 0.2 M/M, respectively. However,  $T$  values differ from each other as 152 °C of NM, 146 °C of SA, 165 °C of DE, and 171 °C of RS. Therefore, for the relevant scenario conditions, the temperature alteration only affects the objective function slightly when other process parameters are kept at 11 h and 0.2 M/M.

In the third one, the same results for all parameters were attained from each algorithm as  $SE_R=8.66$  dB and  $SE_A=29.35$  dB with  $T=150$  °C,  $t=8$  h, and  $C=0.08$  M/M. Besides, in this case, the obtained results are the same as the optimization problem outcomes in Table 4.6. For the same design phenomenon, the case of achieving the same results in optimization problems having different objective functions with the same conditions demonstrates the high prediction capability of the proposed models.

Furthermore, the results demonstrated that the effects of the inputs on the outputs change depending on the defined problem conditions. For example, the second scenario in Table 4.7 proves that very effective  $SE_A$  and  $SE_R$  values can be obtained at different temperatures with the same duration and molar ratio. Also, results from scenarios 1 and 2 in both Tables 4.6 and 4.7 show that the same objective values can be acquired at different production parameters.

The acquired results also demonstrate that when the objective function of the relevant problem is determined as maximizing the  $SE_A$  of the nanocomposite, considerable results up to 67 dB can be obtained with a minimum value of  $SE_R$  as far as possible. On the other hand, effective  $SE_A$  values with minimum reflection effectiveness can be achieved, as seen from scenario 1 in Table 4.6. Another significant outcome of this thesis study is that, in the optimization problems, the proposed models predicted a higher total SE of nanocomposite than that of the used experimental dataset.

As mentioned before, this interval of process parameters was identified considering the growth of  $MnO_2$  nanowires on the GF in our experimental conditions. Changing the hydrothermal process parameters according to distinct combinations in a certain interval affects the structure in various aspects (e.g., the aspect ratio of  $MnO_2$

nanowires and their homogeneous distribution on the GF structure). Accordingly, the morphological aspect of materials can be very effective on their EMI SE in several ways, such as the number of trapping centers in the structure, the electrical conductivity, permittivity and permeability characteristics of the nanocomposite. Therefore, results from the mathematical processes can give the most influential parameter combinations to obtain satisfying SE characteristics of the nanocomposite structures without needing extra raw materials and time consumption.

# Chapter 5

## Conclusion

The nanocomposite form of CVD-based GF and MnO<sub>2</sub> nanowires is promising material for a wide variety of application areas owing to their unique properties. Therefore, it is crucial to gain insight into the interaction of the morphological and crystallographic forms of MnO<sub>2</sub> nanomaterials synthesized on the CVD-based GF with hydrothermal process parameters to comprehend the process-performance relationship. Furthermore, since all production parameters in considered intervals might not be performed experimentally, the mathematical consideration of the experimental processes plays a key role in decreasing the time, cost, and raw material consumption by giving an estimation capability.

Ever-growing data science subject brings along popular data modeling algorithms to get insight into the phenomena through existing data. Additionally, great numbers of studies on adapting the relevant algorithms into engineering problem are performed. However, as mentioned in Chapter 1, available methods include some insufficient approaches in terms of complex engineering design. Therefore, this thesis is based on proposing a systematic mathematical perspective for design optimization.

In line with the aim of this thesis study, multiple nonlinear neuro-regression modeling-based optimization approach was carried out considering Graphene Foam/MnO<sub>2</sub> nanocomposite structure as EMI shielding material. Because the production parameters effect the various nanomaterials' feature through crystallographic and morphologic structure, the hydrothermal process parameters effect on the shielding effectiveness of final GF/MnO<sub>2</sub> nanocomposite were investigated. Therefore, the optimization problem was defined considering the temperature, duration, and KMnO<sub>4</sub>/HCl molar ratios as design variables, while the objective functions were identified as maximizing the SE<sub>A</sub> with minimum SE<sub>R</sub> of nanocomposite. The dataset

was obtained from the experimental studies performed within the scope of a collaborative project study (2021-GAP-MÜMF-0042) funded by İzmir Kâtip Çelebi University, Scientific Research Projects Unit.

In the modeling stage, hybrid models were proposed for each objective functions because the valid accuracy could not be achieved using standard regression models. In the optimization step, three distinct scenario was considered for each problem.

In case of considering the  $SE_A$  as objective function, significant results were attained up to 67 dB for  $SE_A$  with minimum  $SE_R$ , 8 dB. On the contrary, unsatisfying results for the physical phenomenon were estimated when objective function is considered as minimizing  $SE_R$ . However, a considerable result was still achieved from the RS algorithm in the first scenario, as 56.25 dB for  $SE_A$  and 8 dB for  $SE_R$ .

From reliability regard, achieving the same or similar results through different direct search algorithms based on independent bases of each other increases the prospect of acquiring global optimum. Moreover, considering different scenarios allows the user to evaluate alternative results. In optimization problems, the constraint conditions are defined depending on the concerned phenomenon needs and/or manufacturing process feasibility. Most cases might not enable precise control of the respective parameters, so the input intervals in continuous search space can become unpractical, even if obtaining good results through mathematical procedures. Hence, in terms of applicability, the preferred modeling approach has a vital role in obtaining a robust objective function for the optimization problems.

Furthermore, even though very effective predictions can be made via proposed methodology, it must be performed for different design processes because the concerned problem would inherently have distinct features. Therefore, the situation requirements considered elaborately. However, it is believed that the introduced methodology in this thesis study is applicable enough to utilize the materials design-concerned studies possessing controllable parameters. From this point of view, the proposed method has high potential regarding feasibility for any materials science-concerned studies since it can meet their bases as part of processing-structure-properties-performance relationships.

## References

- [1] Gupta S, Tai NH. Carbon materials and their composites for electromagnetic interference shielding effectiveness in X-band. *Carbon* 2019; 152: 159-187.
- [2] Chung DDL. Materials for electromagnetic interference shielding. *Materials Chemistry and Physics* 2020; 255: 123587.
- [3] Chung DDL. Electromagnetic interference shielding effectiveness of carbon materials. *Carbon* 2001; 39.2: 279-285. [https://doi.org/10.1016/S0008-6223\(00\)00184-6](https://doi.org/10.1016/S0008-6223(00)00184-6)
- [4] Ji H, Zhao R, Zhang N, Jin C, Lu X, Wang C. Lightweight and flexible electrospun polymer nanofiber/metal nanoparticle hybrid membrane for high-performance electromagnetic interference shielding. *NPG Asia Materials* 2018; 10(8): 749-760. <https://doi.org/10.1038/s41427-018-0070-1>
- [5] Shahzad F, Alhabeab M, Hatter CB, Anasori B, Man Hong S, Koo CM, et al. Electromagnetic interference shielding with 2D transition metal carbides (MXenes). *Science* 2016; 353(6304): 1137-1140. <https://doi.org/10.1126/science.aag2421>
- [6] Kolanowska A, Janas D, Herman AP, Jędrysiak RG, Giżewski T, Boncel S. From blackness to invisibility—carbon nanotubes role in the attenuation of and shielding from radio waves for stealth technology. *Carbon* 2015; 126: 31-52. <https://doi.org/10.1016/j.carbon.2017.09.078>
- [7] Kumar N, Dixit A. *Nanotechnology for defence applications*. Springer International Publishing; 2019.
- [8] Chen H, Ma W, Huang Z, Zhang Y, Huang Y, Chen Y. Graphene-based materials toward microwave and terahertz absorbing stealth technologies. *Advanced Optical Materials* 2019; 7(8): 1801318. <https://doi.org/10.1002/adom.201801318>
- [9] Wei H, Zhang Z, Hussain G, Zhou L, Li Q, Ostrikov KK. Techniques to enhance magnetic permeability in microwave absorbing materials. *Applied Materials Today* 2020; 19: 100596. <https://doi.org/10.1016/j.apmt.2020.100596>

- [10] Ruiz-Perez F, López-Estrada SM, Tolentino-Hernández RV, Caballero-Briones F. Carbon-based radar absorbing materials: A critical review. *Journal of Science: Advanced Materials and Devices* 2022; 100454. <https://doi.org/10.1016/j.jsamd.2022.100454>
- [11] Jia Z, Lan D, Lin K, Qin M, Kou K, Wu G, et al. Progress in low-frequency microwave absorbing materials. *Journal of Materials Science: Materials in Electronics* 2018; 29(20): 17122-17136. <https://doi.org/10.1007/s10854-018-9909-z>
- [12] Zhang L, Yu X, Hu H, Li Y, Wu M, Wang Z, et al. Facile synthesis of iron oxides/reduced graphene oxide composites: application for electromagnetic wave absorption at high temperature. *Scientific reports* 2015; 5(1): 1-9. <https://doi.org/10.1038/srep09298>
- [13] Novoselov KS, Geim AK, Morozov SV, Jiang DE, Zhang Y, Dubonos SV, et al. Electric field effect in atomically thin carbon films. *Science* 2004; 306(5696): 666-669. <https://doi.org/10.1126/science.1102896>
- [14] Chang J, Jin M, Yao F, Kim TH, Le VT, Yue H, et al. Asymmetric supercapacitors based on graphene/MnO<sub>2</sub> nanospheres and graphene/MoO<sub>3</sub> nanosheets with high energy density. *Advanced Functional Materials* 2013; 23(40): 5074-5083. <https://doi.org/10.1002/adfm.201301851>
- [15] Chen D, Wang GS, He S, Liu J, Guo L, Cao MS. Controllable fabrication of mono-dispersed RGO-hematite nanocomposites and their enhanced wave absorption properties. *Journal of Materials Chemistry A* 2013; 1(19): 5996-6003. <https://doi.org/10.1039/C3TA10664K>
- [16] Deng LJ, Gu YZ, Xu WX, Ma ZY. Preparation of TiO<sub>2</sub> nanocrystals/graphene composite and its photocatalytic performance. *Chinese Journal of Chemical Physics* 2014; 27(3): 321-326. <https://doi.org/10.1063/1674-0068/27/03/321-326>
- [17] Güneş F. A direct synthesis of Si-nanowires on 3D porous graphene as a high performance anode material for Li-ion batteries. *RSC Advances* 2016; 6(2): 1678-1685. <https://doi.org/10.1039/C5RA18353G>
- [18] Li C, Shi G. Three-dimensional graphene architectures. *Nanoscale* 2012; 4(18): 5549-5563.

- [19] Yue HY, Huang S, Chang J, Heo C, Yao F, Adhikari S, et al. ZnO Nanowire Arrays on 3D Hierarchical Graphene Foam: Biomarker Detection of Parkinson's Disease. *ACS Nano* 2014; 8(2): 1639-1646. <https://doi.org/10.1021/nn405961p>
- [20] Hadi A, Karimi-Sabet J, Moosavian SMA, Ghorbanian S. Optimization of graphene production by exfoliation of graphite in supercritical ethanol: A response surface methodology approach. *The Journal of Supercritical Fluids* 2016; 107: 92-105. <https://doi.org/10.1016/j.supflu.2015.08.022>
- [21] Güneş F, Han GH, Kim KK, Kim ES, Chae SJ, et al. Large-area graphene-based flexible transparent conducting films. *Nano* 2009; 4(02): 83-90. <https://doi.org/10.1142/S1793292009001538>
- [22] Chae SJ, Güneş F, Kim KK, Kim ES, Han GH, Kim SM, et al. Synthesis of large-area graphene layers on poly-nickel substrate by chemical vapor deposition: wrinkle formation. *Advanced Materials* 2009; 21(22): 2328-2333. <https://doi.org/10.1002/adma.200803016>
- [23] Zhu Y, Murali S, Cai W, Li X, Suk JW, Potts JR, et al. Graphene and graphene oxide: synthesis, properties, and applications. *Advanced Materials* 2010; 22(35): 3906-3924. <https://doi.org/10.1002/adma.201001068>
- [24] Güneş F, Aykaç A, Erol M, Erdem Ç, Hano H, Uzunbayir B. Synthesis of hierarchical hetero-composite of graphene foam/ $\alpha$ -Fe<sub>2</sub>O<sub>3</sub> nanowires and its application on glucose biosensors. *Journal of Alloys and Compounds* 2022; 895: 162688.
- [25] Mattevi C, Kim H, Chhowalla M. A review of chemical vapour deposition of graphene on copper. *Journal of Materials Chemistry* 2011; 21(10): 3324-3334.
- [26] Chen X, Zhang L, Chen S. Large area CVD growth of graphene. *Synthetic Metals* 2015; 210: 95-108.
- [27] Liang J, Wang Y, Huang Y, Ma Y, Liu Z, Cai J, et al. Electromagnetic interference shielding of graphene/epoxy composites. *Carbon* 2009; 47(3): 922-925. <https://doi.org/10.1016/j.carbon.2008.12.038>
- [28] Wen B, Wang XX, Cao WQ, Shi HL, Lu MM, Wang G, et al. Reduced graphene oxides: the thinnest and most lightweight materials with highly efficient microwave attenuation performances of the carbon world. *Nanoscale* 2014; 6(11): 5754-5761. <https://doi.org/10.1039/C3NR06717C>



- [29] Shu R, Zhang J, Guo C, Wu Y, Wan Z, Shi J, et al. Facile synthesis of nitrogen-doped reduced graphene oxide/nickel-zinc ferrite composites as high-performance microwave absorbers in the X-band. *Chemical Engineering Journal* 2020; 384: 123266. <https://doi.org/10.1016/j.cej.2019.123266>
- [30] Dong S, Zhang X, Li X, Chen J, Hu P, Han J. SiC whiskers-reduced graphene oxide composites decorated with MnO nanoparticles for tunable microwave absorption. *Chemical Engineering Journal* 2020; 392: 123817. <https://doi.org/10.1016/j.cej.2019.123817>
- [31] Zhang H, Xie A, Wang C, Wang H, Shen Y, Tian X. Novel rGO/ $\alpha$ -Fe<sub>2</sub>O<sub>3</sub> composite hydrogel: synthesis, characterization and high performance of electromagnetic wave absorption. *Journal of Materials Chemistry A* 2013; 1(30): 8547-52. <https://doi.org/10.1039/C3TA11278K>
- [32] Song C, Yin X, Han M, Li X, Hou Z, Zhang L et al. Three-dimensional reduced graphene oxide foam modified with ZnO nanowires for enhanced microwave absorption properties. *Carbon* 2017; 116: 50-8. <https://doi.org/10.1016/j.carbon.2017.01.077>
- [33] Fang H, Guo H, Hu Y, Ren Y, Hsu PC, Bai SL. In-situ grown hollow Fe<sub>3</sub>O<sub>4</sub> onto graphene foam nanocomposites with high EMI shielding effectiveness and thermal conductivity. *Composites Science and Technology* 2020; 188: 107975. <https://doi.org/10.1016/j.compscitech.2019.107975>
- [34] Julien CM, Mauger A. Nanostructured MnO<sub>2</sub> as electrode materials for energy storage. *Nanomaterials* 2017; 7(11): 396.
- [35] Sohal N, Maity B, Shetti NP, Basu S. Biosensors based on MnO<sub>2</sub> nanostructures: A review. *ACS Applied Nano Materials* 2021; 4(3): 2285-2302. <https://dx.doi.org/10.1021/acsanm.0c03380>
- [36] Lan B, Sun M, Lin T, Cheng G, Yu L, Peng S, et al. Ultra-long  $\alpha$ -MnO<sub>2</sub> nanowires: control synthesis and its absorption activity. *Materials Letters* 2014; 121: 234-237. <http://dx.doi.org/10.1016/j.matlet.2014.01.055>
- [37] Ong YP, Ho LN, Ong SA, Banjuraizah J, Ibrahim AH, Thor SH, et al. A highly sustainable hydrothermal synthesized MnO<sub>2</sub> as cathodic catalyst in solar photocatalytic fuel cell. *Chemosphere* 2021; 263: 128212. <https://doi.org/10.1016/j.chemosphere.2020.128212>

- [38] Wu X, Yang F, Dong H, Sui J, Zhang Q, Yu J, et al. Controllable synthesis of MnO<sub>2</sub> with different structures for supercapacitor electrodes. *Journal of Electroanalytical Chemistry* 2019; 848: 113332. <https://doi.org/10.1016/j.jelechem.2019.113332>
- [39] Ma J, Zhang Y, Yuan M, Nan, C. Li Ion Exchanged  $\alpha$ -MnO<sub>2</sub> Nanowires as Efficient Catalysts for Li-O<sub>2</sub> Batteries. *Chemical Research in Chinese Universities* 2020; 36(6): 1261-1264. <https://doi.org/10.1007/s40242-020-0077-3>
- [40] Portehault D, Cassaignon S, Baudrin E, Jolivet JP. Morphology control of cryptomelane type MnO<sub>2</sub> nanowires by soft chemistry. Growth mechanisms in aqueous medium. *Chemistry of Materials* 2007; 19(22): 5410-5417. <https://doi.org/10.1021/cm071654a>
- [41] Guan H, Chen G, Zhang S, Wang Y. Microwave absorption characteristics of manganese dioxide with different crystalline phase and nanostructures. *Materials Chemistry and Physics* 2010; 124(1): 639-645. <https://doi.org/10.1016/j.matchemphys.2010.07.027>
- [42] He G, Duan Y, Pang H, Zhang X. Rational design of mesoporous MnO<sub>2</sub> microwave absorber with tunable microwave frequency response. *Applied Surface Science* 2019; 490: 372-382. <https://doi.org/10.1016/j.apsusc.2019.06.037>
- [43] Ding B, Zheng P, Ma PA, Lin J. Manganese oxide nanomaterials: synthesis, properties, and theranostic applications. *Advanced Materials* 2020; 32(10): 1905823. <https://doi.org/10.1002/adma.201905823>
- [44] Song H, Xu L, Chen M, Cui Y, Wu CE, Qiu J, et al. Recent progresses in the synthesis of MnO<sub>2</sub> nanowire and its application in environmental catalysis. *RSC Advances* 2021; 11(56): 35494-35513. <https://doi.org/10.1039/D1RA06497E>
- [45] Song L, Duan Y, Liu J, Pang H. Insight into electromagnetic absorbing performance of MnO<sub>2</sub> from two dimensions: Crystal structure and morphology design. *Materials Characterization* 2020; 163: 110300. <https://doi.org/10.1016/j.matchar.2020.110300>
- [46] Hu J, Shen Y, Xu L, Liu Y. Facile preparation of flower-like MnO<sub>2</sub>/reduced graphene oxide (RGO) nanocomposite and investigation of its microwave

- absorption performance. *Chemical Physics Letters* 2020; 739: 136953.  
<https://doi.org/10.1016/j.cplett.2019.136953>
- [47] Mondal J, Srivastava SK.  $\delta$ -MnO<sub>2</sub> nanoflowers and their reduced graphene oxide nanocomposites for electromagnetic interference shielding. *ACS Applied Nano Materials* 2020; 3(11): 11048-11059.
- [48] Zhang Z, Wang S, Lv Y, Chen X, Wu Z, Zou Y. MnO<sub>2</sub> nanostructures deposited on graphene foams for broadband and lightweight electromagnetic absorption. *Journal of Alloys and Compounds* 2019; 810: 151744.  
<https://doi.org/10.1016/j.jallcom.2019.151744>
- [49] Gupta TK, Singh BP, Singh VN, Teotia S, Singh AP, Elizabeth I, et al. MnO<sub>2</sub> decorated graphene nanoribbons with superior permittivity and excellent microwave shielding properties. *Journal of Materials Chemistry A* 2014; 2(12): 4256-4263. <https://doi.org/10.1039/C3TA14854H>
- [50] Li C, Ge Y, Jiang X, Waterhouse GI, Zhang Z, Yu L. Porous Fe<sub>3</sub>O<sub>4</sub>/C microspheres for efficient broadband electromagnetic wave absorption. *Ceramics International* 2018; 44(16): 19171-83.  
<https://doi.org/10.1016/j.ceramint.2018.06.264>
- [51] Singh SK, Akhtar MJ, Kar KK. Impact of Al<sub>2</sub>O<sub>3</sub>, TiO<sub>2</sub>, ZnO and BaTiO<sub>3</sub> on the microwave absorption properties of exfoliated graphite/epoxy composites at X-band frequencies. *Composites Part B: Engineering* 2019; 167: 135-46.
- [52] Gao Y, Wang C, Li J, Guo S. Adjustment of dielectric permittivity and loss of graphene/thermoplastic polyurethane flexible foam: Towards high microwave absorbing performance. *Composites Part A: Applied Science and Manufacturing* 2019; 117: 65-75. <https://doi.org/10.1016/j.compositesa.2018.10.036>
- [53] Wei J, Chu X, Sun XY, Xu K, Deng HX, Chen J, et al. Machine learning in materials science. *InfoMat* 2019; 1(3): 338-58.  
<https://doi.org/10.1002/inf2.12028>
- [54] Himanen L, Geurts A, Foster AS, Rinke P. Data-driven materials science: status, challenges, and perspectives. *Advanced Science* 2019; 6(21): 1900808.  
<https://doi.org/10.1002/advs.201900808>
- [55] Rhone TD, Chen W, Desai S, Torrisi SB, Larson DT, Yacoby A, et al. Data-driven studies of magnetic two-dimensional materials. *Scientific Reports* 2020; 10(1): 1-1. <https://doi.org/10.1038/s41598-020-72811-z>

- [56] He Y, Gong R, Nie Y, He H, Zhao Z. Optimization of two-layer electromagnetic wave absorbers composed of magnetic and dielectric materials in gigahertz frequency band. *Journal of Applied Physics* 2005; 98(8): 084903. <https://doi.org/10.1063/1.2108158>
- [57] Dorraji MS, Rasoulifard MH, Amani-Ghadim AR, Khodabandeloo MH, Felekari M, Khoshrou MR, et al. Microwave absorption properties of polypyrrole-SrFe<sub>12</sub>O<sub>19</sub>-TiO<sub>2</sub>-epoxy resin nanocomposites: Optimization using response surface methodology. *Applied Surface Science* 2016; 383: 9-18. <https://doi.org/10.1016/j.apsusc.2016.04.108>
- [58] Huang Y, Fan Q, Chen J, Li L, Chen M, Tang L, et al. Optimization of flexible multilayered metastructure fabricated by dielectric-magnetic nano lossy composites with broadband microwave absorption. *Composites Science and Technology* 2020; 191:108066. <https://doi.org/10.1016/j.compscitech.2020.108066>
- [59] Green M, Tran AT, Chen X. Obtaining strong, broadband microwave absorption of polyaniline through data-driven materials discovery. *Advanced Materials Interfaces* 2020; 7(18): 2000658.
- [60] Green M, Tran AT, Chen X. Realizing maximum microwave absorption of poly(3, 4-ethylenedioxythiophene) with a data-driven method. *ACS Applied Electronic Materials* 2020; 2(9): 2937-2944.
- [61] Guan ZJ, Li R, Jiang JT, Song B, Gong YX, Zhen L. Data mining and design of electromagnetic properties of Co/FeSi filled coatings based on genetic algorithms optimized artificial neural networks (GA-ANN). *Composites Part B: Engineering* 2021; 226: 109383. <https://doi.org/10.1016/j.compositesb.2021.109383>
- [62] Baek SM, Lee WJ. Design method for radar absorbing structures using reliability-based design optimization of the composite material properties. *Composite Structures* 2021; 262: 113559.
- [63] Darvishzadeh A, Nasouri K. Manufacturing, modeling, and optimization of nickel-coated carbon fabric for highly efficient EMI shielding. *Surface and Coatings Technology* 2021; 409: 126957.
- [64] Nasouri K, Shoushtari AM. Designing, modeling and manufacturing of lightweight carbon nanotubes/polymer composite nanofibers for

- electromagnetic interference shielding application. *Composites Science and Technology* 2017; 145: 46-54.
- [65] Sidi Salah L, Chouai M, Danlée Y, Huynen I, Ouslimani N. Simulation and optimization of electromagnetic absorption of polycarbonate/CNT composites using machine learning. *Micromachines* 2020; 11(8): 778. <https://doi.org/10.3390/mi11080778>
- [66] Green M, Van Tran AT, Chen X. Maximizing the microwave absorption performance of polypyrrole by data-driven discovery. *Composites Science and Technology* 2020; 199: 108332.
- [67] Toktas A, Ustun D, Tekbas M. Multi-objective design of multi-layer radar absorber using surrogate-based optimization. *IEEE Transactions on Microwave Theory and Techniques* 2019; 67(8): 3318-29.
- [68] Polatoğlu İ, Aydın L. A new design strategy with stochastic optimization on the preparation of magnetite cross-linked tyrosinase aggregates (MCLTA). *Process Biochemistry* 2020; 99: 131-8.
- [69] Polatoğlu İ, Aydın L, Nevruz BÇ, Özer S. A novel approach for the optimal design of a biosensor. *Analytical Letters* 2020; 53(9): 1428-45. <https://doi.org/10.1080/00032719.2019.1709075>
- [70] Aydın L, Artem HS, Oterkus S. (Ed.) *Designing Engineering Structures using Stochastic Optimization Methods*, 1st ed. CRC Press; 2020. <https://doi.org/10.1201/9780429289576>
- [71] Ceylan AB, Aydın L, Nil M, Mamur H, Polatoğlu İ, Sözen H. A new hybrid approach in selection of optimum establishment location of the biogas energy production plant. *Biomass Conversion and Biorefinery* 2021; 1-16. <https://doi.org/10.1007/s13399-021-01532-8>
- [72] Aydın KB, Aydın L, Güneş F. Modeling and Optimum Design of Carbon Nanotube/Polyvinyl Alcohol Hybrid Nanofibers as Electromagnetic Interference Shielding Material. *Integrating Materials and Manufacturing Innovation* 2022; 11: 391–406. <https://doi.org/10.1007/s40192-022-00270-7>
- [73] Antony J. *Design of Experiments for Engineers and Scientists*. 2nd ed. Elsevier; 2014.
- [74] Vecchio RD. *Understanding Design of Experiments: a Primer for Technologists*. Hanser/Gardner Publications, Inc., Cincinnati; 1997.

- [75] Cavazzuti M. Optimization Methods: from Theory to Design Scientific and Technological Aspects in Mechanics. Springer Science & Business Media; 2012.
- [76] Antony J. Some Key Things Industrial Engineers Should Know About Experimental Design. Logistics Information Management; 1998.
- [77] Montgomery DC, Runger GC, Hubele NF. Engineering Statistics. 5th ed. John Wiley & Sons; 2009.
- [78] Gunst RF, Mason RL. How to Construct Fractional Factorial Experiments. ASQC Quality Press; 1991.
- [79] Montgomery DC. Design and Analysis of Experiments. 8th ed. John Wiley & Sons; 2017.
- [80] Turhan, F. 1100 serisi alüminyum malzemelerde tig kaynağı ile oluşan kaynak dikiş geometrisinin optimizasyonu (master's thesis). İzmir: İzmir Katip Çelebi University Fen Bilimleri Enstitüsü; 2017. <https://tez.yok.gov.tr/>
- [81] Aydın L, Artem HS. Comparison of stochastic search optimization algorithms for the laminated composites under mechanical and hygrothermal loadings. Journal of Reinforced Plastics and Composites. 2011; 30(14):1197-212.
- [82] Savran, M. Development of vibration performances of hybrid laminated composite materials by using stochastic methods (master's thesis). İzmir: İzmir Katip Çelebi University Fen Bilimleri Enstitüsü; 2017. <https://tez.yok.gov.tr/>
- [83] Pelletier JL, Vel SS. Multi-objective optimization of fiber reinforced composite laminates for strength, stiffness and minimal mass. Computers & Structures. 2006; 84(29-30):2065-80.
- [84] Rao SS. Engineering optimization: theory and practice. 4th ed. John Wiley & Sons; 2019.
- [85] Rao RV, Savsani VJ. Mechanical design optimization using advanced optimization techniques. Springer; 2012.
- [86] Ombach J. A Short Introduction to Stochastic Optimization. Schedae Informaticae 2014; 23. <https://doi.org/10.4467/20838476SI.14.001.3018>
- [87] Karaboğa D. Yapay Zeka Optimizasyon Algoritmaları. Nobel Akademik Yayıncılık; 2014.

- [88] Ozturk S, Aydin L, Celik E. A comprehensive study on slicing processes optimization of silicon ingot for photovoltaic applications. *Solar Energy* 2018; 161:109-24.
- [89] Grabusts P, Musatovs J, Golenkov V. The application of simulated annealing method for optimal route detection between objects. *Procedia Computer Science* 2019; 149:95-101.
- [90] Aydin L, Artem HS. Design and optimization of fiber composites. Ed.: Seydibeyoğlu MÖ, Amar KH, Misra M. *Fiber Technology for Fiber-Reinforced Composites*. Woodhead Publishing; 2017. 299-315.
- [91] Storn R, Price K. Minimizing the real functions of the ICEC'96 contest by differential evolution. In *Proceedings of IEEE international conference on evolutionary computation*; 1996 May 20; 842-844.
- [92] Das S, Suganthan PN. Differential evolution: A survey of the state-of-the-art. *IEEE Transactions on Evolutionary Computation* 2010; 15(1):4-31.
- [93] Satya Eswari J, Venkateswarlu C. Dynamic modeling and metabolic flux analysis for optimized production of rhamnolipids. *Chemical Engineering Communications* 2016; 203(3):326-38.
- [94] Arunachalam, V. Optimization using Differential Evolution (master's thesis). London: The University of Western Ontario; 2008.
- [95] Nelder JA, Mead R. A simplex method for function minimization. *The Computer Journal*. 1965; 7(4):308-13.
- [96] Fan SK, Liang YC, Zahara E. A genetic algorithm and a particle swarm optimizer hybridized with Nelder–Mead simplex search. *Computers & industrial engineering*. 2006; 50(4):401-25.
- [97] Horst R, Hoang, T. *Global Optimization: Deterministic Approaches*, 3rd Edition, Springer-Verlag, Berlin; 1996.
- [98] Horst R, Pardalos PM, *Handbook of Global Optimization*, Kluwer Academic Publishers, Netherlands; 1995.
- [99] Pardalos PM, Romeijn HE. *Handbook of Global Optimization, Volume 2*, Springer New York, NY; 2002.
- [100] Zabinsky ZB. *Random search algorithms*. Department of Industrial and Systems Engineering, University of Washington, USA 2009.

- [101] Savran M, Sayi H, Aydin L. *Mathematica and optimization*. Ed.: Aydin L, Artem HS, Oterkus S. Designing engineering structures using stochastic optimization methods. CRC Press; 2020. 24-43.
- [102] Jamil M, Yang XS, Zepernick HJ. (2013). Test functions for global optimization: a comprehensive survey. Ed.: Yang XS, Cui Z, Xiao R, Gandomi AH, Karamanoglu M. *Swarm intelligence and bio-inspired computation: theory and applications*. Newnes; 2013. 193-222.
- [103] Ingber L. Simulated annealing: practice versus theory. *Mathematical and Computer Modelling* 1993; 18(11): 29-57. [https://doi.org/10.1016/0895-7177\(93\)90204-C](https://doi.org/10.1016/0895-7177(93)90204-C)
- [104] Vo-Duy T, Ho-Huu V, Do-Thi TD, Dang-Trung H, Nguyen-Thoi T. A global numerical approach for lightweight design optimization of laminated composite plates subjected to frequency constraints. *Composite Structures* 2017; 159: 646-655. <https://doi.org/10.1016/j.compstruct.2016.09.059>
- [105] Aydın KB, Aydin L, Güneş F. Stochastic Optimization of TiO<sub>2</sub>-Graphene Nanocomposite by Using Neuro-Regression Approach for Maximum Photocatalytic Degradation Rate. *ISSC2021: Proceedings of the 5th International Students Science Congress*; 2021 May 21-22; Izmir, Turkey. 345-351.
- [106] Fattahi A, Liang R, Kaur A, Schneider O, Arlos MJ, Peng P, *et al.* Photocatalytic degradation using TiO<sub>2</sub>-graphene nanocomposite under UV-LED illumination: Optimization using response surface methodology. *Journal of Environmental Chemical Engineering* 2019; 7(5):103366. <https://doi.org/10.1016/j.jece.2019.103366>



# Appendices

# Appendix A

## Traditional Regression Model Forms Obtained for Each Output

$$L1 = 11.5353 - 0.00143494 x_1 - 0.137192 x_2 - 5.03046 x_3$$

$$LR1 = (13.3846 - 0.0958014 x_1 + 0.369965 x_2 - 4.37463 x_3)/(1.36354 - 0.0101025 x_1 + 0.042065 x_2 - 0.276936 x_3)$$

$$SON1 = 7.521 + 0.0230394 x_1 - 0.0000223909 x_1^2 + 0.293349 x_2 - 0.00288939 x_1 x_2 - 0.00601727 x_2^2 + 1.59207 x_3 + 0.0999399 x_1 x_3 + 0.983936 x_2 x_3 - 117.787 x_3^2$$

$$SONR1 = (32595.8 + 1.04658 * 10^7 x_1 + 1.58761 * 10^7 x_1^2 + 9.40566 * 10^6 x_2 + 1.98094 * 10^8 x_1 x_2 + 3.99786 * 10^7 x_2^2 - 393477. x_3 - 3.34183 * 10^7 x_1 x_3 + 341209. x_2 x_3 - 27015.1 x_3^2)/(-245901. - 7.74532 * 10^7 x_1 + 467499. x_1^2 - 7.35794 * 10^7 x_2 + 6.69771 * 10^7 x_1 x_2 - 3.13402 * 10^8 x_2^2 + 4.06779 * 10^6 x_3 + 3.64731 * 10^8 x_1 x_3 + 1.54575 * 10^6 x_2 x_3 + 278019. x_3^2)$$

$$FOTN1 = 2.54011 - 5.59775 \text{Cos}[x_1] + 3.5402 \text{Cos}[x_2] + 2.6306 \text{Cos}[x_3] + 1.29119 \text{Sin}[x_1] + 1.59967 \text{Sin}[x_2] - 4.72293 \text{Sin}[x_3]$$

$$FOTNR1 = (-1.42217 * 10^9 + 4.16495 * 10^9 \text{Cos}[x_1] - 1.51965 * 10^9 \text{Cos}[x_2] - 1.36443 * 10^9 \text{Cos}[x_3] + 1.58737 * 10^{10} \text{Sin}[x_1] + 5.6623 * 10^7 \text{Sin}[x_2] - 4.98881 * 10^8 \text{Sin}[x_3])/(-2.38404 * 10^9 + 3.05625 * 10^9 \text{Cos}[x_1] - 1.77479 * 10^9 \text{Cos}[x_2] - 2.64413 * 10^9 \text{Cos}[x_3] + 9.15519 * 10^9 \text{Sin}[x_1] + 1.80315 * 10^9 \text{Sin}[x_2] + 1.7911 * 10^9 \text{Sin}[x_3])$$

$$\begin{aligned}
SOTN1 = & 0.886571 - 1.68926 \cos[x1] + 2.07224 \cos[x1]^2 + \\
& 1.17636 \cos[x2] - 2.19985 \cos[x1] \cos[x2] + 1.49666 \cos[x2]^2 + \\
& 0.916279 \cos[x3] - 1.72678 \cos[x1] \cos[x3] + 1.22247 \cos[x2] \cos[x3] + \\
& 0.946317 \cos[x3]^2 + 0.650879 \sin[x1] - 0.527579 \cos[x1] \sin[x1] + \\
& 0.895095 \cos[x2] \sin[x1] + 0.687137 \cos[x3] \sin[x1] + 1.05714 \sin[x1]^2 - \\
& 0.0267343 \sin[x2] + 0.461293 \cos[x1] \sin[x2] - 0.459445 \cos[x2] \sin[x2] + \\
& 0.0292193 \cos[x3] \sin[x2] + 0.290978 \sin[x1] \sin[x2] - 2.89767 \sin[x2]^2 - \\
& 1.03979 \sin[x3] - 4.21364 \cos[x1] \sin[x3] - 3.14717 \cos[x2] \sin[x3] - \\
& 0.968275 \cos[x3] \sin[x3] - 5.45237 \sin[x1] \sin[x3] - \\
& 21.6817 \sin[x2] \sin[x3] - 23.4097 \sin[x3]^2
\end{aligned}$$

$$\begin{aligned}
SOTNR1 = & (-1.19906 * 10^{11} + 3.78753 * 10^{11} \cos[x1] - 6.12028 * \\
& 10^{10} \cos[x1]^2 - 4.32779 * 10^{11} \cos[x2] + 3.45022 * \\
& 10^{11} \cos[x1] \cos[x2] - 9.80331 * 10^{10} \cos[x2]^2 - 4.72371 * \\
& 10^{11} \cos[x3] + 3.73637 * 10^{11} \cos[x1] \cos[x3] - 4.2651 * \\
& 10^{11} \cos[x2] \cos[x3] - 1.16315 * 10^{11} \cos[x3]^2 + 7.92053 * \\
& 10^{11} \sin[x1] - 3.84107 * 10^{11} \cos[x1] \sin[x1] + 7.29197 * \\
& 10^{11} \cos[x2] \sin[x1] + 7.82796 * 10^{11} \cos[x3] \sin[x1] - 5.87031 * \\
& 10^{10} \sin[x1]^2 + 1.95346 * 10^{11} \sin[x2] - 1.47051 * \\
& 10^{11} \cos[x1] \sin[x2] + 1.7268 * 10^{11} \cos[x2] \sin[x2] + 1.91784 * \\
& 10^{11} \cos[x3] \sin[x2] - 2.90531 * 10^{11} \sin[x1] \sin[x2] - 2.18728 * \\
& 10^{10} \sin[x2]^2 - 7.82903 * 10^{10} \sin[x3] + 5.73232 * \\
& 10^{10} \cos[x1] \sin[x3] - 6.86185 * 10^{10} \cos[x2] \sin[x3] - 7.68912 * \\
& 10^{10} \cos[x3] \sin[x3] + 1.09273 * 10^{11} \sin[x1] \sin[x3] + 3.63642 * \\
& 10^{10} \sin[x2] \sin[x3] - 3.59128 * 10^9 \sin[x3]^2) / (-9.71461 * 10^{10} + \\
& 2.9054 * 10^{11} \cos[x1] - 4.63368 * 10^{10} \cos[x1]^2 - 3.52763 * \\
& 10^{11} \cos[x2] + 2.60745 * 10^{11} \cos[x1] \cos[x2] - 8.03865 * \\
& 10^{10} \cos[x2]^2 - 3.85668 * 10^{11} \cos[x3] + 2.87838 * \\
& 10^{11} \cos[x1] \cos[x3] - 3.44183 * 10^{11} \cos[x2] \cos[x3] - 9.56995 * \\
& 10^{10} \cos[x3]^2 + 5.69145 * 10^{11} \sin[x1] - 2.83769 * \\
& 10^{11} \cos[x1] \sin[x1] + 5.03289 * 10^{11} \cos[x2] \sin[x1] + 5.62555 * \\
& 10^{11} \cos[x3] \sin[x1] - 5.08093 * 10^{10} \sin[x1]^2 + 1.53553 * \\
& 10^{11} \sin[x2] - 1.21468 * 10^{11} \cos[x1] \sin[x2] + 1.36521 *
\end{aligned}$$

$$10^{11} \cos[x_2] \sin[x_2] + 1.65518 * 10^{11} \cos[x_3] \sin[x_2] - 2.54507 * 10^{11} \sin[x_1] \sin[x_2] - 1.67596 * 10^{10} \sin[x_2]^2 - 4.16425 * 10^{10} \sin[x_3] + 3.49748 * 10^{10} \cos[x_1] \sin[x_3] - 8.14852 * 10^{10} \cos[x_2] \sin[x_3] - 4.11503 * 10^{10} \cos[x_3] \sin[x_3] + 7.80625 * 10^{10} \sin[x_1] \sin[x_3] - 8.01173 * 10^{10} \sin[x_2] \sin[x_3] - 1.44653 * 10^9 \sin[x_3]^2)$$

$$FOLN1 = 11.759 - 0.228389 \log[x_1] - 1.18755 \log[x_2] - 0.622925 \log[x_3]$$

$$FOLNR1 = (1371.18 - 118786. \log[x_1] + 216733. \log[x_2] - 101961. \log[x_3]) / (-8918.12 - 11126.2 \log[x_1] + 24329.3 \log[x_2] - 10324.7 \log[x_3])$$

$$SOLN1 = -4.00089 + 2.01248 \log[x_1] + 0.965765 \log[x_1]^2 + 1.80241 \log[x_2] - 1.99022 \log[x_1] \log[x_2] + 2.22921 \log[x_2]^2 - 4.0979 \log[x_3] + 3.28405 \log[x_1] \log[x_3] + 1.05468 \log[x_2] \log[x_3] + 3.5837 \log[x_3]^2$$

$$SOLNR1 = (19888.4 + 534928. \log[x_1] + 844971. \log[x_1]^2 + 354886. \log[x_2] + 1.52099 * 10^6 \log[x_1] \log[x_2] + 290885. \log[x_2]^2 - 299945. \log[x_3] - 973138. \log[x_1] \log[x_3] - 505989. \log[x_2] \log[x_3] + 234980. \log[x_3]^2) / (120332. + 1.05746 * 10^6 \log[x_1] - 408658. \log[x_1]^2 - 273931. \log[x_2] + 836878. \log[x_1] \log[x_2] - 828633. \log[x_2]^2 + 755219. \log[x_3] - 1.0446 * 10^6 \log[x_1] \log[x_3] - 702414. \log[x_2] \log[x_3] - 1.32095 * 10^6 \log[x_3]^2)$$

$$FOEN1 = 14.8728 - 8.90472 * 10^{-10} E^{(0.1 x_1)} - 5.07018 * 10^{-6} E^{x_2} - 4.3921 E^{x_3}$$

$$FOENR1 = (1.96044 * 10^7 + 102897. E^{(0.1 x_1)} + 2.42599 * 10^8 E^{x_2} + 1.29338 * 10^7 E^{x_3}) / (-1.87716 * 10^8 + 10496.5 E^{(0.1 x_1)} + 2.66814 * 10^7 E^{x_2} - 1.23906 * 10^8 E^{x_3})$$

$$SOEN1 = 13.2886 + 9.95255 * 10^{-9} E^{(0.1 x_1)} - 1.49075 * 10^{-17} E^{(0.2 x_1)} - 0.0000194884 E^{x_2} - 1.22525 * 10^{-10} E^{(2 x_2)} -$$

$$1.13984 * 10^{\dots} - 13 E^{(0.1 x1 + x2)} + 2.7418 E^{x3} - 5.1281 E^{(2 x3)} + 2.11787 * 10^{\dots} - 9 E^{(0.1 x1 + x3)} + 0.0000317487 E^{(x2 + x3)}$$

$$SOENR1 = (1.08006 + 378205. E^{(0.1 x1)} + 2.0972 * 10^8 E^{(0.2 x1)} + 1653.03 E^{x2} + 6.2088 * 10^7 E^{(2 x2)} + 6.7891 * 10^7 E^{(0.1 x1 + x2)} + 2.23283 E^{x3} + 1.02865 E^{(2 x3)} + 273317. E^{(0.1 x1 + x3)} - 3907.42 E^{(x2 + x3)}) / (0.238536 - 3.59707 * 10^6 E^{(0.1 x1)} + 2.19455 * 10^7 E^{(0.2 x1)} - 15111.3 E^{x2} - 5.66467 * 10^8 E^{(2 x2)} + 9.28326 * 10^7 E^{(0.1 x1 + x2)} - 0.225891 E^{x3} + 0.720992 E^{(2 x3)} - 2.61312 * 10^6 E^{(0.1 x1 + x3)} + 35808.1 E^{(x2 + x3)})$$

$$L2 = 37.7458 - 0.239738 x1 + 1.21893 x2 + 84.6594 x3$$

$$LR2 = (4.33801 * 10^7 + 1.04446 * 10^9 x1 + 3.63882 * 10^7 x2 + 4.34938 * 10^7 x3) / (-8.47869 * 10^8 + 7.67826 * 10^7 x1 - 3.82944 * 10^8 x2 - 1.12546 * 10^9 x3)$$

$$SON2 = 19.8069 + 0.0481983 x1 - 0.000216207 x1^2 + 0.0648245 x2 + 0.000278626 x1 x2 - 0.119924 x2^2 + 30.6067 x3 - 0.811006 x1 x3 + 22.9276 x2 x3 - 113.022 x3^2$$

$$SONR2 = (840562. + 3.03201 * 10^8 x1 + 3.07393 * 10^9 x1^2 + 1.78486 * 10^7 x2 + 5.93576 * 10^8 x1 x2 + 1.97985 * 10^7 x2^2 + 2.03089 * 10^6 x3 + 2.70325 * 10^8 x1 x3 + 2.06764 * 10^7 x2 x3 + 125318. x3^2) / (-1.61451 * 10^7 - 5.08257 * 10^9 x1 + 2.50566 * 10^8 x1^2 - 3.36806 * 10^8 x2 - 1.14631 * 10^9 x1 x2 - 3.53178 * 10^8 x2^2 - 5.11783 * 10^7 x3 - 6.8554 * 10^9 x1 x3 - 5.40593 * 10^8 x2 x3 - 3.2285 * 10^6 x3^2)$$

$$FOTN2 = 0.867741 + 3.55931 Cos[x1] - 1.65152 Cos[x2] + 0.629997 Cos[x3] + 4.58265 Sin[x1] - 27.6931 Sin[x2] + 85.5825 Sin[x3]$$

$$FOTNR2 = (-1.02431 * 10^9 + 1.20758 * 10^9 Cos[x1] - 8.34399 * 10^8 Cos[x2] - 9.91948 * 10^8 Cos[x3] + 3.46424 * 10^9 Sin[x1] + 6.15883 * 10^8 Sin[x2] - 2.91461 * 10^8 Sin[x3]) / (-8.78095 * 10^7 + 1.024 * 10^8 Cos[x1] - 7.42341 * 10^7 Cos[x2] - 8.40999 * 10^7 Cos[x3] + 2.91992 * 10^8 Sin[x1] + 4.68161 * 10^7 Sin[x2] - 3.18696 * 10^7 Sin[x3])$$

$$\begin{aligned}
SOTN2 = & 1.80032 - 2.71109 \cos[x1] + 2.30504 \cos[x1]^2 + \\
& 2.87851 \cos[x2] - 3.89364 \cos[x1] \cos[x2] + 4.10302 \cos[x2]^2 + \\
& 1.88869 \cos[x3] - 2.87327 \cos[x1] \cos[x3] + 3.14924 \cos[x2] \cos[x3] + \\
& 1.97834 \cos[x3]^2 + 1.86609 \sin[x1] - 2.80047 \cos[x1] \sin[x1] + \\
& 3.31754 \cos[x2] \sin[x1] + 1.93566 \cos[x3] \sin[x1] + 2.25734 \sin[x1]^2 + \\
& 4.77977 \sin[x2] - 2.84386 \cos[x1] \sin[x2] + 3.64954 \cos[x2] \sin[x2] + \\
& 6.24746 \cos[x3] \sin[x2] + 8.25001 \sin[x1] \sin[x2] - 22.107 \sin[x2]^2 - \\
& 11.2136 \sin[x3] + 26.3314 \cos[x1] \sin[x3] - 57.2579 \cos[x2] \sin[x3] - \\
& 11.1271 \cos[x3] \sin[x3] - 4.47435 \sin[x1] \sin[x3] - \\
& 513.298 \sin[x2] \sin[x3] - 116.107 \sin[x3]^2
\end{aligned}$$

$$\begin{aligned}
SOTNR2 = & (-5.33047 * 10^9 + 1.65735 * 10^{10} \cos[x1] - 2.66822 * \\
& 10^9 \cos[x1]^2 - 1.88534 * 10^{10} \cos[x2] + 1.49222 * \\
& 10^{10} \cos[x1] \cos[x2] - 4.18403 * 10^9 \cos[x2]^2 - 2.09546 * \\
& 10^{10} \cos[x3] + 1.63554 * 10^{10} \cos[x1] \cos[x3] - 1.85046 * \\
& 10^{10} \cos[x2] \cos[x3] - 5.14861 * 10^9 \cos[x3]^2 + 3.40367 * \\
& 10^{10} \sin[x1] - 1.66317 * 10^{10} \cos[x1] \sin[x1] + 3.12854 * \\
& 10^{10} \cos[x2] \sin[x1] + 3.375 * 10^{10} \cos[x3] \sin[x1] - 2.66225 * \\
& 10^9 \sin[x1]^2 + 9.53746 * 10^9 \sin[x2] - 6.82217 * 10^9 \cos[x1] \sin[x2] + \\
& 8.28876 * 10^9 \cos[x2] \sin[x2] + 9.42642 * 10^9 \cos[x3] \sin[x2] - 1.25958 * \\
& 10^{10} \sin[x1] \sin[x2] - 1.14643 * 10^9 \sin[x2]^2 - 3.81103 * \\
& 10^9 \sin[x3] + 2.46615 * 10^9 \cos[x1] \sin[x3] - 3.5472 * \\
& 10^9 \cos[x2] \sin[x3] - 3.7391 * 10^9 \cos[x3] \sin[x3] + 3.87758 * \\
& 10^9 \sin[x1] \sin[x3] + 1.31258 * 10^9 \sin[x2] \sin[x3] - 1.81853 * \\
& 10^8 \sin[x3]^2) / (-3.31829 * 10^9 + 9.87013 * 10^9 \cos[x1] - 1.572 * \\
& 10^9 \cos[x1]^2 - 1.20891 * 10^{10} \cos[x2] + 8.91928 * \\
& 10^9 \cos[x1] \cos[x2] - 2.76365 * 10^9 \cos[x2]^2 - 1.31081 * \\
& 10^{10} \cos[x3] + 9.75742 * 10^9 \cos[x1] \cos[x3] - 1.2098 * \\
& 10^{10} \cos[x2] \cos[x3] - 3.23654 * 10^9 \cos[x3]^2 + 1.92004 * \\
& 10^{10} \sin[x1] - 9.60206 * 10^9 \cos[x1] \sin[x1] + 1.71747 * \\
& 10^{10} \cos[x2] \sin[x1] + 1.90062 * 10^{10} \cos[x3] \sin[x1] - 1.74629 * \\
& 10^9 \sin[x1]^2 + 5.15761 * 10^9 \sin[x2] - 3.9909 * 10^9 \cos[x1] \sin[x2] + \\
& 4.60054 * 10^9 \cos[x2] \sin[x2] + 4.74153 * 10^9 \cos[x3] \sin[x2] - 8.15273 *
\end{aligned}$$

$$10^9 \sin[x1] \sin[x2] - 5.54637 * 10^8 \sin[x2]^2 - 1.90395 * 10^9 \sin[x3] + 1.34213 * 10^9 \cos[x1] \sin[x3] - 5.62073 * 10^8 \cos[x2] \sin[x3] - 1.87296 * 10^9 \cos[x3] \sin[x3] + 2.4266 * 10^9 \sin[x1] \sin[x3] + 3.33102 * 10^9 \sin[x2] \sin[x3] - 8.17469 * 10^7 \sin[x3]^2)$$

$$FOLN2 = 214.956 - 38.1575 \log[x1] + 10.5513 \log[x2] + 10.4834 \log[x3]$$

$$FOLNR2 = (118926. + 384387. \log[x1] - 86839. \log[x2] - 437235. \log[x3]) / (-882810. + 193511. \log[x1] - 48974.8 \log[x2] - 69419.9 \log[x3])$$

$$SOLN2 = 67.652 - 6.48765 \log[x1] - 5.30895 \log[x1]^2 + 17.3755 \log[x2] + 7.22388 \log[x1] \log[x2] + 1.96101 \log[x2]^2 - 6.81263 \log[x3] - 11.4682 \log[x1] \log[x3] + 24.576 \log[x2] \log[x3] - 5.256 \log[x3]^2$$

$$SOLNR2 = (1.43543 + 9.37542 \log[x1] + 8.51279 \log[x1]^2 + 5.29568 \log[x2] + 15.7347 \log[x1] \log[x2] + 2.58494 \log[x2]^2 - 1.32302 \log[x3] - 11.917 \log[x1] \log[x3] - 2.9905 \log[x2] \log[x3] + 2.68263 \log[x3]^2) / (-1.61663 - 21.9001 \log[x1] + 7.59261 \log[x1]^2 - 10.9758 \log[x2] - 4.71163 \log[x1] \log[x2] - 1.22313 \log[x2]^2 + 13.5309 \log[x3] + 2.75376 \log[x1] \log[x3] - 18.9616 \log[x2] \log[x3] - 0.106591 \log[x3]^2)$$

$$FOEN2 = -61.6928 - 1.48773 * 10^{-7} E^{(0.1 x1)} + 0.0000450478 E^{x2} + 73.9162 E^{x3}$$

$$FOENR2 = (4.76996 * 10^6 + 9.75278 * 10^8 E^{(0.1 x1)} - 2.25083 * 10^9 E^{x2} + 7.28009 * 10^6 E^{x3}) / (-9.66769 * 10^7 + 4.83071 * 10^7 E^{(0.1 x1)} - 1.89945 * 10^8 E^{x2} - 1.62937 * 10^8 E^{x3})$$

$$SOEN2 = 7.50008 - 3.10198 * 10^{-8} E^{(0.1 x1)} - 5.76995 * 10^{-16} E^{(0.2 x1)} - 0.000404145 E^{x2} - 2.49072 * 10^{-9} E^{(2 x2)} + 3.76949 * 10^{-13} E^{(0.1 x1 + x2)} + 6.81228 E^{x3} + 6.09743 E^{(2 x3)} - 3.53662 * 10^{-8} E^{(0.1 x1 + x3)} + 0.000739806 E^{(x2 + x3)}$$

$$\begin{aligned}
SOENR2 = & (1.07739 + 365611.E^{(0.1 x1)} + 2.23425 * 10^8 E^{(0.2 x1)} + \\
& 463.643 E^{x2} + 1.37486 * 10^7 E^{(2 x2)} - 1.33107 * 10^8 E^{(0.1 x1 + x2)} + \\
& 2.46546 E^{x3} + 1.16555 E^{(2 x3)} + 552231.E^{(0.1 x1 + x3)} + \\
& 16711.7 E^{(x2 + x3)}) / (-0.566628 - 7.40058 * 10^6 E^{(0.1 x1)} + 1.10932 * \\
& 10^7 E^{(0.2 x1)} - 11622.5 E^{x2} - 3.71294 * 10^8 E^{(2 x2)} + 1.95489 * \\
& 10^7 E^{(0.1 x1 + x2)} - 8.36017 E^{x3} - 2.8891 E^{(2 x3)} - 1.23064 * \\
& 10^7 E^{(0.1 x1 + x3)} - 493612.E^{(x2 + x3)})
\end{aligned}$$



# Appendix B

## Publications from the Thesis

### Conference Papers

1. Aydın KB, Aydın L, Güneş F. Stochastic Optimization of TiO<sub>2</sub>-Graphene Nanocomposite by Using Neuro-Regression Approach for Maximum Photocatalytic Degradation Rate. ISSC2021: Proceedings of the 5th International Students Science Congress; 2021 May 21-22; Izmir, Turkey. 345-351.
2. Aydın KB, Aydın L, Savran M, Sayı H, Ayakdaş O, Artem HS. Stochastic Optimization of Graphene Sheets Subjected to Drilling Operation Using Neuro-Regression Approach for Maximum Mechanical Strength. ISSC2020: Proceedings of the 4th International Students Science Congress; 2020 Sep 18-19; Izmir, Turkey. 281-289.

### Journal Articles

1. Aydın KB, Aydın L, Güneş F. Modeling and Optimum Design of Carbon Nanotube/Polyvinyl Alcohol Hybrid Nanofibers as Electromagnetic Interference Shielding Material. Integrating Materials and Manufacturing Innovation 2022; 11:391–406. <https://doi.org/10.1007/s40192-022-00270-7>

### Projects

1. Grafen Tabanlı Nanokompozit Yapının Sentezi, Optimizasyonu ve Elektromanyetik Dalga Soğurma Özellikleri (2021-GAP-MÜMF-0042)
2. Grafen Tabanlı Nanokompozitlerin Elektromanyetik Dalga Soğurma Özelliklerinin Stokastik Yöntemlerle Geliştirilmesi (2022-TYL-FEBE-0018)

# Curriculum Vitae

**Name Surname** : Kemal Bartu Aydın

## **Education:**

MSc (2020–2023) – İzmir Kâtip Çelebi University, Dept. of Materials Science & Eng.

BSc (2014–2020) – İzmir Kâtip Çelebi University, Dept. of Materials Science & Eng.

## **Work Experience:**

08/2019–09/2019 – Production Engineer (Internship) / Şafak Döküm, *İzmir, Turkey*

07/2017–09/2017 – Production Engineer (Internship) / VESTEL, *Manisa, Turkey*

## **Publications:**

1. Aydın KB, Aydın L, Güneş F. Modeling and Optimum Design of Carbon Nanotube/Polyvinyl Alcohol Hybrid Nanofibers as Electromagnetic Interference Shielding Material. *Integrating Materials and Manufacturing Innovation* 2022; 11:391–406. <https://doi.org/10.1007/s40192-022-00270-7>
2. Aydın KB, Aydın L, Güneş F. Stochastic Optimization of TiO<sub>2</sub>-Graphene Nanocomposite by Using Neuro-Regression Approach for Maximum Photocatalytic Degradation Rate. *ISSC2021: Proceedings of the 5th International Students Science Congress*; 2021 May 21-22; Izmir, Turkey. 345-351.
3. Aydın KB, Aydın L, Savran M, Sayı H, Ayakdaş O, Artem HS. Stochastic Optimization of Graphene Sheets Subjected to Drilling Operation Using Neuro-Regression Approach for Maximum Mechanical Strength. *ISSC2020: Proceedings of the 4th International Students Science Congress*; 2020 Sep 18-19; Izmir, Turkey. 281-289.